GAS DELIVERABILITY USING THE METHOD OF DISTRIBUTED VOLUMETRIC SOURCES

A Thesis

by

XIAOZE JIN

Submitted to the Office of Graduate Studies of
Texas A&M University
in partial fulfillment of the requirements for the degree of

MASTER OF SCIENCE

December 2008

Major Subject: Petroleum Engineering

GAS DELIVERABILITY USING THE METHOD OF DISTRIBUTED VOLUMETRIC SOURCES

A Thesis

by

XIAOZE JIN

Submitted to the Office of Graduate Studies of
Texas A&M University
in partial fulfillment of the requirements for the degree of

MASTER OF SCIENCE

Approved by:

Chair of Committee,	Peter P. Valkó
Committee Members,	Ahmad Ghassemi
	Theofanis Strouboulis
Head of Department,	Stephen A. Holditch

December 2008

Major Subject: Petroleum Engineering

ABSTRACT

Gas Deliverability Using the Method of Distributed Volumetric Sources.

(December 2008)

Xiaoze Jin, B.S., University of Science and Technology of China

Chair of Advisory Committee: Dr. Peter P. Valkó

Productivity index (PI) is an important indicator of a well's production capacity. For conventional reservoirs, well productivity is usually calculated using the pressure response of the reservoir in its pseudosteady-state period. There are numerous studies for different well completion schemes which developed correlations for pseudosteady-state productivity index for specific cases, such as horizontal wells and fractured wells. Most of the developed models for complex well completion schemes use some approximations for productivity index calculation and they have some limitations in use. Furthermore, as the petroleum industry goes toward producing lower quality reservoirs like low- and ultra low-permeability reservoirs, the period of transient flow covers a larger part of the well lifetime and these pseudosteady-state productivity calculations become less applicable in prediction of the reservoir's production behavior. The Distributed Volumetric Sources (DVS) method seems able to fill this gap. Our method is able to predict the productivity index of a general well completion scheme for transient as well as pseudosteady-state flow periods.

In this study, we focus on a typical well completion scheme — vertical well intersected by a vertical fracture of finite conductivity. Parametric study is performed by varying the proppant pack permeability with a linear distribution, varying fracture width

with an elliptical distribution and varying fracture height with an elliptical distribution. The details of hydraulic fracture are integrated into the calculation of well productivity. By combining the well productivity with gas material balance, production forecasting of the hydraulically fractured wells could be easily obtained. The result of production forecasting could be used to aid in decision making of choosing the best stimulation treatment. Field examples are presented to illustrate the application of this technology for production modeling the complicated reservoir cases involving fracture stimulation.

DEDICATION

To my family and all my friends who have always stood by me

ACKNOWLEDGMENTS

I would like to express my deepest gratitude and appreciation to my advisor and committee chair, Dr. Peter P. Valkó, for believing in me and helping me out when everything looked bleak. His constant encouragement and creative ideas have always motivated me to work beyond my ability.

I would also like to thank Dr. Ahmad Ghassemi and Dr. Theofanis Strouboulis for serving as my committee members. Thank you for your effort.

Finally, I would like to thank the Crisman Institute in the Petroleum Engineering Department at Texas A&M University for sponsoring me during my endeavor for a master degree in petroleum engineering.

TABLE OF CONTENTS

CHAPTER Page

Page

LIST OF FIGURES

FIGURE Page

FIGURE Page

FIGURE Page

FIGURE Page

LIST OF TABLES

TABLE Page

TABLE Page

CHAPTER I

INTRODUCTION

1.1 General Background

Natural gas production has become increasingly important in the U.S. and the wellhead revenue generated from it is now greater than the wellhead revenue generated from oil production. Many wells, particularly gas wells in low-permeability formations, require hydraulic fracturing to be commercially viable. In order to maximize potential profits derived from accelerated production, reduced operating costs, and possibly increased ultimate recovery, one has to investigate the economics aspects of hydraulic fracturing.

Economic design of fracture treatments generally has three basic requirements[1]: (1) to evaluate what oil and/or gas production rates and recoveries might be expected from various fracture lengths and fracture conductivities for a given reservoir and relate these to cash flow income, (2) to determine the fracture treatment requirements to achieve the desired fracture lengths and conductivities and relate these to costs, (3) to select the fracture lengths and conductivities where the income and costs combine to maximize economic returns. Ideally, a reservoir performance simulator will provide predictions of the production rates and recoveries for various fracture lengths and conductivities; a hydraulic fracturing simulator usually is required to compute treatment volumes, types of materials, and pumping schedules necessary to achieve various fracture lengths and conductivities.

This thesis follows the style of *SPE Journal*.

However, despite all the progress made in reservoir simulation, such a task might be challenging even today.

The main objectives of this study are to develop a model, which can supersede the reservoir simulator to predict the performance of fractured wells. We first calculate the transient and stabilized productivity of complex well/fracture configurations using the distributed volumetric source (DVS) method, which is original developed by Amini and Valkó[2,3]. Combining productivity with material balance, we can forecast the production of the fractured well. The production can then be taken as input for an economic evaluation model. One can run a series of "what-if" scenarios to choose the best fracture treatment size and geometry for the well.

We now proceed with presenting a review of the current methodologies applied in the industry for fractured well performance evaluation.

1.2 Literature Review

In this section, an overview of previous work regarding the hydraulic fracture treatment design and evaluation will be presented. Existing approaches to predict production increase from a hydraulic fracture treatment will be reviewed. Also, the source/sink solution techniques will be briefly described. The motivation here is to identify the missing components in the current practice and to see how these gaps can be filled.

1.2.1 Modern Fracturing - Enhancing Natural Gas Production[4]

Hydraulic fracturing has been established as the premier production enhancement procedure in the petroleum industry. For the first 40 years since its inception, hydraulic fracturing has been primarily for low-permeability reservoirs; in the last two decades, it has expanded into medium- to high-permeability formations through the tip screenout (TSO) process. For natural gas wells, a reservoir above 0.5 md should be considered as a medium permeability reservoir. Above 5 md it should be considered as a high permeability formation. In all high permeability cases, the fracture should be a TSO treatment.

Valkó and Economides[5] and co-workers as in Romero et al.[6] (2002) introduced a physical optimization technique to maximize the productivity index of a hydraulically fractured well. It was called the Unified Fracture Design (UFD, Economides et al., 2002a) approach. A new concept was introduced: the dimensionless Proppant Number, N_{prop}, given by:

$$N_{prop} = I_x^2 C_{fD} = \frac{4k_f x_f w}{kx_e^2} = \frac{4k_f x_f wh}{kx_e^2 h} = \frac{2k_f}{k}\frac{V_p}{V_r} \quad \text{.....} \quad (1.1)$$

Where I_x is the penetration ratio, C_{fD} is the dimensionless fracture conductivity, V_r is the reservoir drainage volume, V_p is the volume of the proppant in the pay (the total volume injected times the ratio of the net height to the fracture height), k_f is the proppant pack permeability, k is the reservoir permeability, x_e is the well drainage dimension, h_f is the

fracture height and h is the reservoir thickness. The proppant permeability for gas wells will have to be adjusted because of turbulence effects.

A well in a reservoir developed on a certain pattern has a finite drainage area. During most of its lifetime, it is producing in a stabilized flow regime called pseudo-steady state (or more precisely, boundary-dominated state). During the stabilized flow regime, the productivity index of a well (PI), defined by the production rate divided by the pressure drawdown, is calculated as:

$$J = \frac{q}{\bar{p} - p_{wf}} \quad \text{……..……. (1.2)}$$

The dimensionless productivity index, J_D, is defined as

$$J_D = \frac{\mu B}{2\pi kh} J \quad \text{……...…..…….. (1.3)}$$

For an unstimulated well in a circular reservoir, J_D is given by the well-known formula:

$$J_D = \frac{1}{\ln(0.472 \frac{r_e}{r_w}) + s} \quad \text{……..……..…… (1.4)}$$

with the skin factor, s, representing deviation from the base case (without any near-wellbore damage or stimulation).

For a fracture stimulated well, J_D is affected by the volume of proppant placed into the pay layer, by the permeability ratio of the proppant bed and the reservoir, and by the geometry of the created fracture. All these factors can be characterized by two dimensionless numbers-the dimensionless fracture conductivity, C_{fD}, and the penetration ratio, I_x as defined before. The combination of the two dimensionless numbers is the dimensionless proppant number as defined in Equ. 1.1.

Valkó and Economides also found that for a given value of N_{prop}, there is an optimal dimensionless fracture conductivity at which the productivity index is maximized. More details are summarized in Section 1.2.6.

1.2.2 Flow Patterns in Hydraulically Fractured Wells

The productivity improvement as a result of fracturing a well will depend on the initial condition of the formation-i.e. whether it is damaged prior to the treatment. The primary mechanism that improves production from a fractured well is the change in flow pattern[7] within the reservoir. In a natural completion or matrix-acidized well, there is a radial flow pattern. In flow from a fractured well, there is a large portion of production that will be channeled through the fracture, particularly in the presence of any near-wellbore formation damage.

After a fractured gas well is placed on production, a pressure drawdown moves down the fracture away from the well. Four different flow periods will result over time: linear flow in the fracture, bi-linear flow in the fracture and formation, linear flow in the formation and, finally, pseudo-radial flow into the fracture. These different flow patterns are shown schematically in **Fig. 1.1**.

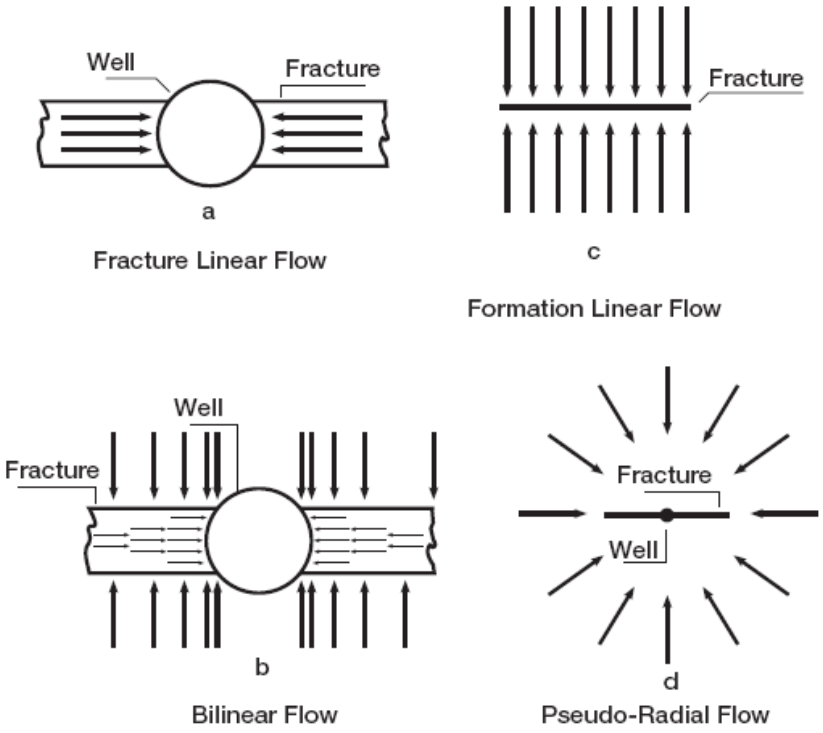

Fig. 1.1—Flow patterns for a hydraulically fractured well[8]

However, for those fractures with variable height and/or conductivity, some of these flow regimes might be obscured or totally missing.

1.2.3 Reservoir Models

Reservoir models are the engine that creates the output from the various applications. There are numerous different kinds of reservoir models, of widely varying complexity, that are of interest in advanced reservoir simulations.

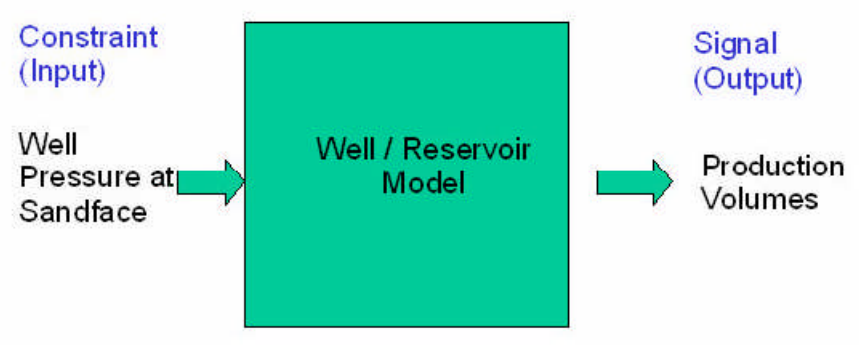

Fig. 1.2— Schematic explanation of well/reservoir model with Bottomhole Flowing Pressures (BHFPs) as input and production rates as output[9]

A reservoir model can be thought of as a "black box", which has an input and an output. The input is either a production rate or flowing pressure constraint and the output is either a simulated flowing pressure response or a simulated production rate response. Some models, such as multi-phase model may have multiple constraints and/or outputs. **Fig. 1.2** and **Fig. 1.3** show the concept of well/reservoir modeling as simple flow charts.

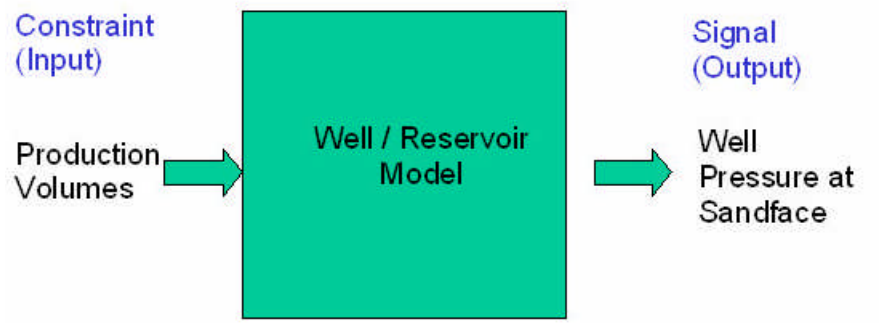

Fig. 1.3—Schematic explanation of well/reservoir model with production rates as input and Bottomhole Flowing Pressures (BHFPs) as output[9]

There is a list of useful models, as shown in **TABLE 1.1**, in production performance analysis. Models that have internal boundary condition types 3) and/or 5) are history match models. All other are type-curve or decline curve models.

TABLE 1.1—Elements for reservoir model building[9]

Fluid Properties	Formation Properties
1. Single phase constant 2. Single phase variable 3. Multi-phase variable 4. Non-Darcy flow	1. constant 2. k(p) 3. k(x, y) 4. k(z) 5. porosity (p) 6. porosity (x, y)

Well Geometry	External Boundary Conditions	Internal Boundary Conditions
1. Vertical well 2. Infinite conductivity fracture 3. Finite conductivity fracture 4. Horizontal well	1. Volumetric circle 2. Volumetric rectangle 3. Volumetric multi-layer 4. Radial composite closed 5. Radial composite open (infinite acting) 6. Connected tanks 7. Constant pressures	1. Constant pressure drawdown 2. Constant rate drawdown 3. Variable rate/pressure drawdown 4. Multi-well drawdown 5. Drawdown/Buildup

1.2.4 Infinite-acting Flow and Boundary-dominated Flow

Flow in a reservoir is often characterized as being one of two types, namely transient or boundary-dominated[9].

Transient flow takes place during the early life of a well, when the reservoir boundaries have not been felt, and the reservoir is said to be infinite-acting. During this period, the size of the reservoir has no effect on the well performance, and from analysis

of pressure or production, nothing can be deducted about the reservoir size. In theory, the size of the reservoir does have an effect even at very early times, but in reality, this effect is so small as to be negligible and not quantifiable with any kind of confidence. Transient flow forms the basis of a domain of reservoir engineering called Pressure Transient Analysis, also known as well test interpretation.

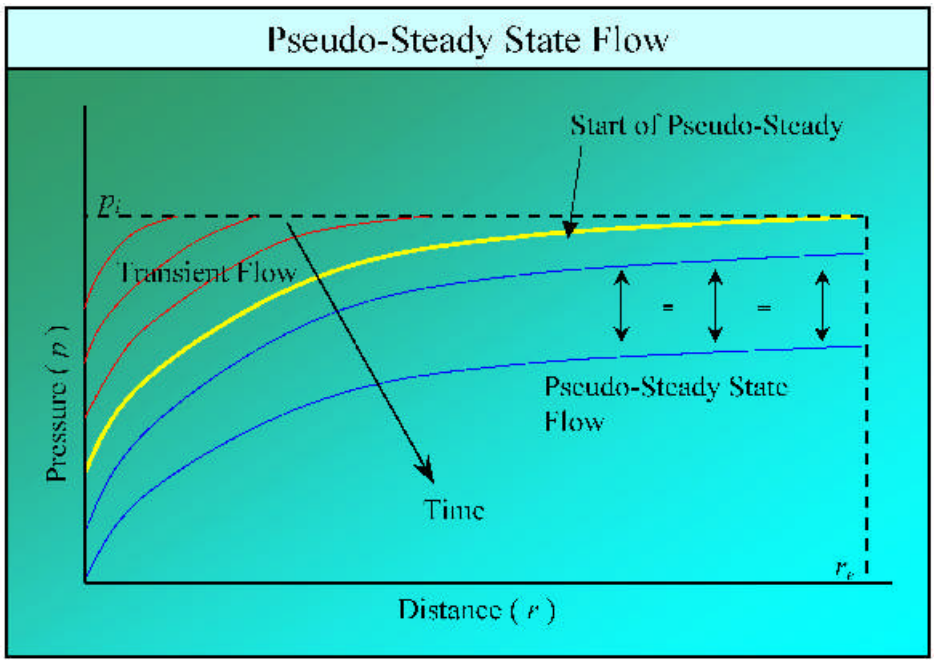

Fig. 1.4—Transient flow and pseudo-steady state flow profile in a tank reservoir model[9]

The field of well testing relies heavily on equations of flow for a well flowing at constant rate. Initially, the flow regime is transient, but eventually when all the reservoir boundaries have been felt, the well will flow at steady state, if a constant pressure boundary exists, or at pseudo-steady state, if all the boundaries are no-flow boundaries.

During pseudo-steady state, the pressure throughout the reservoir declines at the same rate as shown in **Fig. 1.4**. The concept of pseudo-steady state is applicable to a situation where the well is flowing at a constant flow rate.

When a well is flowing at a constant flowing well-bore pressure, as is often the case in production operations, there is a period of time during which boundaries have no influence, and the flow behavior is “transient”. However, after a period of time, when the radius of investigation has reached the outer boundary, the boundary starts to influence the well performance, and the pressure drops throughout the reservoir. But unlike pseudo-steady state flow, where the pressure drop is uniform throughout the reservoir, the pressure at the well is kept constant and the pressure at the boundary is dropping due to depletion. This is a case where the boundary is affecting the reservoir pressure, and hence the production rate, but it cannot be called pseudo-steady state, because the pressure drop in the reservoir is not uniform, so it is called boundary-dominated flow as shown in **Fig. 1.5**.

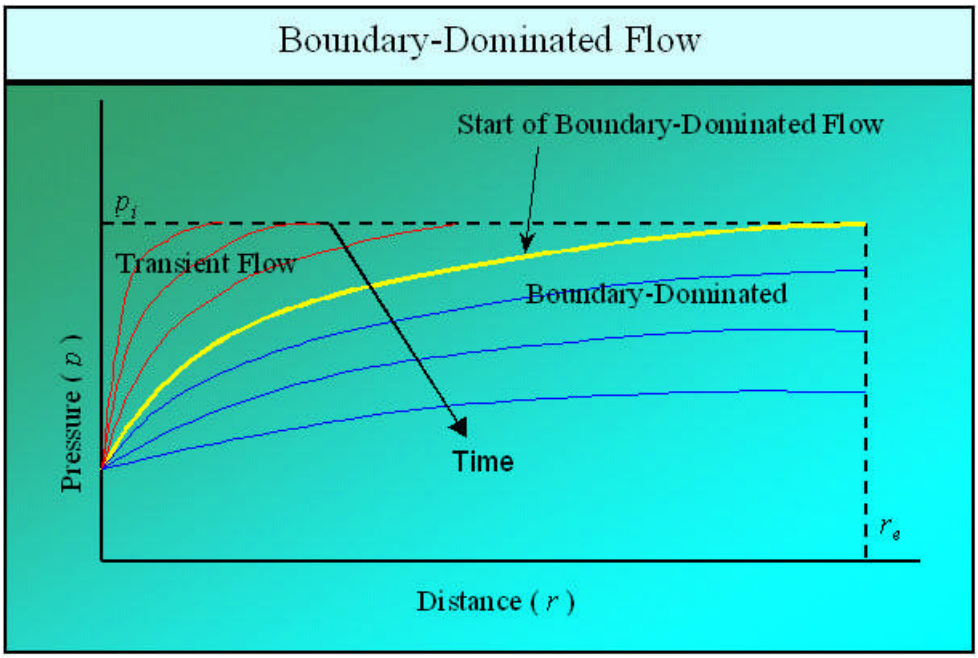

Fig. 1.5—Transient flow and boundary-dominated flow profile in a reservoir model[9]

Thus, boundary-dominated flow is a generic name for the well performance when the boundaries have a measurable effect. Pseudo-steady state flow is only one type of boundary-dominated flow, which takes place when the well is flowing at a constant rate.

1.2.5 Equivalence of Constant Rate and Constant Pressure Solutions

A well produced at a constant rate exhibits a varying (declining) bottomhole flowing pressure, whereas a well produced at a constant bottomhole pressure exhibits a varying decline rate.

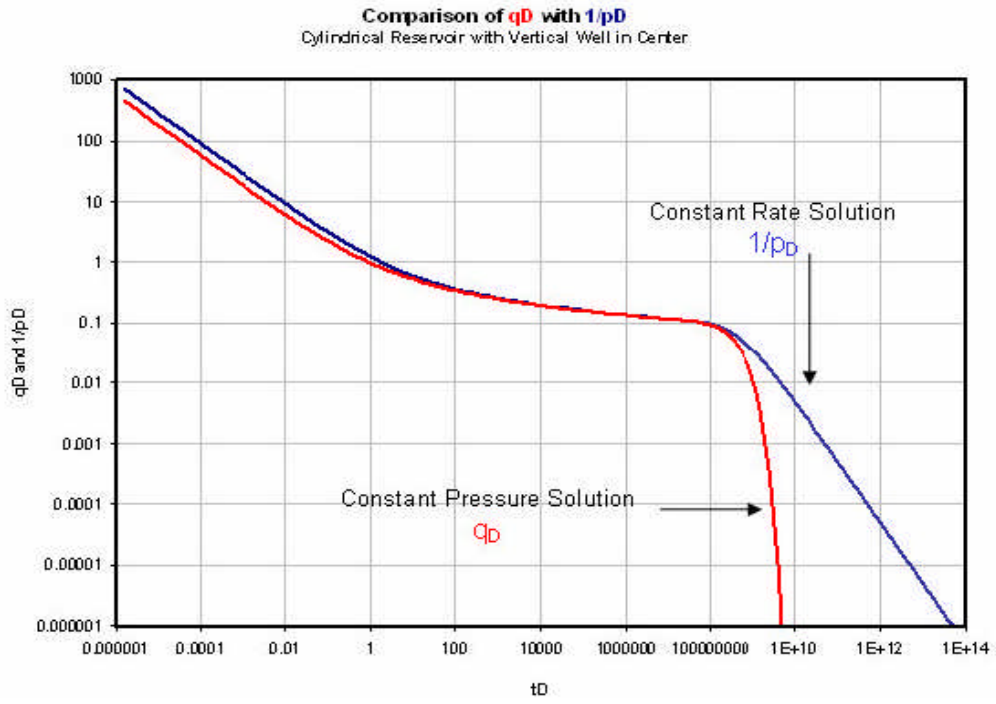

Fig. 1.6—Comparison of constant pressure solution and constant rate solution for a cylindrical reservoir with a vertical well in center (Dimensionless rate and reciprocal of dimensionless pressure versus dimensionless time)[9]

There is a strong symmetry between the two solutions as shown in **Fig. 1.6**, as both are obtained from the same equation, namely the equation that governs fluid flow in porous media. The symmetry is not exact, however, because the boundary conditions under which the two solutions are obtained are different.

The constant rate solution can be converted to a constant bottomhole pressure solution (and vice versa) using the principle of superposition. The constant bottomhole pressure solution would be obtained by superposing a large number of very short constant rate solutions in time. When plotted against superposition time, the superposed constant rate solution is very similar to the constant pressure solution, provided the

discretization intervals are sufficiently small. It turns out that the two solutions are quite similar during transient flow anyway, and therefore superposition is not required to make one look like the other.

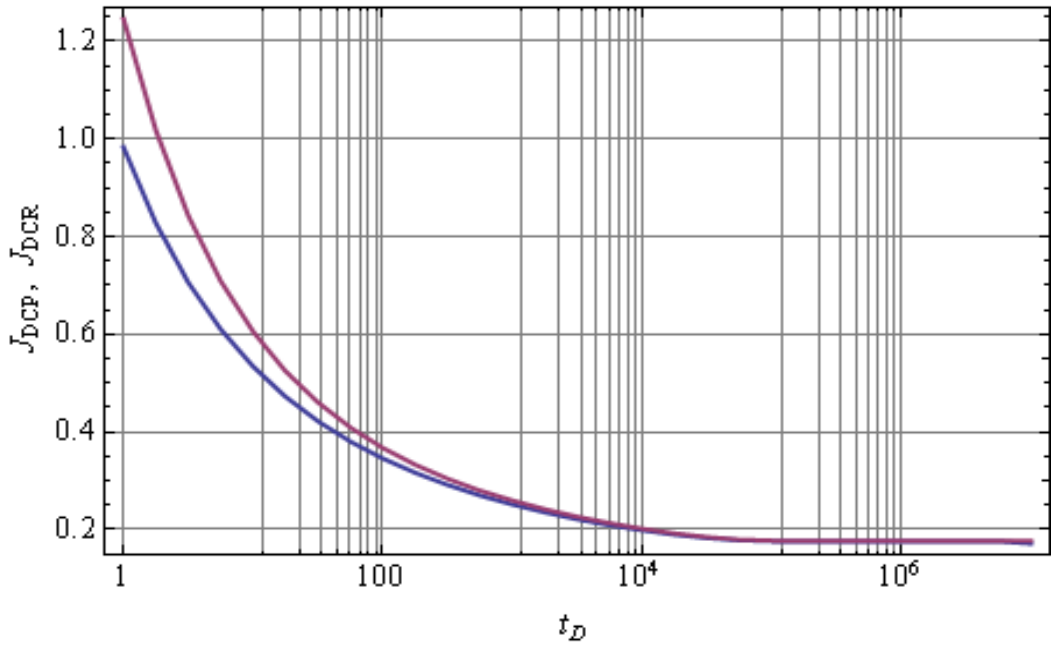

Fig. 1.7—Comparison of J_D from constant pressure solution and constant rate solution for a circular reservoir with a vertical well in center[10]

However, they quickly diverge once boundary dominated flow begins. The constant rate solution behaves like the harmonic stem of the Arps type curves, while the constant pressure solution declines exponentially.

Kumar (2008) solved the flow equations with different boundary conditions and concluded that the difference in J_D from constant pressure solution and constant rate solution is not significant as shown in **Fig. 1.7**.

1.2.6 Hydraulic Fracture Sizing and Optimization

Currently, the optimization of hydraulic fracture design has taken in three categories.

- **Pseudo-steady State Curves**

McGuire and Sikora[11] (1960) presented the first pseudo-steady state set of curves to estimate the gain in PI that can be obtained for an oil well from alteration of reservoir flow pattern by a fracture. Increases in PI, commonly called the stimulation ratio, are plotted vs. dimensionless fracture length and fracture permeability contrast. The curves were generated from an electric analog laboratory model by measuring electrical potential difference. However, the assumptions behind these curves restrict their use to pseudo-steady state conditions for slightly compressible reservoir fluids, as found in undersaturated oil wells.

Tannich and Nierode[12] (1985) presented another set of pseudo-steady state curves for gas wells. The shapes of these curves are similar to the shapes of the McGuire-Sikora curves, but the correlating parameters are a little different. PI ratio is plotted vs. fractional fracture length and a conductivity group called relative turbulent conductivity, C_{rB}. The Tannich-Nierode curves were generated from many computer calculations for a fractured gas well with a finite-difference reservoir simulator and correlation of the results.

Such a plot used to be popular to select treatment size and fracture dimensions simultaneously. Unfortunately, it is not obvious which curve is to select and what point

to select on a given curve, because this type of presentation blurs the cost the creating a propped fracture.

- **Economic Optimization via Net Present Value (NPV)**

Ideally, the reservoir deliverability, well producing systems, fracture mechanics, fracturing fluid characteristics, proppant transport mechanism, operational constraints, and economics should be considered and integrated, to obtain the most cost-effective design and to maximize the benefit of a well stimulation treatment.

Balen[13] et al. (1988) introduced the concept of net present value (NPV) as a systematic approach in the optimization of hydraulic fractures. In their method, the optimum hydraulic fracture design is achieved by coupling of production forecasting, fracture geometry requirements and treatment scheduling. The technique involves certain steps to determine the optimum size of the treatment:

- Optimize the reservoir deliverability,
- Maximize the proppant coverage for a given fracture penetration,
- Optimize the pump rate and fluid based on viscosity and fluid loss of selected fluids,
- Minimize the treatment cost, and
- Maximize the economic returns based on the NPV.

Based on the constructed NPV curves, one could then compare the various stimulation scenarios. Hence, the optimum fracture size is defined as the one that corresponds to the maximum NPV.

There is nothing implicitly wrong with the NPV approach, but it is particularly applicable to unrestricted fracturing where the length and the width can be optimized by adjusting injection variables such as the injection rate and fluid rheology.

- **Physical Optimization via Dimensionless Proppant Number (N_{prop})**

Valkó and Economides[5] (2002) presented a physical optimization of fracture design in their book: *Unified Fracture Design* (UFD). Algorithms are available to calculate J_D as a function of C_{fD} with N_{prop} as a parameter, as shown in **Fig. 1.8** for low-permeability hydraulic fracture design with proppant number smaller than or equal to 0.1 and **Fig. 1.9** for high-permeability hydraulic fracture design with proppant number larger than 0.1.

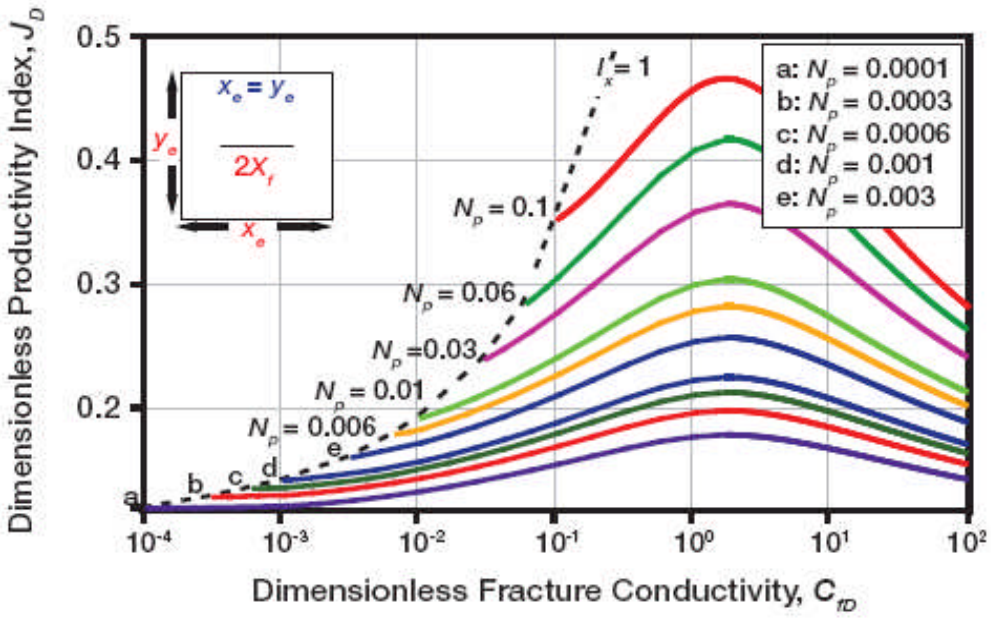

Fig. 1.8—Dimensionless productivity index as a function of dimensionless fracture conductivity with dimensionless proppant number as a parameter, for N_{prop}<=0.1[5]

They also found that for a given value of N_{prop}, there is an optimal dimensionless fracture conductivity, C_{fDopt} at which the productivity index is maximized.

Although large poppant number lead to larger dimensionless productivity index, the absolute maximum for J_D is 1.909. At "low" proppant number, the optimal C_{fD}=1.6. At larger proppant numbers, the optimum C_{fD} is larger as can be seen in **Fig. 1.9**. When the propped volume increases or the reservoir permeability decreases, the optimal compromise happens at larger dimensionless fracture conductivities, as the penetration ratio cannot exceed one.

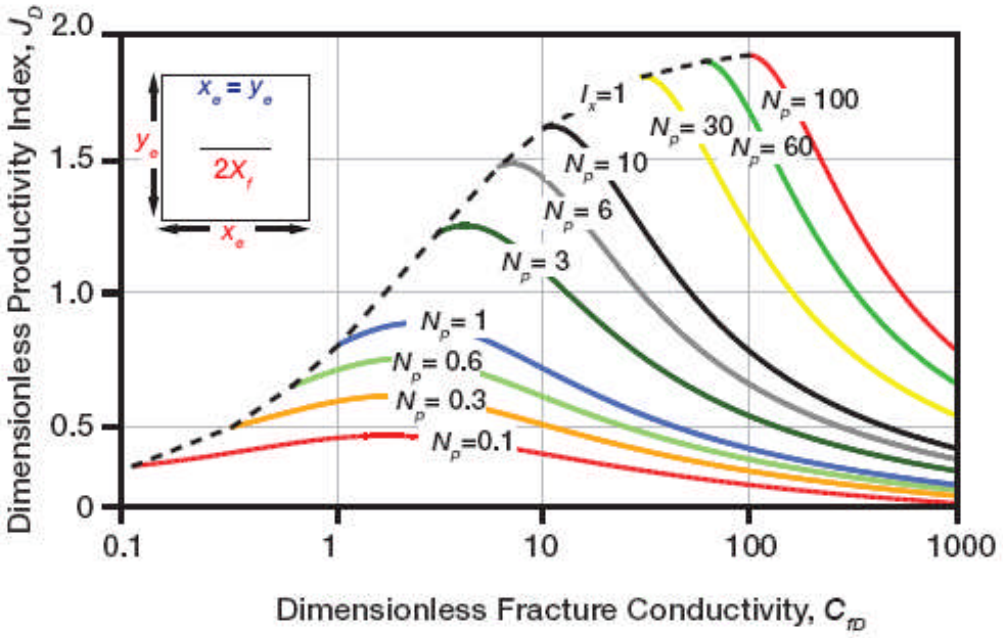

Fig. 1.9—Dimensionless productivity index as a function of dimensionless fracture conductivity with dimensionless proppant number as a parameter, for N_{prop}>0.1[5]

A reasonable optimization scheme for fracture design can be readily established because once the optimum dimensionless fracture conductivity is identified, the optimum fracture dimensions of length and width are determined by two equations:

$$x_{fopt} = \left(\frac{k_f V_p / 2}{C_{fD,opt} kh} \right)^{0.5} \quad \text{……..……..…….. (1.6)}$$

$$w_{fopt} = \left(\frac{C_{fD,opt} kV_p / 2}{k_f h} \right)^{0.5} \quad \text{……..……...…….. (1.7)}$$

1.2.7 Prediction of Fractured Well Performance

There have been two basic categories of methods commonly used for predicting the production from hydraulically fractured wells: 1) analytical solutions and 2) finite-difference reservoir simulation.

For hydraulically fractured wells, there are several ways to incorporate the stimulation effect into the dimensionless pseudo-steady state productivity index indirectly:

- the pseudo-skin concept:

$$J_D = \frac{1}{\ln \frac{r_e}{r_w} - \frac{3}{4} + s_f} \quad \text{…..……...…….……..…..…… (1.8)}$$

- Prats' (1961)[14] equivalent wellbore radius concept:

$$J_D = \frac{1}{\ln \frac{r_e}{r_w'} - \frac{3}{4}} \quad \text{……...……...…..…… (1.9)}$$

- Cinco-Ley and Sameniego's (1981)[15] f-factor concept:

$$J_D = \frac{1}{\ln \frac{r_e}{x_f} - \frac{3}{4} + f} \quad \text{……...…….....…...…..} \quad (1.10)$$

These concepts can be used as an approximation to the PI of hydraulically fractured wells. But none of them account for the details of fluid flow from reservoir to fractures. Moreover, they might be convenient to use these concepts in the transient flow period but it is not a good one to represent the whole life of any fractured wells, especially for those wells in low and ultra low permeability reservoirs. Obviously, a robust method of predicting the productivity index of hydraulically fractured wells is needed in the industry.

In the finite-difference reservoir simulation, fracture is first modeled implicitly using the approximation concepts of productivity index of the hydraulically fractured wells. Right now, people in the industry tend to model the fracture explicitly in the reservoir simulator. Lots of works published were developing finite-difference models by using local grid refinement (LGR) technique, e.g. Bennett et al.(1986)[16], Ehrl et al. (2000)[17], to name a few. Although this method works fine, it is very time consuming for the engineer, because complicated gridding schemes are necessary to correctly represent the fracture geometry. In addition, the detailed description of the fracture properties from a fracture simulation was not usually passed through to the reservoir model, resulting in the assumption of constant properties for the fracture. This method of simulation is not very efficient and can lead to inconsistencies in the data used in the different simulations.

Typically, a reservoir simulator is used for field development planning, but it is not practical for design of individual well completions. Analytical solutions to the radial diffusivity equation are often used to estimate production benefits from changes in completion practices.

Recently, there are publications describing the idea of transferring the output from a fracture model to a reservoir simulation model. It was first presented by Behr et al. (2003)[18], then, further developed by Shaoul et al. (2005)[19] as well as applications of their model (2007)[20]. Although the new idea seems appealing to someone, there is no big help with regarding to efficiency and robustness compared to the traditional finite-difference simulator. The idea is only that developing a tool which works as a link between their commercial fracture simulator and reservoir simulator. Put it simple, the output of the fracture simulator is transferred to reservoir simulator as input.

Nodal analysis is a Schlumberger patented technology for petroleum system analysis. It is widely used for any kind of system, homogeneous or heterogenous reservoirs with any inner boundary conditions. Meng et al. (1982)[21] applied the nodal analysis method for prediction of fractured wells performance. Although it works, it is not so convenient to use it as optimization fracture design treatment tool. It will be cumbersome if we need to run a series of "what-if" production forecast scenarios for comparison.

1.2.8 Deliverability Testing[22]

Both the theoretical and empirical gas-flow equations are used extensively in the natural gas industry to analyze deliverability tests. The theoretical equations, developed

by Houpeurt[23], are exact solutions to the generalized radial flow diffusivity equation, while the Rawlins and Schellhardt[24] equation is derived empirically. All basic equations were developed with radial flow in a homogeneous, isotropic reservoir assumed and therefore are not applicable to the analysis of deliverability tests from reservoirs with heterogeneities, such as natural fractures or layered pay zones. These equations also cannot be used to analyze tests from hydraulically fractured wells, especially during the initial, fracture-dominated, linear flow period. Finally, these equations assume that wellbore storage effects have ceased. Unfortunately, wellbore-storage distortion may affect the entire test period in short tests, especially those conducted in low-permeability reservoirs.

The data used in deliverability tests analysis could be from well testing analysis or from direct measurements of flowing pressures and rates. There are four most common types of gas-well deliverability tests: flow-after-flow, single-point, isochronal, and modified isochronal tests, with each of which has their own advantages and disadvantages. The main issue concerned with the deliverability tests is that they all require at least one stabilized flow, which requires a long time especially in low-permeability reservoirs. Thus, sometimes, it is not practical and economic to conduct a deliverability test in field.

1.2.9 Application of Source and Green Functions

Although most of the solutions to the flow problem in porous media have been investigated in a similar case in the heat transfer and the solution is originated from heat transfer, Gringarten and Ramey's[25] work is the first application of the Green's and

Source function to the problem of unsteady-state fluid flow in the reservoirs. They introduced proper Green's functions for a series of source shapes and boundary conditions. They showed that the point source solution is actually a more general form of theory of Green's function. He used the integration of the response to an instantaneous source solution to get the response for a continuous source solution. The application of the Newman's principle in breaking a problem in 3D to the product of three 1D solutions is also discussed in this paper.

The major disadvantage of this method is the inherent singularity of the solution wherever the source is placed. Since the source is assumed to have no volume (point, line, or plane source), the source is considered to be at infinite pressure at any time zero and it is not possible to calculate the exact pressure as a function of time at the point where the source is placed. The provided solution for finite cases is in the form of an infinite series which converges very slowly when we approach to the source's coordinates. This makes the process of calculation inefficient when we approach the source. To handle this problem, we have to assume an arbitrary point with a certain distance from the source and calculate the solution there. The solution by this method is only a function of the distance from the source, regardless of the coordinates, so it might raise some questions about the reliability of the solution when we specifically deal with anisotropic systems and/or complex well completion schemes.

The application of source and Green's function later was extended to the unsteady state pressure distribution for more complex well completion schemes by others. The developed solutions do not suffer the singularity problem, because the line

source solution is integrated over the length or area of the source, but they still need reference points to perform calculations. Moreover, the assumption of the source not having a volume has led us to develop different solutions for each special case.

The distributed volumetric source (DVS) method is developed by Amini and Valkó[2,3] to remove this singularity problem and provide a faster and more reliable solution to the problems of transient and pseudosteady-state fluid flow in a reservoir with closed boundaries. In this method, every source, regardless of its size and dimensions, is assumed to contain a volume. So the initial value pressure in the source is never infinite. This assumption provides us the opportunity to treat all kinds of sources in a similar way. In other words, DVS solution for a uniform flux source is unique no matter it is a point, a vertical or horizontal well with partial penetration, or a fracture.

The main concept of the DVS method is to introduce an instantaneous volumetric source inside the reservoir and calculate the analytical 3D response of the system as a product of three 1D responses based on Newman's principle. The solution will provide the well-testing derivative of the response to a continuous source in analytical form. This can be integrated over time to provide the pressure response to a continuous source.

Results from the new solution are combined with the material balance equation for a closed boundary reservoirs to predict the production behavior of the system in form of transient and pseudosteady-state dimensionless Productivity Index (PI). This has important applications in production engineering in terms of finding the optimum completion scheme for development of a certain reservoir.

The new method has shown to provide a fast, robust, and reliable way to pressure transient analysis, and well performance prediction whenever complex well/fracture configuration is considered.

We now give a brief description of our method of solution.

1.3 Statement of the Problem

In production engineering application, productivity of a well is calculated using the pressure response of the reservoir in its pseudosteady-state period. There are numerous studies for different well completion schemes — such as horizontal wells and fractured wells — which developed correlations for pseudosteady-state productivity index for specific cases. Most of the developed models for complex well completion schemes use some approximations for productivity index calculation and they have some limitations in use. Furthermore, as the petroleum industry goes toward producing lower quality reservoirs like low- and ultra low-permeability reservoirs, the period of transient flow covers larger part of the well lifetime and these pseudosteady-state productivity calculations become less applicable in prediction of the reservoir's production behavior.

The DVS method seems able to fill this gap. Our method is able to predict the productivity index of a general well completion scheme for transient as well as pseudosteady-state flow periods.

1.3.1 Solution Approach

As stated in the previous section, it is very important to hydraulically fracture treating a well in an optimization design. The capital investment required to hydraulic fracturing a well is usually very high. It is very costly to correct mistakes made during this design process. The controllable factors that determine the performance of fractured wells are the fracture length, fracture conductivity and fracture height. For evaluation purpose, the fracture face could also be rectangular or elliptical. In our method of predicting fractured well performance, both the geometry of the sources and the conductivity of sources will also be varied. This methodology, which will be explained in detail in the coming chapters, is appropriate for use as a screening tool rather than for actual operations.

1.3.2 Concluding Remarks

In this chapter, we gave a general background of modern fracturing stimulation and also motivated the necessity of optimization of the hydraulic fracture stimulation treatment. Along with the design optimization, we will provide production forecasting for each well/fracture configuration.

The literature review leads to the following observations:

- The fracture design procedures currently practiced in the industry include the following:
  - The prediction of well deliverability for various fracture penetrations and conductivities.
  - Parametric studies on the fracture geometry requirements.

- The selection of the appropriate type of fracturing materials.
- The determination of fracture design criteria based on maximum economic returns on the well. Various reservoir simulators, hydraulic fracture propagation simulators, and economic models are often run on a trial-and-error basis until the desired design criteria are met. This is a time-consuming exercise.

- Among the three fracture treatment optimization methods, McGuire and Sikora's pseudosteady state plots, economic optimization via NPV and physical optimization via N_{prop} come to the arsenal of hydraulic fracture industry, in a chronical way, as methodologies of optimum treatment design. But none of them seem as a robust design method. Recently, Marongiu-Procu et. al[26] presented a way of coming the economic and physical optimization of hydraulic fracturing, but the primary point is still the way how to calculate the well productivity, especially for complex well/fracture configurations, which is the common completion scheme for the ultra-low permeability reservoirs.
- Production forecasting of the complex well/fracture systems combining productivity index and material balance is in its early stage. Different techniques have been proposed, though the area is very open to further exploration.
  - DVS method seems the best currently available method to calculate the well productivity for complex well/fracture systems[3, 27]
- The assessment of the effects of uncertainty to various geological and

engineering parameters is vital for reliable economic evaluation, thus prudent decision making. Therefore, the optimization framework must consider uncertainty.

The outline of this thesis is as follows. In **Chapter II**, the basic principles of the DVS method and the method of production forecasting combining dimensionless productivity index and material balance are presented. The utilization of the DVS method as a way to pressure transient analysis and predict well productivity for hydraulically fractured wells is explained, and guidelines for the use of the DVS method are established. Calculation and correlation procedure of gas PVT property is also included in **Appendix A**. The logic of calculating the dimensionless productivity index with the DVS method and forecasting production is described and tabulated. Synthetic example calculations are included in **Appendix B**. In **Chapter III**, we investigate effect of the sizing and the geometry of fracture on productivity of the vertical gas well in further application of the DVS method. Four synthetic cases are computed and the effects of varying propped permeability, varying fracture width and varying fracture height are investigated in details based on one of the synthetic case. In **Chapter IV**, we apply all of our developments to three field examples. We get the field data about the fracture size and geometry from the case studies in the literature. Finally, in **Chapter V**, we draw conclusions based on this research work.

CHAPTER II

METHODOLOGY

2.1 The Distributed Volumetric Sources (DVS) Method

The method of Distributed Volumetric Sources (DVS) is developed to solve problems of transient and pseudo steady state fluid flow in reservoirs by Amini[2] in his Ph.D. dissertation. The basic building block of the method comprises the calculation of the analytical response of a rectilinear reservoir with closed outer boundaries to an instantaneous volumetric source, also shaped as a rectilinear body. The solution also provides the well-testing derivative of the response to a continuous source in analytical form. This can be integrated over time to provide the pressure response to a continuous source. For production engineering applications, we cast the results into a transient/pseudo-steady productivity index form. The main advantage of the new solution is its applicability over the more complex fracture/well configurations.

The DVS method has shown to provide a fast, robust and reliable way to pressure transient analysis and well performance prediction whenever complex well/fracture configuration is considered.

2.1.1 Basic Principles of the DVS Method

The first step of the DVS method is to develop the pressure response of a rectilinear reservoir with closed boundaries to an instantaneous withdrawal from the source. The porous media is assumed to be an anisotropic, homogeneous reservoir shaped as a box. The box is oriented in line with the three principal directions of the

permeability field. The source is assumed to be a smaller rectilinear box with its surfaces parallel to the reservoir boundaries. It is assumed to have the same media properties as the reservoir. **Fig. 2.1** shows the schematic of the system, which we will refer it to "box-in-box" model. The instantaneous unit withdrawal is distributed uniformly in the volume of the source. In short, we will refer to the solution as instantaneous source response of the box-in-box and will denote the response observed at a location (x_D, y_D, z_D) as $p_{\delta D}(box-pars; x_D, y_D, z_D, t_D)$. The box-pars notation stands for all the information contained in the problem specification: (x_e, y_e, z_e, k_x, k_y, k_z, c_x, c_y, c_z, w_x, w_y, w_z). For the meaning of the variables, see **Fig. 2.1**.

The results is obtained from Newman's principle as

$$p_{\delta D}(box-pars; x_D, y_D, z_D, t_D) = f(x-pars; x_D, t_{Dx}) \times f(y-pars; y_D, t_{Dy}) \times f(z-pars; z_D, t_{Dz}) \quad \text{..... (2.1)}$$

where $f()$ represents the solution of a 1D problem with the source distributed along a finite section of the "linear" reservoir. The structure of Equ. 2.1 already indicates that all anisotropy is handled in the parameters of the 1D solution. In short, this comprises the main advantage of the DVS method: once an effective method is available to accurately calculate $f()$, the additional programming requirement is minimal. The details are provided by Valkó et al.[3].

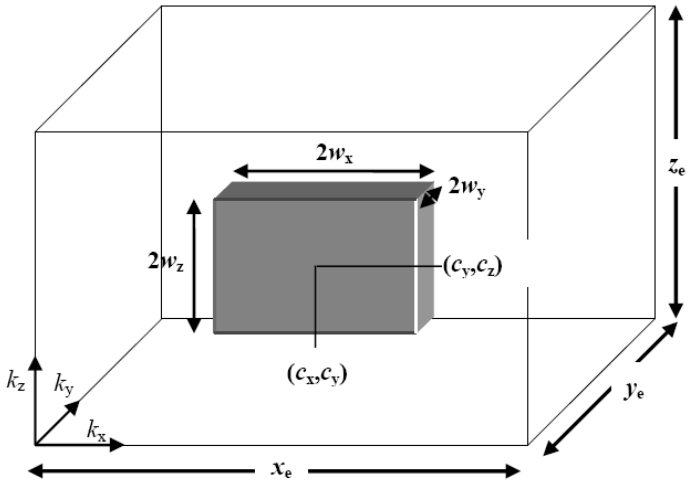

Fig. 2.1—Schematic of the box-in-box model[2]

To obtain the response of the reservoir to a continuous unit source distributed uniformly in the small box, we numerically integrate the solution, Equ. 2.1 over time:

$$p_{uD}(x_D, y_D, z_D, t_D) = \int_0^{t_D} p_{\delta D}(x_D, y_D, z_D, \tau) d\tau \quad \text{……..……. (2.2)}$$

To obtain wellbore flowing pressure, we can calculate $p_{uD}(x_D, y_D, z_D, t_D)$ at the geometric center of the well. The instantaneous source solution (which is equal to the well testing pressure derivative function), $p_{\delta D}(x_D, y_D, z_D, \tau)$ and the continuous source solution (which is the well testing pressure function), $p_{uD}(x_D, y_D, z_D, t_D)$ can be used as type-curves for pressure transient analysis.

The box-in-box model can be used directly to reproduce some well-know results for *uniform flux* and *infinite conductivity* sources, such as fully penetrating vertical well, partially penetrating vertical well, horizontal well, fully penetrating vertical fracture. All

these calculations can be done basically using the DVS method. We will refer to these cases as single box models.

More important, the box-in-box model can be used to model more complicated cases using the familiar concept of superposition in space. For instance, a vertical well intersected by a vertical fracture of *finite conductivity* is represented by n boxes put next to each other in the fracture. Then, the actual distribution of inflow between the boxes is determined from a system of linear equations. The system matrix coefficients are time-dependent and are calculated with repeated application of the analytical solution from the single box model. Also, the coefficients depend on the dimensionless fracture conductivity. With the same way we can deal with other two cases are horizontal well intersected by a vertical fracture of finite conductivity longitudinally or transversely. Obviously, finite conductivity fracture/well systems are more time consuming to calculate. In fact, the most computationally demanding case is the horizontal well intersected by a transverse fracture, because it needs a two dimensional array of boxes to represent the finite conductivity fracture. Accordingly, we can refer these cases to multiple box models.

2.1.2 DVS Method as a Way to Predict Well Productivity

The further use of DVS method was developed by Valkó et al.[3] as a way to predict productivity of complex well/fracture systems. The applicability and reliability of the results were compared with the study of Chen and Asaad[28] for the pseudo-steady state productivity index of horizontal wells.

In production engineering, the productivity index is defined as the ability of the reservoir to produce hydrocarbon per unit pressure drop in the reservoir (volume/time/pressure).

$$J = \frac{q}{p_{avg} - p_{wf}} \quad \text{……..……} \quad (2.3)$$

In which

q = Flow Rate

p_{avg} = Average Reservoir Pressure

p_{wf} = Well Flowing Pressure

Introducing the Dimensionless parameters as the followings the expression for the dimensionless productivity index would be obtained.

$$p_{D,trad} = \frac{2\pi kh}{qB\mu}(p_i - p) \quad \text{……...……...……} \quad (2.4)$$

$$J_D = \frac{\mu B}{2\pi kh} J \quad \text{……...……...…} \quad (2.5)$$

With:

p_i = Initial Reservoir Pressure

k = Reservoir Permeability

h = Reservoir Thickness

B = Formation Volume Factor

μ = Fluid Viscosity

Combining Eqs. 2.3 through 2.5 we have:

$$J_D = \frac{1}{p_{D,trad} - p_{D,avg,trad}} \quad \text{……...…….. (2.6)}$$

Assuming a constant and small compressibility during depletion we can write:

$$c_t = -\frac{1}{V}\frac{\partial V}{\partial p} \quad \text{……...……...…….. (2.7)}$$

$$V = \phi Ah \quad \text{……...……...…… (2.8)}$$

$$\frac{\partial p}{\partial V} = \frac{1}{\phi Ahc_t} \quad \text{……...……..….. (2.9)}$$

$$\Delta p = p_i - p_{avg} = \frac{\Delta V}{\phi Ahc_t} = \frac{N_p B}{\phi Ahc_t} = \frac{qBt}{\phi Ahc_t} \text{ (Constant flow rate production) …...…. (2.10)}$$

Using the definition for dimensionless pressure and applying it on Eq. 2.10 we have:

$$p_{D,avg,trad} = 2\pi \frac{kt}{\phi \mu c_t A} = 2\pi t_{DA} \quad \text{……...……..…….. (2.11)}$$

Where:

$$t_{DA} = \frac{kt}{\phi \mu c_t A} \text{ (Dimensionless time defined based on drainage area) …… (2.12)}$$

Combination of Eqs. 2.11 and 2.6 would lead us to an expression correlating the dimensionless productivity index as a function of dimensionless pressure and dimensionless time (Eq. 2.13)

$$J_D = \frac{1}{p_{D,trad} - 2\pi t_{DA}} \quad \text{……...……. (2.13)}$$

Based on the new dimensionless variables defined in the DVS method, we will get

$$J_D = \frac{1}{2\pi c_{trad}(p_{uD} - t_D)} \quad \text{……..…..…… (2.14)}$$

where,

$$c_{trad} = \frac{z_e \sqrt{k_x k_x}}{L k} \quad \text{..... (2.15)}$$

$$p_{uD} = \int_0^{t_D} p_{\delta D}(t_D^{'}).dt_D^{'} \quad \text{..... (2.16)}$$

$$t_D = \frac{k}{\phi \mu c_t L^2} t \quad \text{..... (2.17)}$$

$$k = (k_x k_y k_z)^{\frac{1}{3}}$$
$$L = (x_e y_e z_e)^{\frac{1}{3}} \text{ (k and L are reference permeability and length) ..... (2.18)}$$

There is a relationship between t_{DA} and t_D

$$t_{DA} = c_{trad}\, t_D \quad \text{..... (2.19)}$$

The dimensionless productivity index is time dependent in the transient flow regime and constant in the pseudo-steady state.

In field units, the productivity index is expressed as

$$PI = \frac{z_e \sqrt{k_x k_y}}{141.2 B \mu} J_{D,trad} \quad \text{..... (2.20)}$$

Where k is in md, μ in cp, B in resBBL/STB, q in STB/D, pwf and pi in psi, t in hr, ct in 1/psi, φ is dimensionless and PI is in (STB/D/psi).

2.2 Production Forecasting

The pseudo-steady state solution for slightly compressible fluid can be solved as following, if the original diffusivity equation is derived in terms of real gas pseudopressure of Al-Hussainy and Ramey[29]

$$q_{sc} = \frac{\sqrt{k_x k_y}\,h}{1424T} \times J_D \times \left[m(\bar{p}) - m(p_{wf})\right] \quad \text{……..……..……..……..} \quad (2.21)$$

Where real gas pseudopressure function, m(p), is defined in **TABLE 2.1**.

To describe the part of the production during the transient period as well, we need a description of J_D covering the whole time span. First of all, we must state, that strictly speaking such a complete presentation is possible only for well defined flow history. Mathematically, the easiest is to handle the constant-rate type flow history. In such case, the late-time stabilized part is called pseudo-steady state. Other types of flow histories, e.g. the one implicitly defined by constant wellbore pressure, may lead to slightly different productivity indices at any moment of time and even their stabilized value might differ from the pseudo-steady state one according to Helmy and Wattenbarger's work[30].

Of course it is possible to calculate a productivity index curve for any specified rate history but that would be unpractical in general. In reality, we do not know ahead the production history that will happen in the fractured well in the future. Fortunately, the productivity index curve obtained with constant-rate condition is generally a good average indicator and any particular production history can be forecasted with reasonable accuracy with it. We can use the results of DVS method as mentioned before

to generate the combined J_D curve that describes both the transient and the stabilized (pseudo-steady state) production regime.

A rather straightforward approach to forecast the production from a fractured well is depicted in **TABLE 2.1**.

TABLE 2.1—Production forecast method (Field units)[4]

1. Prepare pseudopressure function $m(p) = 2\int_{p_0}^{p} \frac{p'}{(\mu Z)_{p'}} dp'$
2. Specify initial pressure p_i
3. Specify wellbore flowing pressure p_{wf}
4. Take a time interval Δt
5. Calculate production rate and production in the time interval $q_{sc} = \frac{\sqrt{k_x k_y}\, h}{1424\, T} \times J_{D,t_{DA}} \times \left[m(\bar{p}) - m(p_{wf})\right]$ and $\Delta G_p = q_{sc} \Delta t$
6. Apply material balance and calculate new average pressure $\bar{p} = \frac{p_i Z}{Z_i}\left(1 - \frac{G_p}{G_i}\right)$
7. Repeat steps 1-6.

The notation $J_{D,,tDA}$ in step 5 means that we should use the dimensionless productivity index corresponding to the dimensionless equivalent of the current time (elapsed from the start of the production.)

2.3 Calculation Logic

When forecasting the production of a fractured well by combining the productivity index and material balance, the calculation procedure involves iterative loops as described in Step 7 of **TABLE 2.1**. In one iterative loop, the most important step is Step 5 of **TABLE 2.1**. As can be seen in the equation, $J_{D,tDA}$ and the wellbore flowing pressure are the two important values to calculate production rate, q_{sc} in Mscf/day. One has to specify the wellbore flowing pressure, p_{wf} before calculation while the $J_{D,tDA}$ value for each iterative loop (time interval) is calculated using DVS method. After we calculate the production rate, we can calculate the cumulative production of the time interval. This is where the combination of dimensionless productivity index and material balance happens. We will show how to calculate the $J_{D,tDA}$ with the DVS method and how to execute the combination for production forecasting in the next sections.

The iterative calculation will stop until certain criterion is met, which is specified by the engineer. Such criteria[31] include:

- Time span of forecast in days
- Economic limit for gas production rate in Mscf/D

Obviously, the calculation will stop whichever criterion is met first. In one iterative loop, there are basically two big parts involved as shown below.

2.3.1 Dimensionless Productivity Index (J_D) Calculation

As indicated above, we need first to calculate the dimensionless productivity index corresponding to the dimensionless equivalent time, $J_{D,tDA}$ using the DVS method.

Actually, this is the most advantageous feature that we have in our method for post-fracture evaluation of complex well/fracture systems in a closed rectangular reservoir. Moreover, the calculation speed is fast and the result is accurate.

TABLE 2.2—Dimensionless productivity index calculation

$$J_D = \frac{1}{2\pi c_{trad}(p_{uD} - t_D)} \quad \text{(2.14)}$$

Where,

$$c_{trad} = \frac{z_e\sqrt{k_x k_x}}{Lk} \quad \text{(2.15)}$$

$$p_{uD} = \int_0^{t_D} p_{\delta D}(t_D^{'}).dt_D^{'} \quad \text{(2.16)}$$

The instantaneous solution $p_{\delta D}$ is from DVS method as shown below:

$$p_{\delta D}(box - pars; x_D, y_D, z_D, t_D) = f(x - pars; x_D, t_{Dx}) \times f(y - pars; y_D, t_{Dy}) \times f(z - pars; z_D, t_{Dz}) \quad \text{(2.1)}$$

$$t_D = \frac{k}{\phi\mu c_t L^2} t \quad \text{(2.17)}$$

$$k = (k_x k_y k_z)^{\frac{1}{3}}$$

(k and L are reference permeability and length). (2.18)

$$L = (x_e y_e z_e)^{\frac{1}{3}}$$

There is a relationship between t_{DA} and t_D:

$$t_{DA} = c_{trad}\ t_D \quad \text{(2.19)}$$

To calculate the $J_{D,tDA}$, one simply needs to take a time interval, Δt, as shown in Step 4 in **TABLE 2.1**. Then, add this time interval into the previous time period and get

the current time, t, which means the current time is elapsed from the start of production after the fracturing treatment (If it is the first iterative loop, the first time interval will be the current time). The dimensionless time, t_D, can be calculated using Equ. 2.17 in **TABLE 2.2**. In this calculation, c_t should be evaluated at the current average pressure in the reservoir.

The dimensionless pressure p_{uD} can be calculated based on the dimensionless time t_D and the corresponding instantaneous solution $p_{\delta D}$ from DVS method, as shown in Equ. 2.16. A conversion factor, c_{trad}, need to be calculated using Equ. 2.15, which is based on pay zone height, z_e and reference permeability, k and reference length, L in Equ. 2.18. After we calculated the dimensionless time, t_D, dimensionless pressure, p_{uD} and the conversion factor, c_{trad}, the dimensionless productivity index, J_D can be calculated using Equ. 2.14. All the equations needed for J_D calculation are shown in **TABLE 2.2**.

2.3.2 Combination of J_D and Material Balance

After we calculate the $J_{D,\,tDA}$ value for a specific time, t, from the beginning of the production, what we need to do is to cast the $J_{D,\,tDA}$ value into gas deliverability equations in Step 5 of **TABLE 2.1**.

As seen in Step 5 of **TABLE 2.1**, in addition to $J_{D,\,tDA}$ value, we still need to calculate the real gas pseudopressure, $m(\bar{p})$ at current average pressure, $\bar{p}$ for the specific time, t and $m(p_{wf})$ at wellbore flowing pressure, p_{wf}, which need to be specified at the very beginning (If it is the first time interval, the average pressure will be the

initial reservoir pressure). The pseudopressure can be calculated using the equation in Step 1 of **TABLE 2.1**.

To calculate the real gas pseudopressure, the gas properties calculation and correlation are needed and all of the details will be summarized in **APPENDIX A**.

After we get the $J_{D,\ tDA}$, $m(\bar{p})$ and $m(p_{wf})$ value, we can calculate the production rate for the specific time, t and t_{DA} accordingly. Continue with Step 5, we can calculate the cumulative production for the time interval. Go on to Step 6, the cumulative production for the time being can be obtained by adding all the production for the previous time intervals. The initial-gas-in-place can be calculated using the volumetric method, which is as following:

$$G_i = \frac{Ah\varphi(1-S_w)}{B_{gi}} \quad \text{……...……...……..} \quad (2.22)$$

Then, we can calculate the current average pressure for next iterative calculation.

Till now, we finish one iterative loop and we will obtain a set of data: dimensionless productivity index, $J_{D,tDA}$, production rate, q_{sc} cumulative production, ΔG_p and average reservoir pressure, $\bar{p}$ for the time being, t or t_{DA}.

As stated in Step 7, by just repeating Step 1-6 in **TABLE 2.1**, the iterative loop can be continued until certain criterion is met. Eventually, a series of data sets including dimensionless productivity index, production rates, accumulative productions and average reservoir pressure, can be obtained.

For engineering purpose, we need to graphically show the computation results for a production forecasting run. For each case, there will be four important plots

available to aid the decision-making about the completion schemes for developing the reservoir. Basically, the four plots[30] are:

- Rate versus time
- Cumulative production versus time
- Rate versus cumulative production
- Average reservoir pressure versus time.

For demonstration purpose, a synthetic example is given in **APPENDIX B**.

2.4 Concluding Remarks

In this chapter, we presented the development and implementation of the DVS method that can be used as pressure transient analysis and well productivity prediction. As a further application, we combine the productivity index calculated from DVS method with material balance for production forecasting. The calculation logic is detailed and a synthetic example is given in **APPENDIX B**.

Based on the production forecast results, one can simply screen the completion scheme after running series of scenarios. For more sophisticated applications, one can perform a revenue estimate for various well/fracture systems, based on the production rate and cumulative production. If the treatment costs can be estimated by using a hydraulic fracturing simulator, then, the net revenue curve will be constructed. All of them make up an economic analysis for the completion scheme.

In the next chapter, we will study the multiple box cases as mentioned before. In **Chapter III**, we will focus on vertical well intersected by a vertical fracture of finite

conductivity. We will further investigate the effects of the varying fracture conductivity and varying fracture height on well productivity. In **Chapter IV**, we will apply the full model to field problems.

CHAPTER III

APPLICATION OF DVS METHOD IN GAS PRODUCTION FORECASTING

3.1 Introduction

Fractured well performance modeling is the main stream of this thesis while investigation of the effect of varying geometry and conductivity of the source on well productivity will be the focus of this chapter.

The DVS method is proved to be a robust way to calculate the productivity of complex well/fracture systems. For a typical case, say a vertical well intersected by a vertical fracture of finite conductivity, we can perform a sensitivity study of the fracture parameters on the well productivity and hence, their effects on well production. As stated in Chapter II, the DVS method will provide a J_D curve (J_D versus t_{DA}) with a smooth transition between the transient flow regime and pseudosteady state regime. The J_D is time dependent in the transient flow regime and constant in the pseudo-steady state flow regime. For low or ultra-low permeability gas reservoirs, the transient flow period will last extremely long before it reaches pseudosteady state flow period. Thus, it is imperative to investigate the varying fracture parameter effects on J_D of these two flow periods. For a typical production mode, say time span or economic limit on the production rate, we can evaluate the overall effects of varying fracture conductivity and fracture height on the production rate and cumulative production, which are important factors to maximize the wellhead revenue.

In DVS method, dimensionless productivity index (J_D) is calculated from

$$J_D = \frac{1}{2\pi\, c_{trad}\left(p_{uD} - t_D\right)} \quad \text{..... (3.1)}$$

Where,

$$c_{trad} = \frac{z_e \sqrt{k_x k_x}}{L\,k} \quad \text{..... (3.2)}$$

$$p_{uD} = \int_0^{t_D} p_{\delta D}(t_D^{'}).dt_D^{'} \quad \text{..... (3.3)}$$

$$t_D = \frac{k}{\phi \mu c_t L^2} t \quad \text{..... (3.4)}$$

$$k = (k_x k_y k_z)^{\frac{1}{3}}$$
$$L = (x_e y_e z_e)^{\frac{1}{3}} \quad \text{(k and L are reference permeability and length) ..... (3.5)}$$

t_{DA} is the dimensionless time defined based on drainage area

$$t_{DA} = \frac{kt}{\phi \mu c_t A} \quad \text{..... (3.5)}$$

There is a relationship between t_{DA} and t_D

$$t_{DA} = c_{trad}\, t_D \quad \text{..... (3.6)}$$

In 2002, Valkó and Economides[5] introduced the dimensionless proppant number in *Unified Fracture Design* (UFD), which is turned out to be an extremely useful optimization parameter in fracture design. Based on penetration ratio in the fracture-length direction

$$I_x = \frac{2w_x}{x_e} \quad \text{..... (3.7)}$$

and on the dimensionless fracture conductivity

$$C_{fD} = \frac{k_f w_y}{k w_x} \quad \text{……..……..……} \quad (3.8)$$

the dimensionless proppant number is defined as

$$N_{prop} = I_x^2 C_{fD} = \frac{4k_f w_x 2w_y 2w_z}{k x_e^2 z_e} = \frac{2k_f}{k}\frac{V_{prop}}{V_{res}} \quad \text{……...……...…….} \quad (3.9)$$

Where w_x is the fracture half length, w_y is the fracture half width, w_z is the fracture half height, x_e is the side length of the square drainage area, z_e is the thickness of the formation, k_f is the proppant pack permeability, k is the formation permeability. For the meaning of the different variables, see **Fig. 3.1** and **Fig. 3.2**.

3.2 Effect of Varying Fracture Parameters on PI

In order to investigate the effect of varying fracture parameters on the productivity index, we will compare two cases.

(1) Base Case

For a vertical well with rectangular fracture, the fracture width and fracture height are constant along the fracture length obviously. We also consider a uniform proppant pack permeability distribution inside the rectangular fracture.

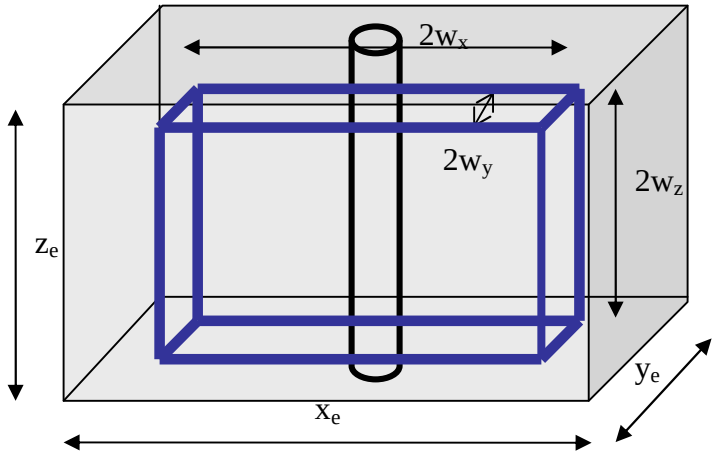

Fig. 3.1—Base case: vertical well with rectangular fracture

(2) Varying Case

For a vertical well with elliptical fracture, the fracture width and fracture height have an elliptical distribution along the fracture length, thus varying fracture width and fracture height along the fracture length. We also use a linear distribution of proppant pack permeability inside the elliptical fracture.

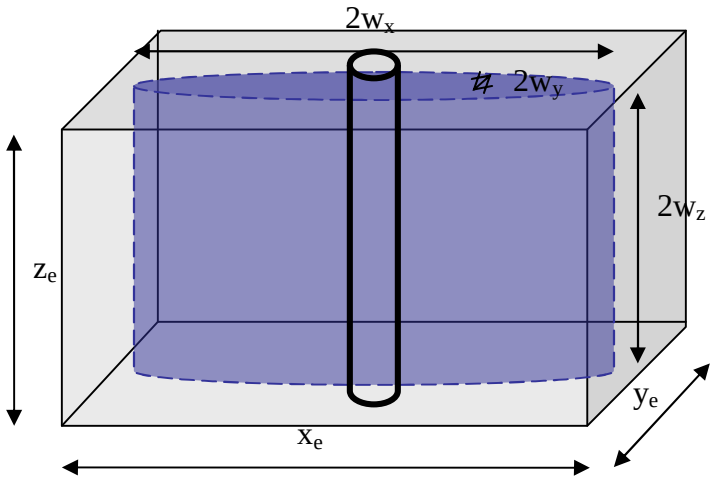

Fig. 3.2—Varying case: vertical well with elliptical fracture

We will refer the first case to be the base case while we will refer the second case to be the varying case.

3.2.1 Investigation Methodology

For the same amount of propped volume inside the fracture, which means the same proppant number, we will transfer the base case to the corresponding varying case. By doing this, we will get a more accurate and representative result to reflect the real case during the hydraulic fracturing treatment.

Investigation study of varying parameter effects on PI is carried out using the procedure as following:

1. **Discretization treatment:** Divide the fracture into proper number of segments, e.g. n = 8, along the fracture length. With discretization treatment, all the effects are included in our computation.
2. **Segment strength assignment:** Assign a value to each segment as its contribution to the whole fracture. We define this value as the strength of the segment. For fracture width and height, the strength of each segment will be obtained from the equivalent-propped-volume transformed ellipsoid by interpolation. While for the proppant pack permeability, we will have two categories: **Case A**: linearly increasing permeability distribution, and **Case B**: linearly decreasing permeability distribution, both of which are distributed from the well-bore to the fracture tips along the fracture length. The permeability distribution inside the fracture is determined by comparing the average proppant pack permeability, k_f with the one near the well-bore, k_{fwb}. If $k_f > kf_{wb}$, a linearly

increasing permeability distribution inside the fracture will be created by linear interpolation between the k_f and k_{fwb}, which is referred to Case A; $k_f<k_{fwb}$, a linearly decreasing permeability distribution will be referred to Case B, which is treated the same way as Case A; otherwise, if $k_f=k_{fwb}$, it will turn out to be a uniformly permeability distribution inside the fracture, which is defined as the base case. At this stage, we should have a distribution of n values for the whole fracture segments.

3. **Calculation:** Calculate the dimensionless productivity index (J_D) for the well/fracture configuration using the DVS method.

Valkó and Economides[5] points out in their book, *Unified Fracture Design (2002),* that for any permeability reservoir, the proppant number would not exceed 1, thus the optimum dimensionless conductivity would be 1.6. Thus, for our study, we propose four scenarios with different proppant numbers: **1.0**, **0.4**, **0.1** and **0.01**. The corresponding dimensionless conductivity will all be set 1.6 while the penetration ratios in the fracture length direction are different from each other, as shown in **TABLE 3.1**.

As the first step of the parametric study, we will validate the new routine (vwvfr) for the varying case with the one (vwcfr) for the base case. The validation plots and data sets are presented and commented. Along the way, new control and calculation functions in the new subroutine (vwvfr) are defined and explained with the corresponding outcomes if certain actions occur. Then, it will lead to three sections to investigate the individual effects of varying proppant pack permeability, varying fracture width and

varying fracture height on PI, separately. Calculated results and explanations are presented in each section.

TABLE 3.1—Data set for the validation

Reservoir data				
x_e, reservoir length, ft	1000			
y_e, reservoir width, ft	1000			
z_e, formation thickness, ft	200			
k_x, permeability along the reservoir length direction, md	1			
k_y, permeability along the reservoir width direction, md	1			
k_z, permeability along the reservoir height direction, md	1			
Fracture data	**1**	**2**	**3**	**4**
c_x, x-coordinate of the center point of fracture	500	500	500	500
c_y, y-coordinate of the center point of fracture	500	500	500	500
c_z, z-coordinate of the center point of fracture	100	100	100	100
w_x, fracture half-length, ft	400	250	125	50
w_y, fracture half-width, ft	0.032	0.02	0.01	0.004
w_z, fracture half-height, ft	80	80	80	80
k_f, average fracture permeability, md	10000	10000	10000	10000
k_{fwb}, fracture permeability near wellbore, md	10000	10000	10000	10000
Penetration Ratio and Dimensionless Fracture Conductivity	**1**	**2**	**3**	**4**
I_x (2wx/xe), penetration ratio in the x-direction	0.8	0.5	0.25	0.1
C_{fD}, dimensionless fracture conductivity	1.6	1.6	1.6	1.6
Dimensionless Proppant Number	**1**	**2**	**3**	**4**
N_{prop}, dimensionless proppant number	1.0	0.4	0.1	0.01

3.2.2 Validation of the Subroutine: GASSIM

The computational power of DVS method is to calculate the instantaneous pressure solution to unsteady state flow problem with both excellent speed and accuracy, which is presented as following:

$$p_{\delta D}(box-pars;x_D,y_D,z_D,t_D) = f(x-pars;x_D,t_{Dx})\times f(y-pars;y_D,t_{Dy})\times f(z-pars;z_D,t_{Dz}) \quad \text{(3.10)}$$

The box-pars notation stands for all the information contained in the problem specification: (x_e, y_e, z_e, k_x, k_y, k_z, c_x, c_y, c_z, w_x, w_y, w_z).

To obtain the response of the reservoir to a continuous unit source distributed uniformly in the small box, we numerically integrate the solution (Eq. 3.10) over time:

$$p_{uD}(x_D,y_D,z_D,t_D)=\int_0^{t_D} p_{\delta D}(x_D,y_D,z_D,\tau)d\tau \quad \text{(3.11)}$$

To obtain wellbore flowing pressure, we can calculate $p_{uD}(x_D,y_D,z_D,t_D)$ at the geometric center of the well. Since the solution is not singular, we do not have to select a surface point arbitrarily.

To develop the DVS method for engineering applications, we will code all the underlying concepts and equations based on *Wolfram Research Mathematica Programming Language*[32]. In the next two sections, we briefly describe the code and present the computational results.

- **Code description**

1. <u>Base Case:</u> Vertical Well with Constant Fracture Routine (vwcfr)

As the instantaneous pressure solution from DVS method (Equ. 3.10) shown, the input for the subroutine are the box-pars in addition to the number of segment, *n* and proppant pack permeability, *kf* and the time, *tDTab*. The interested results of the computation are the dimensionless productivity indices, *JDTab* and the corresponding dimensionless time, *tDTab*. The data sets are expressed as following:

INPUT DATA SET: [n, {xe, ye, ze, kx, ky, kz, cx, cy, cz, wx, wy, wz, kf}, tDTab]

OUTPPUT DATA SET: [tDTab1, JDTab1]

2. <u>Varying Case:</u> Vertical Well With Varying Fracture Routine (vwvfr)

To investigate the effects of varying fracture on PI, we will follow the procedure presented in Section 3.2.1. We need three parameters, *kfwb, switch1, switch2,* to control the discretization requirement as well as the direction to different interpolation functions. The data sets are expressed as following:

INPUT DATA SET:

[n, {xe, ye, ze, kx, ky, kz, cx, cy, cz, wx, wy, wz, kf}, tDTab, kfwb, switch1, switch2]

OUTPPUT DATA SET: [tDTab2, JDTab2]

Segment strength values will be obtained from the interpolation functions, which are defined as following. With the same fracture length as the base case, we create the interpolation functions using the equivalent-proppant-volume.

For fracture width, we use the equivalent-area of the fracture width intersection of the created fracture.

$$y1[x] = \frac{4w_y}{\pi}\sqrt{1-\frac{(x-c_x)^2}{w^2{}_x}} + c_y \quad \text{……..……..……. (3.12)}$$

$$y2[x] = -\frac{4w_y}{\pi}\sqrt{1-\frac{(x-c_x)^2}{w^2{}_x}} + c_y \quad \text{……...……...…… (3.13)}$$

For fracture height, we use the equivalent-area of the fracture height intersection of the created fracture. To keep the fracture height containment inside the formation, we need to define a critical value first. Then, based on this value, there will be two possibilities for the fracture height distribution. If the average fracture height is larger the critical height, we will transform the intersection area using the function 1&2; if the average fracture height is smaller than the critical height, we use function 3&4; otherwise, the fracture will be constant height as the base case.

The critical height is defined as:

$$w_{zcrtical} = \frac{\pi z_e}{8} \text{ ……..……...…….. (3.14)}$$

If $w_z < w_{zcritical}$, the interpolation function is defined as:

$$z1[x] = \frac{4w_z}{\pi}\sqrt{1-\frac{(x-c_x)^2}{w^2{}_x}} + c_z \quad \text{……...……..…….. (3.15)}$$

$$z2[x] = -\frac{4w_z}{\pi}\sqrt{1-\frac{(x-c_x)^2}{w^2{}_x}} + c_z \quad \text{……...…… (3.16)}$$

If $w_z > w_{zcritical}$, the interpolation function is defined as:

$$z3[x] = \frac{2(z_e-2w_z)}{4-\pi}\sqrt{1-\frac{(x-c_x)^2}{w^2{}_x}} + c_z - \frac{\pi(z_e/2)-4w_z}{4-\pi} \quad \text{……...……..…. (3.17)}$$

$$z4[x] = -\frac{2(z_e - 2w_z)}{4-\pi}\sqrt{1-\frac{(x-c_x)^2}{w^2{}_x}} + c_z + \frac{\pi(z_e/2) - 4w_z}{4-\pi} \quad \text{…….....…. (3.18)}$$

For proppant pack permeability, we also define the distribution functions. First, we need an estimate of permeability in the well-bore area noted as kfwb. Then, we compare the average proppant pack permeability noted as kf with kfwb. If kf>kfwb, linearly increasing permeability distribution; if kf<kfwb, linearly decreasing permeability distribution; otherwise, the permeability inside the fracture will be uniform as the base case.

If $k_f < k_{fwb}$, the permeability distribution function is defined as:

$$kfL1[x] = \frac{k_{fwb} - k_f}{w_x/2}\left(x - \frac{c_x - w_x}{2}\right) + k_f \quad \text{……...…… (3.19)}$$

$$kfR1[x] = \frac{k_{fwb} - k_f}{-w_x/2}\left(x - \frac{c_x + w_x}{2}\right) + k_f \quad \text{……...…… (3.20)}$$

TABLE 3.2—Function description for the two subroutines coded in *Mathematica*[31]

Subroutine	Function Description	Actions for validation computation
vwcfr	Compute J_D only with constant fracture height, width and permeability	
vwvfr	Compute J_D with choices of constant or varying fracture parameters: If switch1=1, use varying fracture width; otherwise, use constant ones. If switch2=1, use varying fracture height; otherwise, use constant ones. If $k_{fwb} = k_f$, use constant fracture permeability; otherwise, use varying ones.	By setting switch1= 0, switch2= 0 and $k_{fwb} = k_f$, if vwvfr works, we could expect the same result with the one computed via vwcfr .

If $k_f > k_{fwb}$, the permeability distribution function is defined as:

$$kfL2[x] = \frac{k_f - k_{fwb}}{-w_x/2}\left(x - \frac{c_x - w_x}{2}\right) + k_f \quad \text{……..…… (3.21)}$$

$$kfR2[x] = \frac{k_f - k_{fwb}}{w_x/2}\left(x - \frac{c_x + w_x}{2}\right) + k_f \quad \text{……...…... (3.22)}$$

The comparison of the two subroutines is summarized in **TABLE 3.2**.

With knowledge of the code, we proceed to the computed results as the validation part.

- **Computational Results for Validation**

Use the related data in **TABLE 3.1** for the input of the two routines, vwcfr and vwvfr, we can compute the JD curve for each proppant number case. By overlying the results, we get the following plots as shown in **Fig. 3.3** for N_{prop}=1.0, **Fig. 3.4** for N_{prop}=0.4, **Fig. 3.5** for N_{prop}=0.1, **Fig. 3.6** for N_{prop}=0.01.

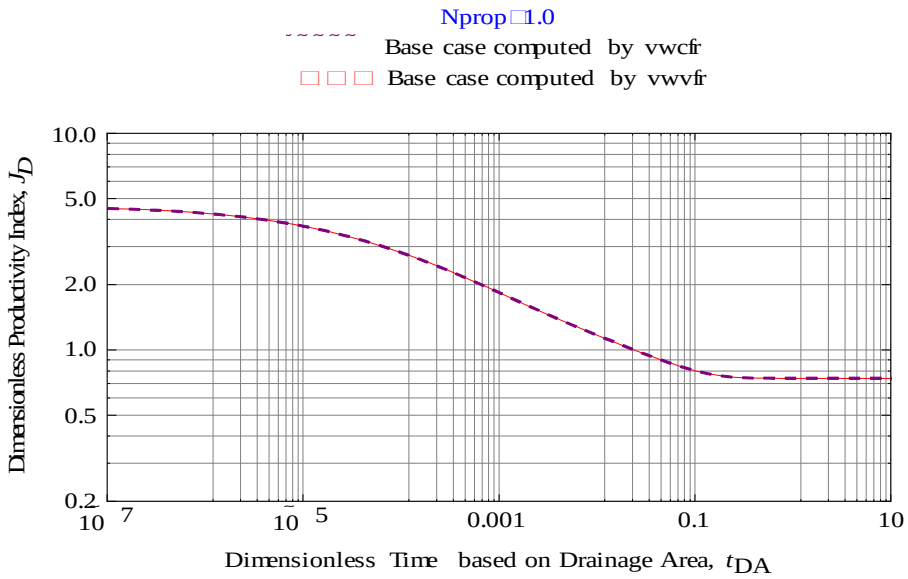

Fig. 3.3—Comparison of results using vwcfr and vwvfr by overlaying (N_{prop}=1.0): dimensionless productivity index for a vertically fractured well as a function of dimensionless time based on drainage area

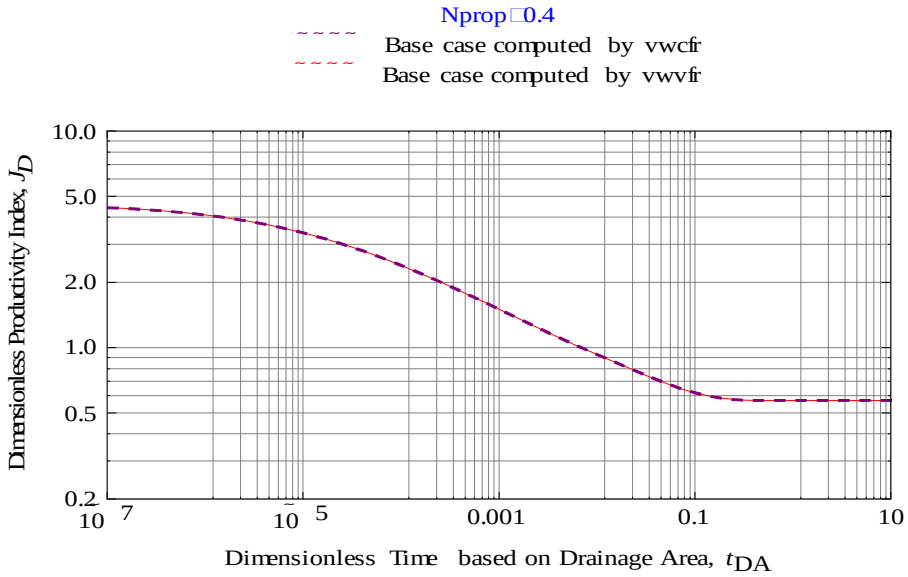

Fig. 3.4—Comparison of results using vwcfr and vwvfr by overlaying (N_{prop}=0.4): dimensionless productivity index for a vertically fractured well as a function of dimensionless time based on drainage area

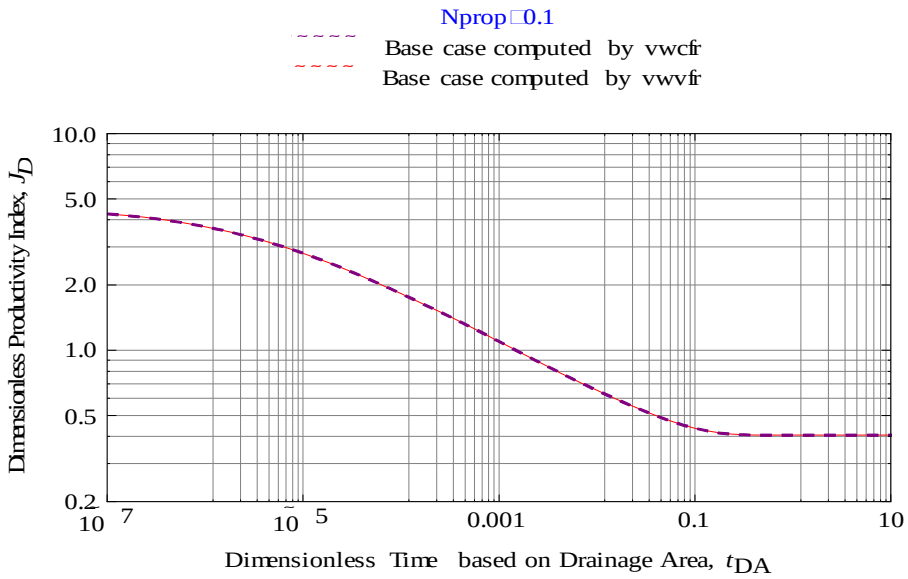

Fig. 3.5—Comparison of results using vwcfr and vwvfr by overlaying (N_{prop}=0.1): dimensionless productivity index for a vertically fractured well as a function of dimensionless time based on drainage area

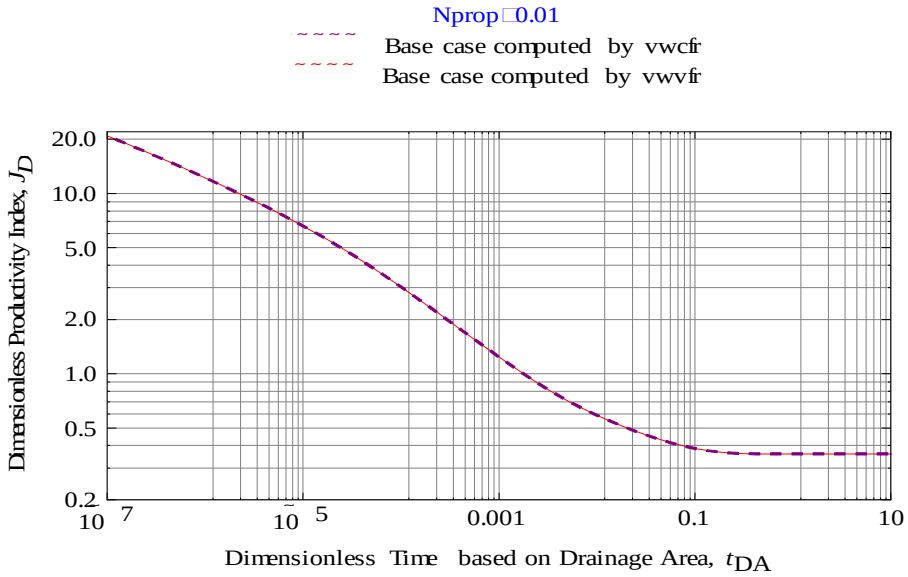

Fig. 3.6—Comparison of results using vwcfr and vwvfr by overlaying (N_{prop}=0.01): dimensionless productivity index for a vertically fractured well as a function of dimensionless time based on drainage area

From the overlying plots and J_D values table, we could see a very good match which indicates that the routine for computing vertical fracture with varying parameters works properly as we expected.

The calculated J_D values are tabulated in **TABLE 3.3**. Again, it approves the validation of the routine vwvfr.

TABLE 3.3—Comparison of computing results from routines vwcfr and vwvfr

Nprop=0.4	Dimensionless Time based on Drainage Area, t_{DA}		Dimensionless Productivity Index, J_D	
	vwcfr	vwvfr	vwcfr	vwvfr
Transient Flow Region	1.00E-12	1.00E-12	4.609596	4.609596
	1.00E-11	1.00E-11	4.609451	4.609451
	1.00E-10	1.00E-10	4.608005	4.608005
	1.00E-09	1.00E-09	4.597546	4.597546
	1.00E-08	1.00E-08	4.557084	4.557084
	1.00E-07	1.00E-07	4.432635	4.432635
	1.00E-06	1.00E-06	4.096533	4.096533
	0.00001	0.00001	3.388734	3.388734
	0.0001	0.0001	2.398067	2.398067
	0.001	0.001	1.50471	1.50471
	0.01	0.01	0.93028	0.93028
Pseudo-Steady State Flow Region	0.1	0.1	0.618649	0.618649
	1	1	0.570161	0.570161
	10	10	0.57016	0.57016
	100	100	0.570151	0.570151

For evaluation, we will use the case, N_{prop}=0.4 for parametric study.

3.2.3 Effect of Varying Proppant Pack Permeability on PI While Holding Fracture Width and Height Constant

Holding the fracture width and height constant as shown in **Fig. 3.7** and **Fig. 3.8**, we create a linear distribution of permeability along the fracture length. More

specifically, from the well bore to the fracture tips, the fracture permeability distribution is linearly increasing if the permeability near the well-bore is smaller than average fracture permeability as shown in **Fig. 3.9**, or the fracture permeability distribution is linearly decreasing if the permeability near the well-bore is larger than average fracture permeability as shown in **Fig. 3.10**. The comparison of the two subroutines is summarized in **TABLE 3.4**.

TABLE 3.4—Descriptions for varying fracture permeability cases

Case	Case description	Fracture permeability, md
Base case: $k_f = k_{fwb}$	Uniform permeability distribution along the fracture length	k_f = 10,000 for all x x: distance from well-bore along the fracture length, ft
Case A: $k_f > k_{fwb}$	Linearly increasing permeability distribution from well-bore to fracture tips along the fracture length	$k_f = m\ x + k_{fwb}$ k_{fwb} = 6,000 when x = 0 x: distance from well-bore along the fracture length, ft
Case B $k_f < k_{fwb}$	Linearly decreasing permeability distribution from well-bore to fracture tips along the fracture length	$k_f = m\ x + k_{fwb}$ k_{fwb} = 14,000 when x = 0 x: distance from well-bore along the fracture length, ft

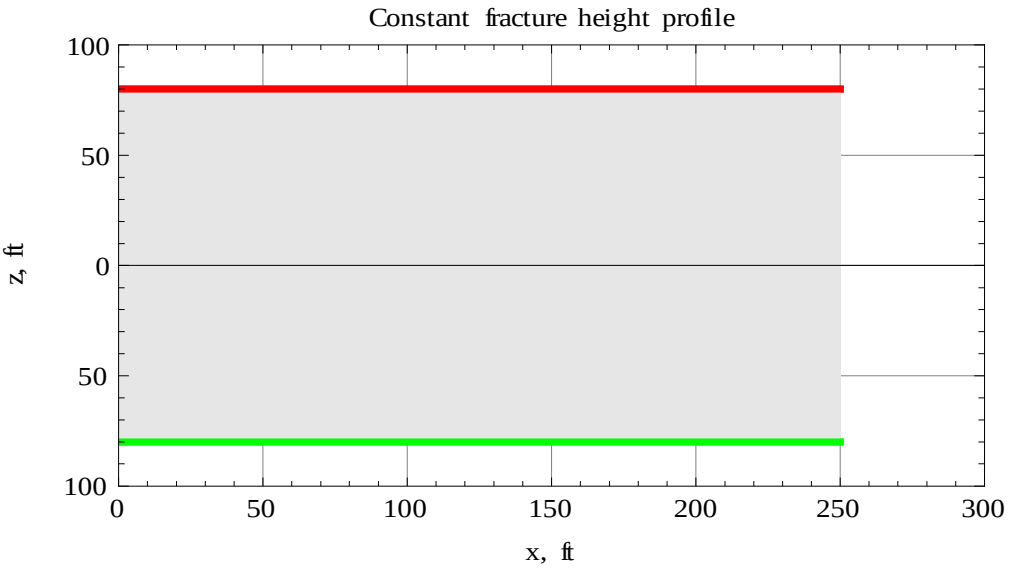

Fig. 3.7—Constant fracture height profile (half wing) used when evaluate the effect of varying fracture permeability on J_D

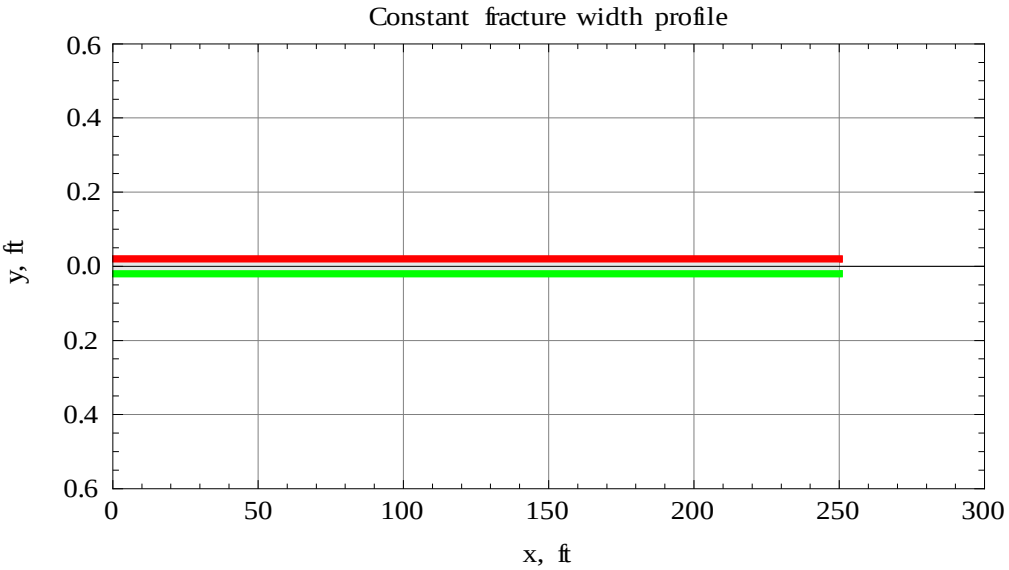

Fig. 3.8—Constant fracture width profile (half wing) used when evaluate the effect of varying fracture permeability on J_D

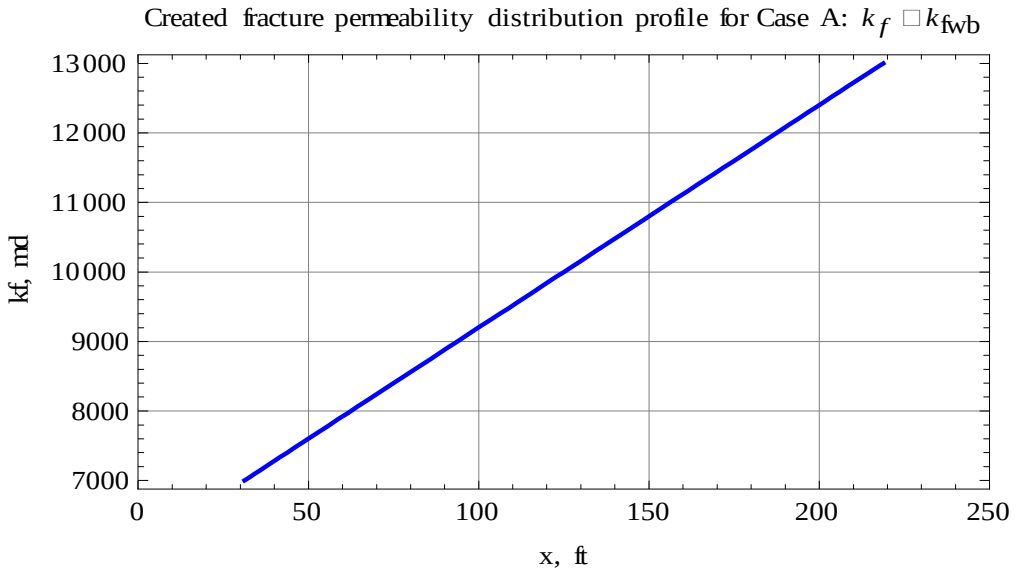

Fig. 3.9—Case A: created fracture permeability distribution profile: linearly increasing permeability distribution along the fracture length (half wing)

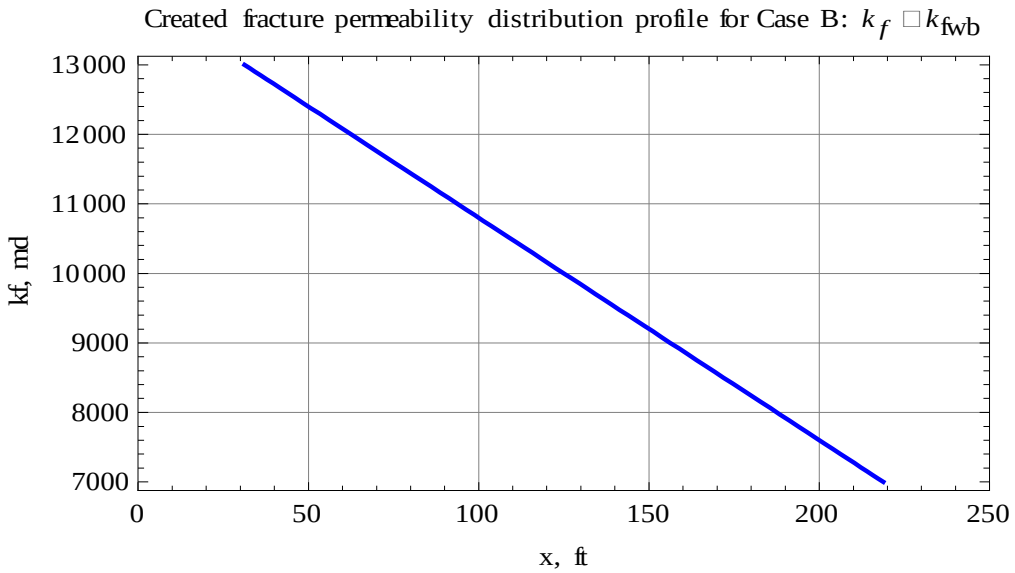

Fig. 3.10—Case B: created fracture permeability distribution profile: linearly decreasing permeability distribution along the fracture length (half wing)

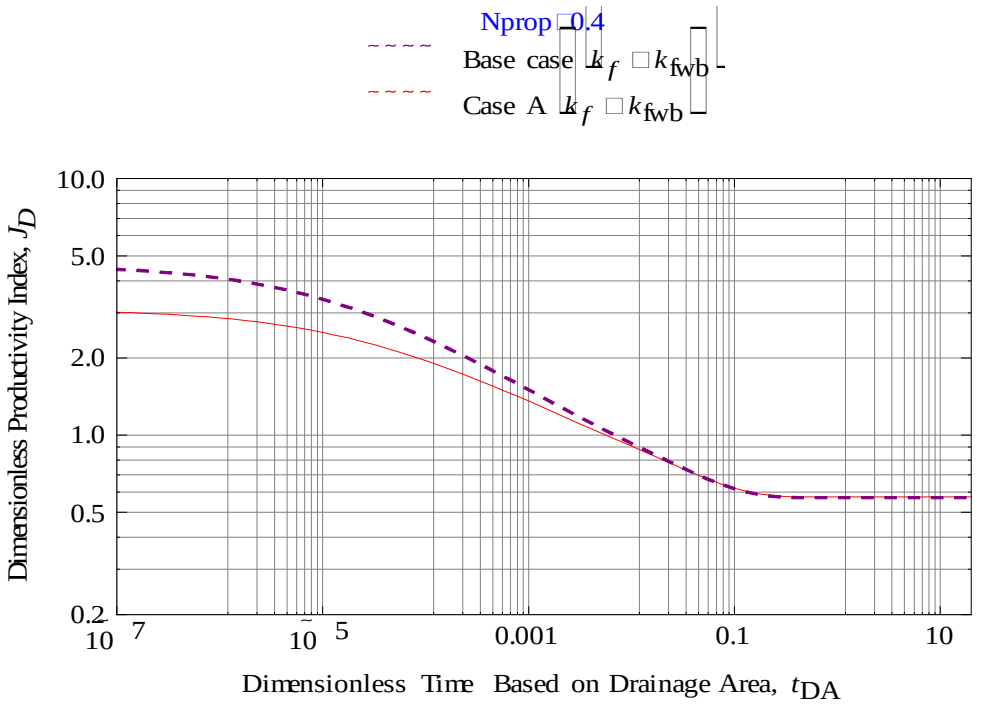

Fig. 3.11—Case A overlaid by base case for comparison: dimensionless productivity index as a function of dimensionless time based on drainage area

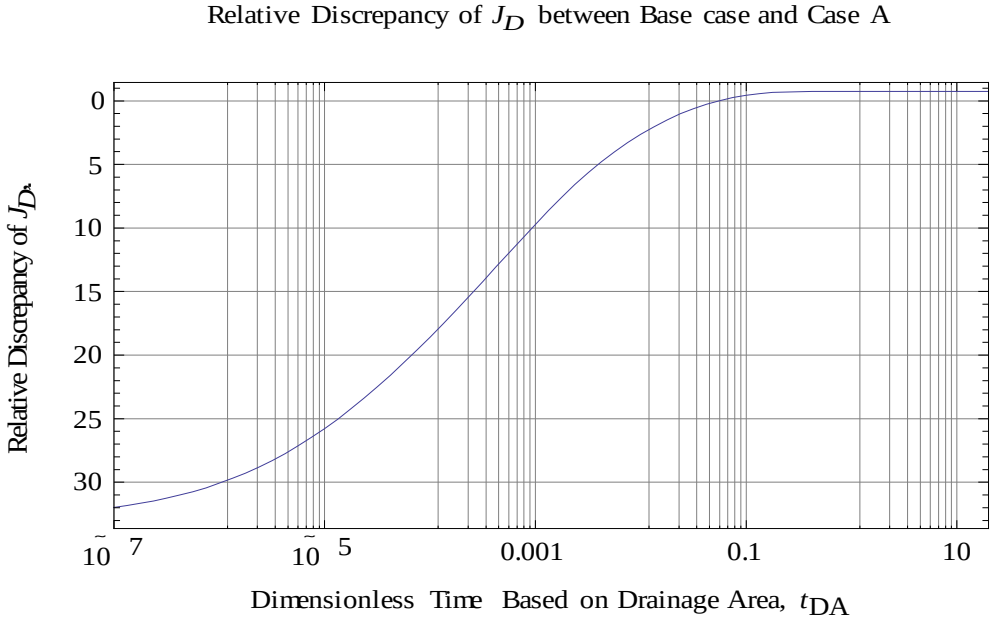

Fig. 3.12—Case A: effect of varying fracture permeability on J_D during early-time transient flow and late-time pseudo-steady state flow

As seen from the comparison plots for Case A, there are big differences of the calculated J_D values for the transient flow region. At the very beginning during the transient flow, the J_D is about 30% less than the base case. This is reasonable because the fracture permeability near the well-bore is smaller than the other area inside the fracture as shown in **Fig. 3.9**. It also means that we will get a decreased early production from the fractured well with Case A. Then, gradually as flow is going on, the difference will be smaller, even zero. In the pseudo-steady state flow region, there is a constant difference of 1.77% larger than the base case, as seen from the **Fig. 3.11**.

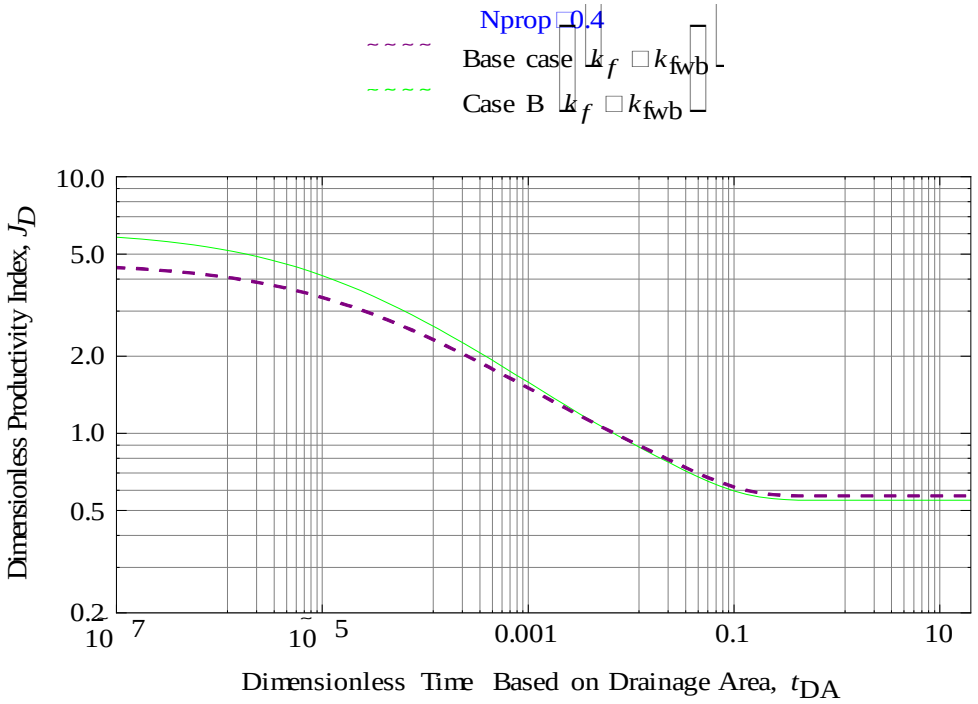

Fig. 3.13—Case B overlaid by base case for comparison: dimensionless productivity index as a function of dimensionless time based on drainage area

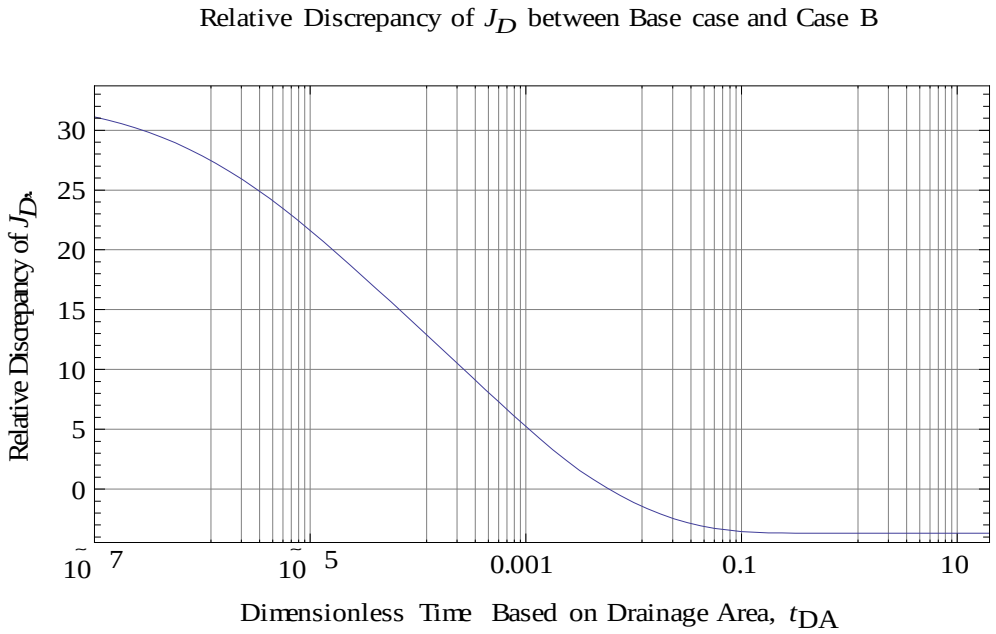

Fig. 3.14—Case B: effect of varying fracture permeability on J_D during early-time transient flow and late-time pseudo-steady state flow

In contrast to Case A, we create a fracture with the near well-bore permeability larger than the other area inside the fracture. The permeability distribution along the fracture length is shown in **Fig. 3.10**. In this case, as shown in **Fig. 3.13**, there is a difference of J_D, which is about 30% larger than the base case at the very beginning of transient flow. But, in the pseudo-steady state flow, the stabilized J_D is 4.20% smaller than the base case. As expected, we will get an increased early production while eventually, after the flow rate stabilize, less is produced. We can compare flow gain and loss in the early transient flow and late stabilized flow. Then, we can know its exact effect on the cumulative production of the well. Case B is the usual situation seen in the real fracture job. The calculated J_D values and relative discrepancy are shown in **TABLE 3.5**.

TABLE 3.5—Comparison of computing results for varying fracture permeability cases

	Dimensionless Time based on Drainage Area, t_{DA}	Dimensionless Productivity Index, J_D			Relative Discrepancy of J_D, %	
		Base case	Case A	Case B	Case A	Case B
Transient Flow Region	1.00E-12	9.219193	3.091145	6.128044	32.94	32.94
	1.00E-11	9.218902	3.091084	6.127781	32.94	32.94
	1.00E-10	9.215998	3.090473	6.125159	32.93	32.92
	1.00E-09	9.188489	3.086051	6.10622	32.88	32.81
	1.00E-08	9.041371	3.068865	6.033284	32.66	32.39
	1.00E-07	8.577661	3.015212	5.812156	31.98	31.12
	1.00E-06	7.467203	2.864184	5.237684	30.08	27.86
	0.00001	5.618524	2.515391	4.121612	25.77	21.63
	0.0001	3.649838	1.952447	2.72331	18.58	13.56
	0.001	2.170482	1.358577	1.583412	-9.71	5.23
	0.01	1.256682	0.905782	0.919861	-2.63	-1.12
Pseudo-Steady-State Flow Region	0.1	0.778741	0.621371	0.596726	0.44	-3.54
	1	0.707806	0.574412	0.549097	0.75	-3.69
	10	0.707806	0.574412	0.549096	0.75	-3.69
	100	0.707792	0.574402	0.549087	0.75	-3.69

3.2.4 Effect of Varying Fracture Width on PI While Holding Fracture Height and Proppant Pack Permeability Constant

The constant fracture width profile is shown in **Fig. 3.15**. As for the varying fracture width case, we suppose the cross-section of the fracture along fracture height direction (z-axis) be an ellipse which is shown in **Fig. 3.16**. The fracture is partitioned into eight segments along the fracture length direction, with each segment having a different width. Based on this treatment of the fracture width, we calculate the

productivity index in order to further investigate the effect of varying fracture width on gas well production. Detailed information about the two cases is shown in **TABLE 3.6**.

TABLE 3.6—Descriptions for varying fracture width cases

Case	Case description	Fracture half-width, ft
Base case	Constant fracture width	$w_y = 0.04$
Varying case	Varying fracture width with a distribution along ellipses	Different values are generated for each fracture segment {0.0246, 0.0398, 0.0472, 0.0505, 0.0505, 0.0472, 0.0398, 0.0246}

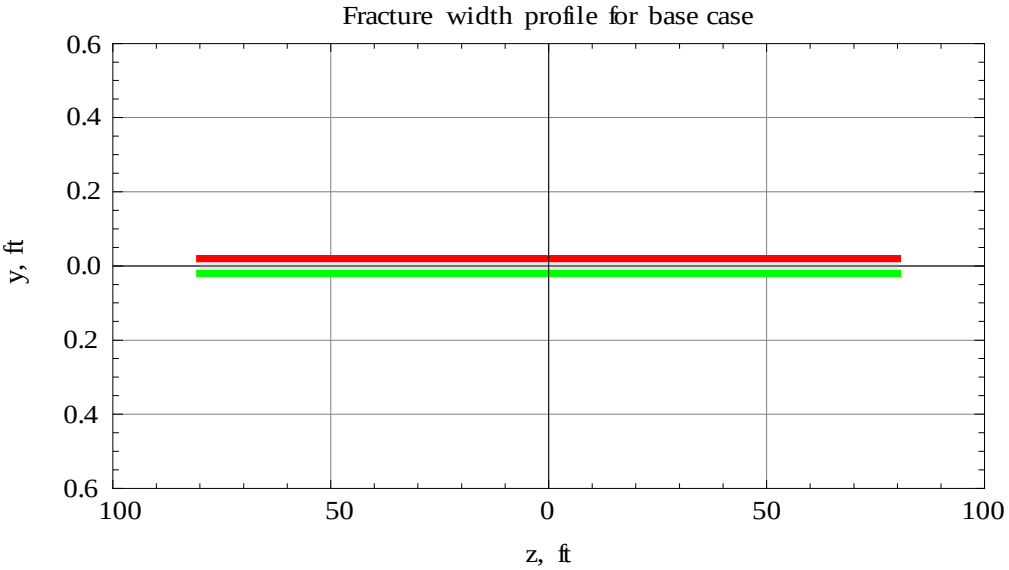

Fig. 3.15—Created fracture width profile for base case

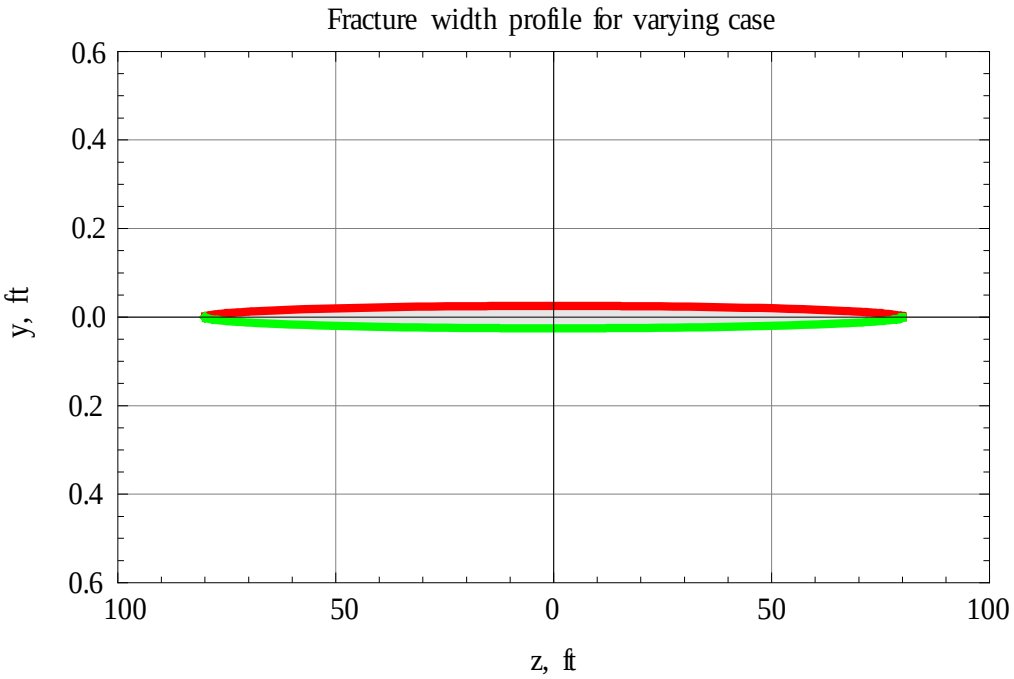

Fig. 3.16—Created fracture width profile for varying case

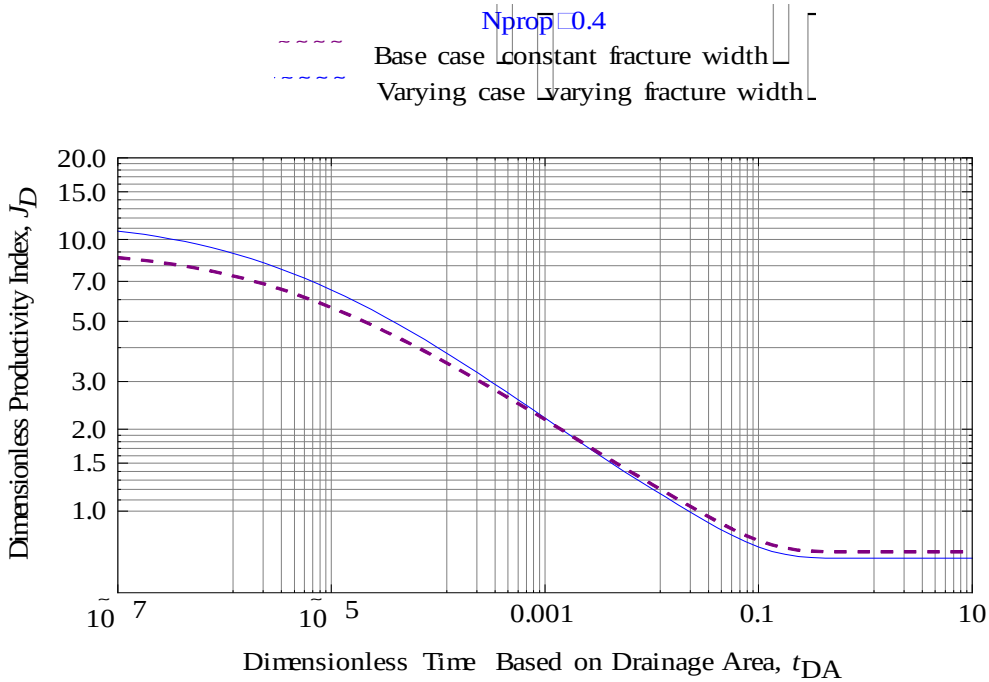

Fig. 3.17—Varying case overlaid by base case: dimensionless productivity index for a vertically fractured well as a function of dimensionless time based on drainage area

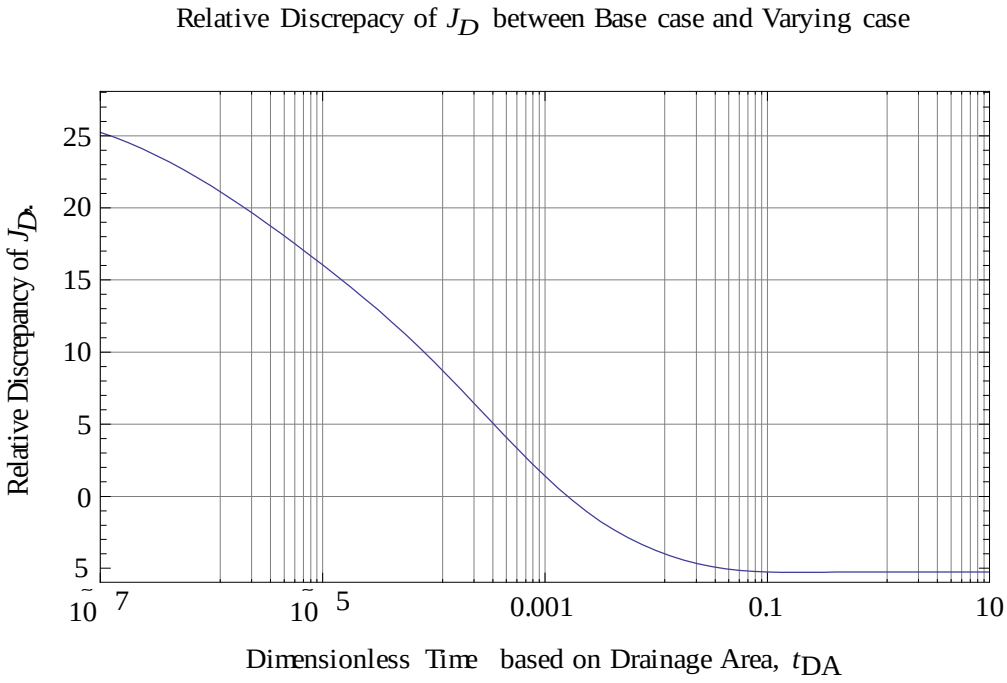

Fig. 3.18—Effect of varying fracture width on J_D during early-time transient flow and late-time pseudo-steady state flow

The effect of varying fracture width on PI is much similar to that of Case B of varying fracture permeability in section 3.2.2. The general trend is by large the same in both the J_D curve and relative difference curve compared to base case. However, the values of J_D and relative difference are not the same at the according flow time as shown in **TABLE 3.6** and **TABLE 3.7**. This means that the varying fracture width and varying fracture permeability of Case B will have the same effect on PI but the magnitude of the effect is different. Generally, the increase of J_D in varying fracture width is less than that of Case B in varying fracture permeability case during the transient flow period, but the decrease of J_D is a little more in the pseudo-steady state flow period. All these will effect the well production.

TABLE 3.7—Comparison of computation results for varying fracture width cases

	Dimensionless Time Based on Drainage Area, t_{DA}	Dimensionless Productivity Index, J_D		Relative discrepancy of J_D, %
		Base case	Varying case	
Transient Flow Region	1.00E-12	9.219193	11.74386	27.38
	1.00E-11	9.218902	11.74348	27.38
	1.00E-10	9.215998	11.73971	27.38
	1.00E-09	9.188489	11.70282	27.36
	1.00E-08	9.041371	11.47657	26.93
	1.00E-07	8.577661	10.74311	25.25
	1.00E-06	7.467203	9.072719	21.50
	0.00001	5.618524	6.52011	16.05
	0.0001	3.649838	3.990487	9.33
	0.001	2.170482	2.200883	1.40
	0.01	1.256682	1.209441	-3.76
Pseudo-Steady-State Flow Region	0.1	0.778741	0.737845	-5.25
	1	0.707806	0.670577	-5.26
	10	0.707806	0.670577	-5.26
	100	0.707792	0.670564	-5.26

3.2.5 Effect of Varying Fracture Height on PI While Holding Fracture Width and Proppant Pack Permeabiltiy Constant

Similar to the way we treat varying fracture width in section 3.2.3, we assume the cross-section of the fracture along the fracture width direction (y-axis) be an ellipse as shown in **Fig. 3.16**. Constant height profile is shown in **Fig. 3.15**. The comparison of the two subroutines is summarized in **TABLE 3.8**.

TABLE 3.8—Description for varying fracture height cases		
Case	Case Description	Fracture half-height, ft
Base case	Constant fracture height	$w_z = 80$
Varying case	Varying fracture height with a distribution along an ellipse	Different values are generated for each segment {51.92, 79.56, 93.20, 99.27, 99.27, 93.20, 79.56, 51.92}

Again, the fracture is partitioned into eight segments along the fracture length. We can get eight fracture heights accordingly. For the base case, the constant fracture half-height is 80 ft with a penetration ratio of 0.8 (I_z = 160/200). With all these information, we calculate the PI for the two cases and the comparison of the results is shown in **TABLE 3.9**.

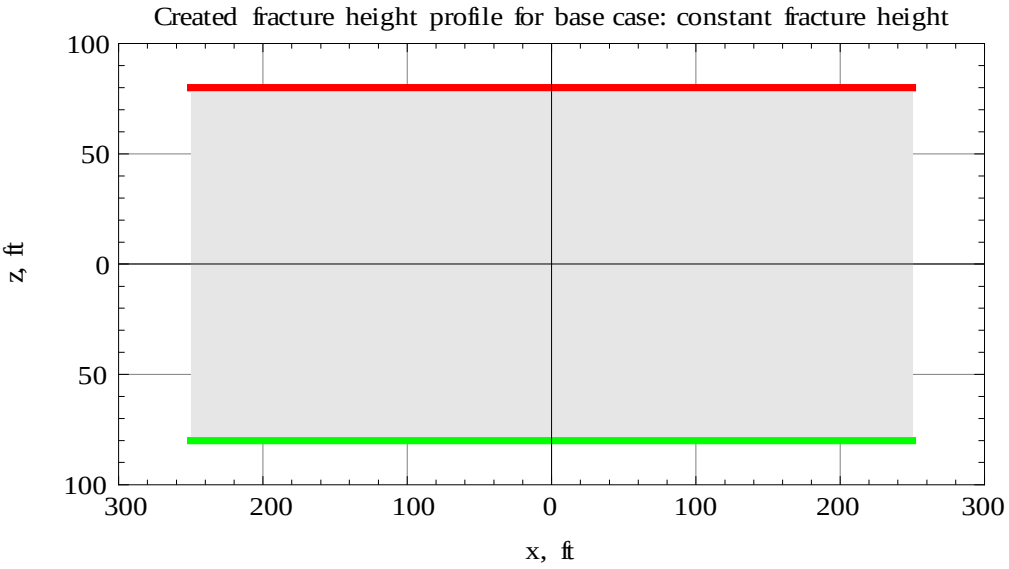

Fig. 3.19—Created constant fracture height profile for base case

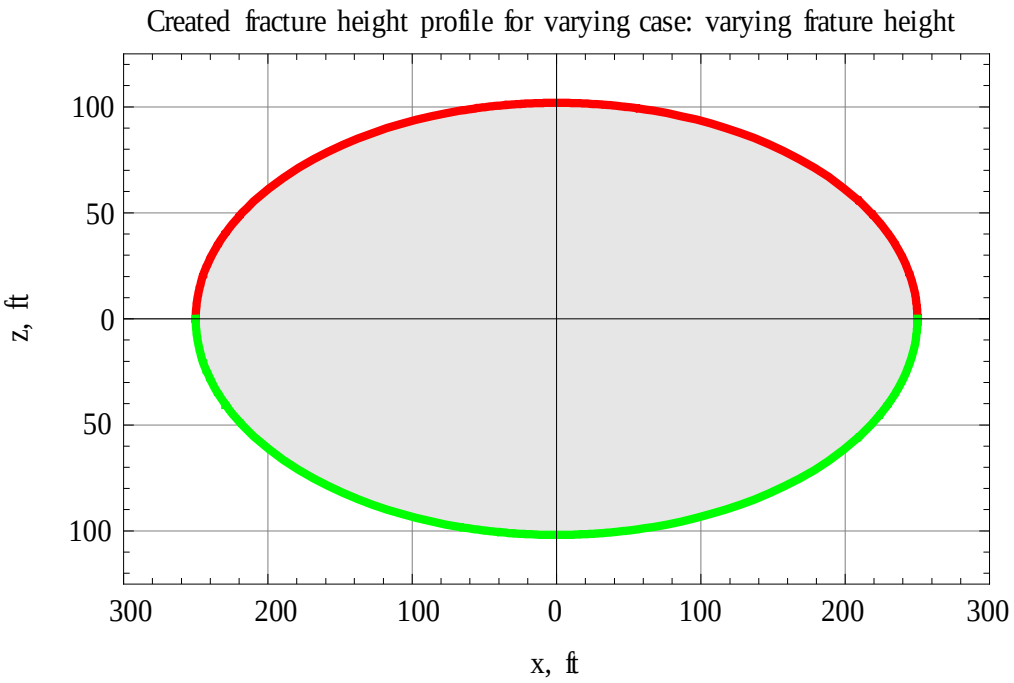

Fig. 3.20—Created varying fracture height profile for varying case

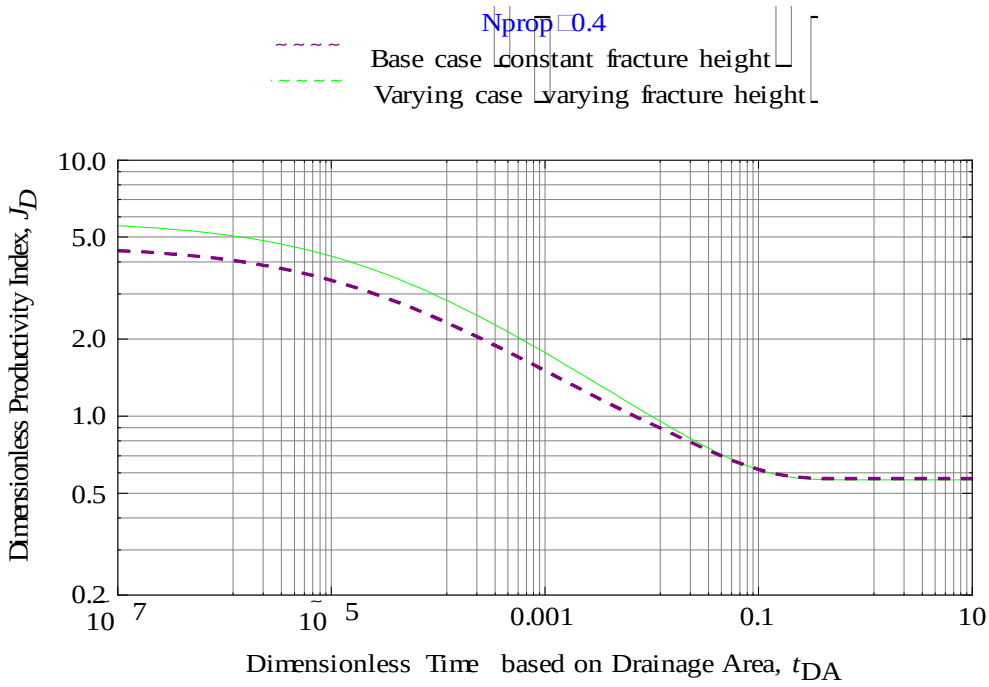

Fig. 3.21—Varying case overlaid by base case: effect of varying fracture height

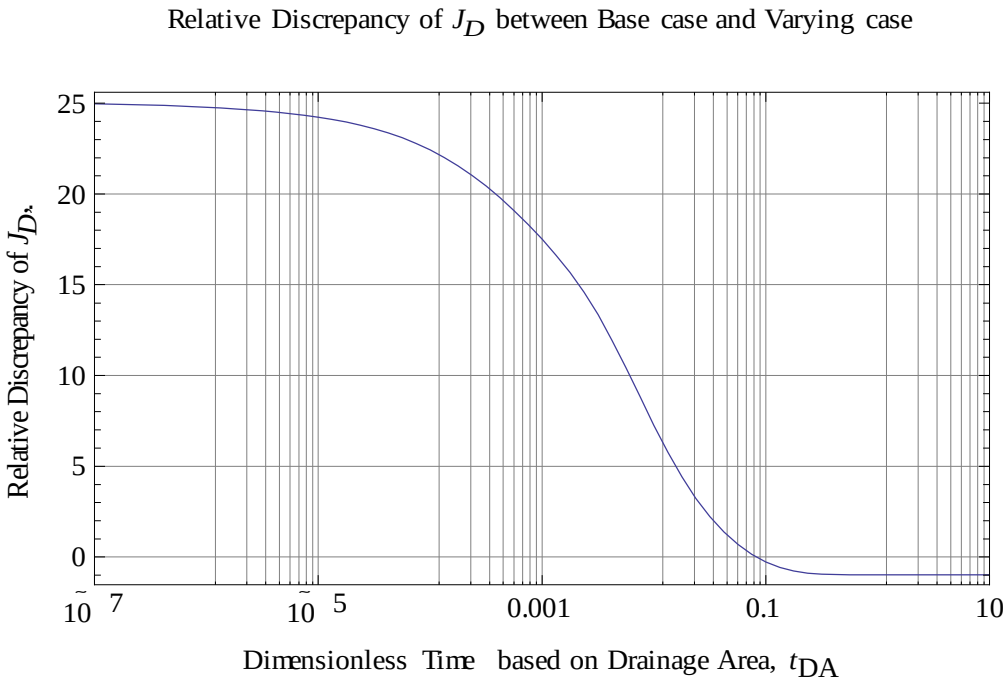

Fig. 3.22—Effect of varying fracture height on J_D during early-time transient flow and late-time pseudo-steady state flow

The effect of varying fracture height on PI is similar to that of varying fracture width on PI.

TABLE 3.9—Comparison of computation results for varying fracture height cases

	Dimensionless Time based on Drainage Area, t_{DA}	Dimensionless Productivity Index, J_D		Relative Discrepancy of J_D, %
		Base case	Varying case	
Transient Flow Region	1.00E-12	4.609596	5.764567	25.06
	1.00E-11	4.609451	5.764382	25.06
	1.00E-10	4.608005	5.76254	25.06
	1.00E-09	4.597546	5.749225	25.05
	1.00E-08	4.557084	5.697717	25.03
	1.00E-07	4.432635	5.539318	24.97
	1.00E-06	4.096533	5.111628	24.78
	0.00001	3.388734	4.209809	24.23

	TABLE 3.9—Continued			
	0.0001	2.398067	2.935883	22.43
	0.001	1.50471	1.768281	17.52
	0.01	0.93028	0.997761	7.25
Pseudo-Steady-State Flow Region	0.1	0.618649	0.61695	-0.27
	1	0.570161	0.564583	-0.98
	10	0.57016	0.564582	-0.98
	100	0.570151	0.564573	-0.98

3.3 Conclusions

After thoroughly investigating all cases related to the vertically fractured wells, we summarize and conclude as following:

- The new routine, vwvfr, is validated through comparing the results from the routine, vwcfr, using constant fracture parameters. It could be used for computing the dimensionless productivity index of a vertically fractured well with the capability of considering the effects of complexity of fracture shape and non-uniformity of fracture permeability obtained after pump job.
- Effect of varying proppant pack permeability on PI

  Case A: $k_{fwb} < k_f$, a linearly increasing permeability distribution along the fracture

  Decrease of PI in transient flow regime and increase of PI in pseudo-steady state flow regime.

  Case B: $k_{fwb} > k_f$, a linearly decreasing permeability distribution along the fracture

  This is common situation

Increase of PI in transient flow regime and decrease of PI in pseudo-steady state flow regime. This is the general case happened in the real fracture job. We prefer to use this case for forecasting the production of the vertically fractured well.

- Effect of varying fracture width on PI

  If a varying fracture width profile is created for a vertically fractured well, it will result in an increase of PI during the transient flow regime and the increase of PI is going to zero as flow feels the reservoir boundary. Eventually, it will pose a decrease of PI in the pseudo-steady state flow regime.

- Effect of varying fracture height on PI

  Similar to effect of varying fracture width on PI, there is an increase of PI in transient flow regime but a decrease of PI in pseudo-steady state flow regime.

3.4 Concluding Remarks

In this chapter, we addressed the necessity of performing the sensitivity analysis in the introduction section. Then, we presented the investigation methodology and continued with a description of the program. Along the way, we validate the new subroutine, named vwvfr and validation results are presented graphically and the concrete data are tabulated for comparison. Finally, we presented the investigation results for varying proppant pack permeability, varying fracture width and varying fracture height. Conclusions are summarized in the end section. In the next chapter, we will apply the model to real field data.

CHAPTER IV

FIELD STUDIES

4.1 Introduction

Tight gas is the term commonly used to refer to low-permeability reservoirs that produce mainly dry natural gas. Holditch[33] (2006) defined the tight gas reservoirs as "a reservoir that cannot be produced at economic flow rates nor recover economic volumes of natural gas unless the well is stimulated by a large hydraulic fracture treatment or produced by use of a horizontal wellbore or multilateral wellbores." It may include tight gas sands, tight-carbonate, gas shale and coalbed methane. All of these reservoirs are called "unconventional gas reservoirs".

As discussed in the previous chapters, it is important to accurately predict the well performance of hydraulically fractured gas wells with a robust production simulator. Since all of the unconventional gas reservoirs need to be hydraulically fracture treated in order to produce at a commercial gas flow rate and produce commercial gas volumes, successfully stimulation must be guaranteed. Normally, scenario analysis is required for choosing the optimum possible treatment. After running a few "what-if" cases, the one with the best performance will be the final choice.

In this chapter, what we do is running several cases to compare the simulated production with real production, the degree of matching of the two will tell the accuracy of our model. We will use the production and completion data from Cotton Valley formation, which is described as tight gas sands (TGS).

4.2 Methodology

Basic parameters sensitive to hydraulically fractured gas well performance are estimated from production data analysis. They are estimated formation permeability, estimated fracture half-length, estimated fracture conductivity and estimated well drainage area. For our program, we need the fracture pack permeability and fracture width. There are two ways that can be used and comparable with each other. The first method is to estimate the proppant pack permeability from correlation function and recalculate the fracture width. The second one is to estimate the fracture width based on propped volume and recalculate the proppant pack permeability. They are described as following:

- **Correlation Function**

  The fracture pack permeability is a function of proppant type, size and closure pressure. The proppant supplier provides the correlation function, based on which we can estimate the proppant pack permeability. Then, we can calculate the estimated fracture width by dividing the estimated fracture conductivity with the estimated proppant pack permeability at closure.

- **Propped Volume**

  Since the mass of the proppant pumped down the well is known from the fracture treatment data, the fracture width can be estimated based on the information of fracture half-length and fracture height. The fracture half-length is estimated by production data analysis. There are lots of methods available to estimate the fracture height, like temperature log, radioactive log, microseismic mapping. But

these data are not readily available. So, we will assume the net pay thickness be the fracture height. The proppant pack porosity is assumed to be 0.3 as experience indicated. The bulk density of the proppant can be obtained from the proppant date provided by the supplier. Then, we can calculate the fracture width by

$$V_b = \frac{M_{prop}}{\rho_b(1-0.3)} \quad \text{……...…….……} \quad (4.1)$$

$$w_f = \frac{V_b}{2x_f h} \quad \text{……..……...…} \quad (4.2)$$

Where, Mprop is the proppant mass pumped down the well, ρ_b is the bulk density of the proppant used, V_b is the proppant volume, x_f is the fracture half-length, h is the net pay thickness.

Since the bottomhole pressure is declining during the production, as shown in **Fig. 4.1**, we will choose the arithmetic average of the pressure during the stabilized period as the input bottomhole pressure.

With all the data ready, we can use them as the input to the model and run the simulation to get the results of the production forecasting, which can be comparable to the production history. The good match between the simulated production and real production will provide the accuracy basis for our production forecasting model. The results of the study are presented as following.

4.3 Field Applications

In this section, three fractured gas wells were analyzed case by case. The process of choosing input data is detailed and the analysis results are presented.

4.3.1 Well Completion Summary

Well A is fracture treated in two stages, Pre-Davis Stage 1 (9658 ft - 9684 ft) and CV Upper Davis Stage 2 (9290 ft - 9440 ft). Stage 1 is perforated and fractured with 40012 lbs of PR6000 20/40 proppant and Stage 2 is perforated and fractured with 250250 lbs of SB Excel 20/40 proppant.

Well B is fracture treated in one stage, Davis & Pre-Davis (9078 ft - 9310 ft). It was perforated and fractured with 873255 lbs of Premium White sand 20/40.

Well C is fracture treated in one stage, Davis & Pre-Davis (9105 ft – 9355 ft). It was perforated and fractured with 543797 lbs of PRC 20/40 proppant.

4.3.2 BHP History

The bottomhole pressure history of Well A, B and C is plotted as **Fig. 4.1**. It is declining sharply at the beginning of production and then stabilized at the rest of the well life.

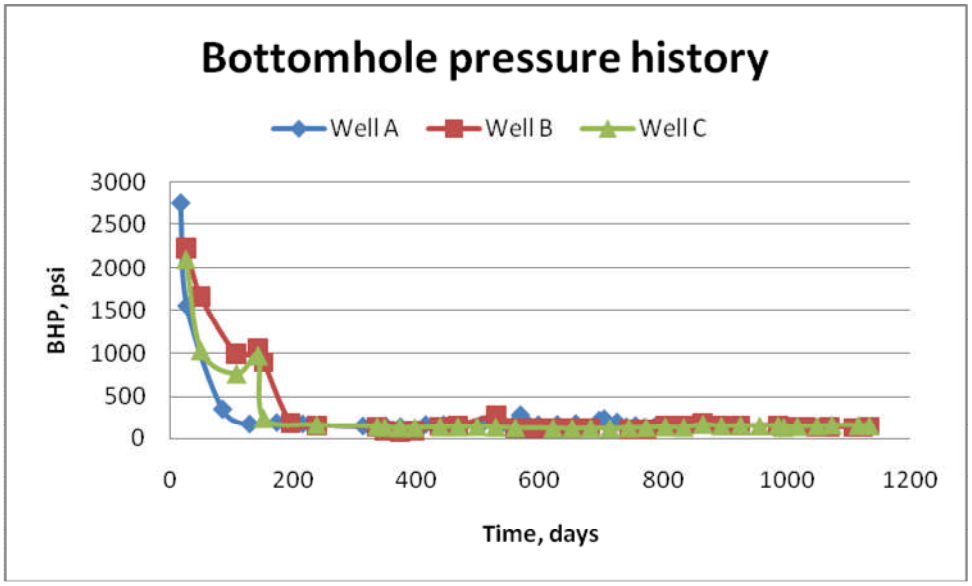

Fig. 4.1—Bottomhole pressure history for Well A, B and C

For production forecasting with our model, we need an input value for the bottomhole pressure. We get this input value from the arithmetic average of the bottomhole pressure at the stabilized stage, which are summarized in **TABLE 4.1** as following.

TABLE 4.1—Bottomhole pressure input data for the model

Well No.	A	B	C
Bottomhole pressure, psia	162	148	139

4.3.3 Estimated Formation and Fracture Parameters

From production data analysis, the estimated parameters are the formation permeability, fracture half-length, fracture conductivity and well drainage area. The results are summarized as in **TABLE 4.2**.

TABLE 4.2—Estimated value based on production data history matching

Parameters	Estimated Value		
	Well A	Well B	Well C
Permeability, md	0.001312	0.001572	0.002039
Fracture half-length, ft	144	265	307.8
Fracture Conductivity, md-ft	200	275	275
Drainage Area, acre	2.25	5.33	7.2

4.3.4 Estimations from Correlation Function and Propped Volume

We summarized the results from the two methods as following.

- **Correlation Function**

From the fracture treatment data, we know that the closure stress is about 5200 psi. Based on the correlation function of permeability to closure stress provided by the proppant supplier, we estimate the proppant pack permeability at 5200 psi closure for each type of proppants pumped down the well. The plot for the stress dependent permeability is shown in **Fig. 4.2**. The estimated permeability at closure for well A, B and C are summarized in **TABLE 4.3**.

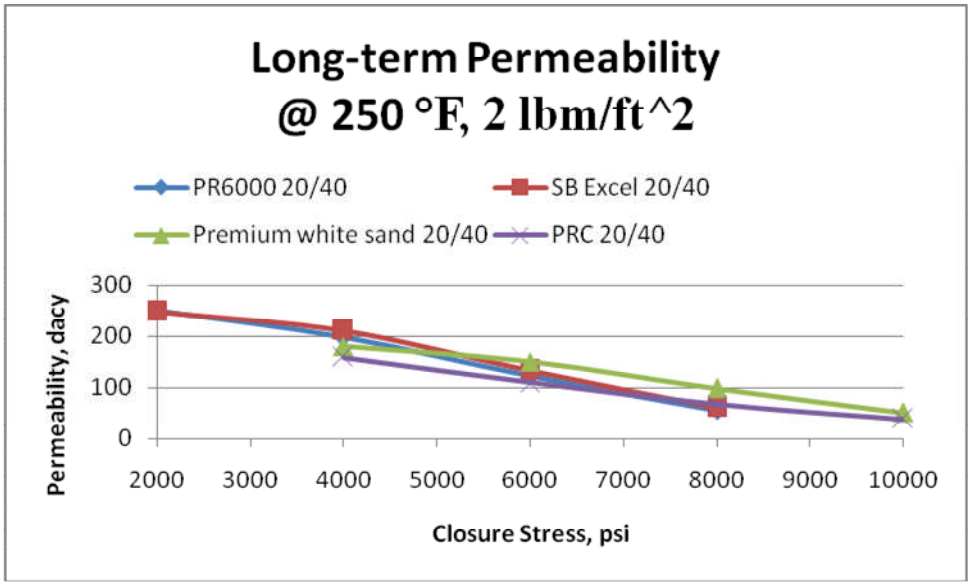

Fig. 4.2—Effect of closure stress on proppant packed permeability

TABLE 4.3—Permeability correlation analysis

Well No.	A		B	C
Estimated conductivity, md-ft	200		275	275
Proppant type/size	PR 6000 20/40	SB Excel 20/40	Premium white sand 20/40	PRC 20/40
Proppant pack permeability from correlation, darcy	150.38	157.08	159.26	130.02
Calculated fracture width, ft	0.001329	0.001273	0.001727	0.002115
Averaged fracture width, ft	0.001301		0.001727	0.002115

- **Propped Volume**

Since the amount of proppant that were pumped down the well is known, the fracture width can be calculated based on the propped volume and estimated fracture length and fracture height. The propped volume can be calculated using Equ. 4.1 while

the fracture width is calculated using Equ. 4.2. The results from propped volume calculations are summarized in **TABLE 4.4**.

TABLE 4.4—Propped volume calculations				
Well No.	A		B	C
Proppant type/size	PR 6000 20/40	SB Excel 20/40	Premium white sand 20/40	PRC 20/40
Proppant mass, lbs	40013	250250	873255	543797
Proppant bulk density, lb/cu. ft	96		100	100
Proppant pack porosity	0.3		0.3	0.3
Propped volume, cu. ft	4319.39		12475.07	7768.529
Proppant concentration, lb/ft^2	6.11		10.98	5.89
Fracture geometry calculations				
Estimated fracture length, ft	288		530	615.6
Estimated fracture height, ft	165		150	150
Calculated fracture width w/o adjustment, ft	0.09090		0.1569	0.08413

The results are summarized in **TABLE 4.5** for comparison. As can be noticed, the fracture width from propped volume calculations is about 70 folds bigger than the one from permeability correlation method for well A, 92 for well B and 40 for well C. The big difference from the two methods may suggest that the estimated fracture length is only the effective length, which means the actual length is far much bigger than the effective length. The phenomenon is “gel damage”. Another reason for the big

difference is that the actual fracture is far breaking out the pay zone while we are using the pay zone height as the fracture height for production data analysis.

TABLE 4.5—Comparison of fracture width estimated from the two methods

Well No.		A	B	C
Fracture width from correlation function	Feet	0.001301	0.001727	0.002115
	Inch	0.015612	0.020724	0.02538
Fracture width from propped volume calculation	Feet	0.09090	0.1569	0.08413
	Inch	1.0908	1.9152	1.00956
Folds		70	92	40

To account for the gel damage effect on fracture length and fracture height containment problem, adjustment factors are needed for fracture length and fracture height in order to using the method of propped volume. The detailed analysis is summarized in **TABLE 4.6**.

TABLE 4.6—Calculations after adjustment

Adjustment factor	Fracture length after adjustment, ft		
	Well A	Well B	Well C
0.3	960	1767	2052
0.5	576	1060	1231
0.7	411	757	879

TABLE 4.6 Continued

Adjustment factor		Fracture height after adjustment, ft		
		Well A	Well B	Well C
1.2		198	180	180
1.5		248	225	225
2.0		330	300	300
Adjustment factor		Calculated fracture width after adjustment, ft		
length	height	Well A	Well B	Well C
0.3	1.2	0.02272	0.03923	0.02103
	1.5	0.01818	0.03138	0.01683
	2.0	0.01363	0.02354	0.01262
0.5	1.2	0.03787	0.06538	0.03505
	1.5	0.03030	0.05231	0.02804
	2.0	0.02272	0.03923	0.02103
0.7	1.2	0.05302	0.09154	0.04908
	1.5	0.04242	0.07323	0.03926
	2.0	0.03181	0.05492	0.02945

4.3.5 Input Data Summary

With careful choice of the estimated values of fracture parameters, we will use it as the input data for our model. Basically, there are two major sets of data. One is for the productivity index computation as in **TABLE 4.7** while the other is for production forecasting as in **TABLE 4.8**.

TABLE 4.7—PI computation					
Well A					
Reservoir Box		Fracture Box		Control Parameters	
xe, ft	313	cx, ft	0.5xe	kfwb, md	155730
ye, ft	313	cy, ft	0.5ye	Switch1	1
ze, ft	165	cz, ft	0.5ze	Switch2	1
kx, md	0.001312	wx, ft	0.5xe		
ky, md	0.001312	wy, ft	0.0006366		
kz, md	0.001312	wz, ft	0.5ze		
		kf, md	153730		
Well B					
Reservoir Box		Fracture Box		Control Parameters	
xe, ft	482	cx, ft	0.5xe	kfwb, md	161260
ye, ft	482	cy, ft	0.5ye	Switch1	1
ze, ft	150	cz, ft	0.5ze	Switch2	1
kx, md	0.001572	wx, ft	0.5xe		
ky, md	0.001572	wy, ft	0.0008634		
kz, md	0.001572	wz, ft	0.5ze		
		kf, md	159260		
Well C					
Reservoir Box		Fracture Box		Control Parameters	
xe, ft	560	cx, ft	0.5xe	kfwb, md	131020
ye, ft	560	cy, ft	0.5ye	Switch1	1
ze, ft	150	cz, ft	0.5ze	Switch2	1
kx, md	0.002039	wx, ft	0.5xe		
ky, md	0.002039	wy, ft	0.001058		
kz, md	0.002039	wz, ft	0.5ze		
		kf, md	130020		

TABLE 4.8—Production forecasting

Well A					
Gas data		Reservoir data		Forecast limit	
Gravity	0.6157	Porosity, fraction	0.08	qend, mscf/d	0
N2 content, mole fraction	0.00066	Water saturation, fraction	0.4	tend, day	852
CO2 content, mole fraction	0.02284	Initial reservoir pressure, psia	4270	pwf, psi	163
H2S content, mole fraction	0	Standard pressure, psia	14.65		
Temperature, F	240	Standard temperature, F	520		
Min. pressure, psia	14.65	Rock compressibility, 1/psi	4.0×10^{-6}		
Max. pressure, psia	4270	Water compressibility, 1/psi	3.6×10^{-6}		
Integration points	100	Adsorption, ft^3/ton	0		
Well B					
Gas data		Reservoir data		Forecast limit	
Gravity	0.6157	Porosity, fraction	0.08	qend, mscf/d	0
N2 content, mole fraction	0.00066	Water saturation, fraction	0.4	tend, day	1133
CO2 content, mole fraction	0.02284	Initial reservoir pressure, psia	4137	pwf, psi	148
H2S content, mole fraction	0	Standard pressure, psia	14.65		
Temperature, F	240	Standard temperature, F	520		
Min. pressure, psia	14.65	Rock compressibility, 1/psi	4.0×10^{-6}		
Max. pressure, psia	4137	Water compressibility, 1/psi	3.6×10^{-6}		
Integration points	100	Adsorption, ft^3/ton	0		
Well C					
Gas data		Reservoir data		Forecast limit	
Gravity	0.6157	Porosity, fraction	0.08	qend, mscf/d	0
N2 content, mole fraction	0.00066	Water saturation, fraction	0.4	tend, day	1133
CO2 content, mole fraction	0.02284	Initial reservoir pressure, psia	4154	pwf, psi	139
H2S content, mole fraction	0	Standard pressure, psia	14.65		
Temperature, F	240	Standard temperature, F	520		
Min. pressure, psia	14.65	Rock compressibility, 1/psi	4.0×10^{-6}		
Max. pressure, psia	4154	Water compressibility, 1/psi	3.6×10^{-6}		
Integration points	100	Adsorption, ft^3/ton	0		

4.3. 6 Results

The comparison plots of simulation data and real production for Well A are listed in this section and results for Well B and Well C are listed in **APPENDIX C**. As can be seen from **Fig. 4.3** to **Fig. 4.6**, the overall matching is very good except the production rate versus cumulative production, since the production rate at the very beginning fluctuates sharply. The same matching are also demonstrated for Well B and Well C as can be seen from the results in **APPENDIX C**.

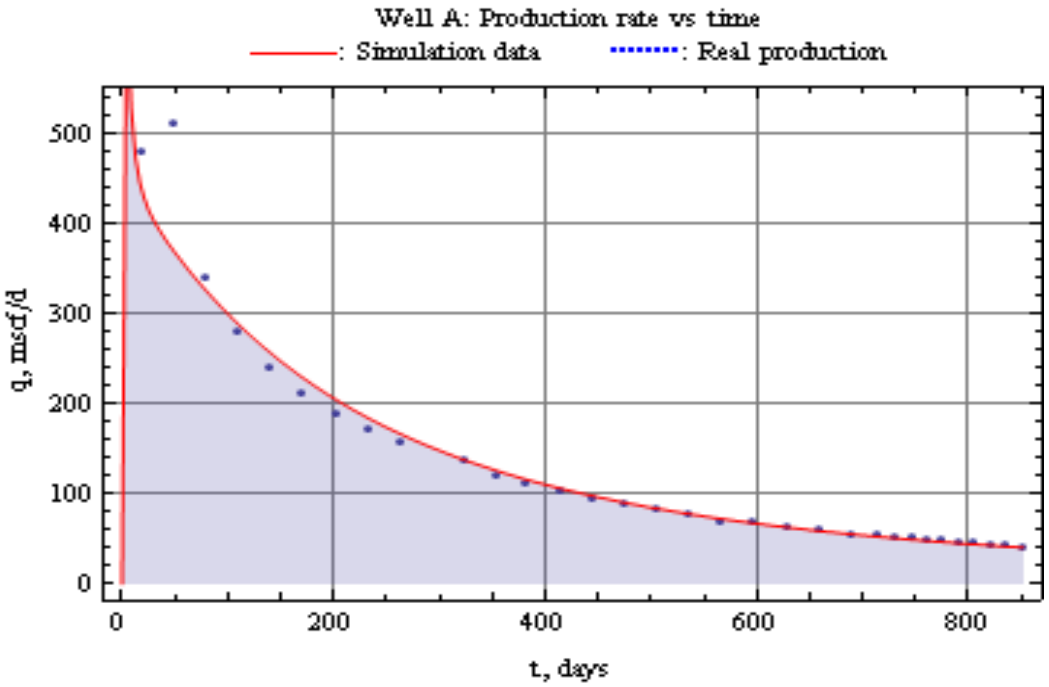

Fig. 4.3—Comparison result of production rate versus time for Well A

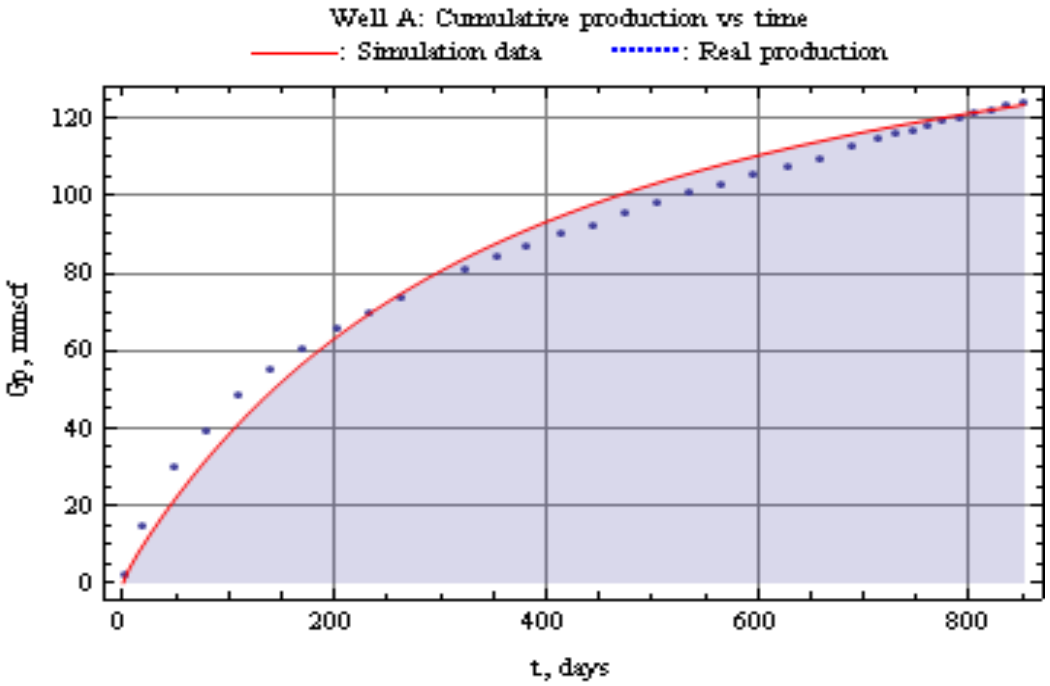

Fig. 4.4—Comparison result of cumulative production versus time for Well A

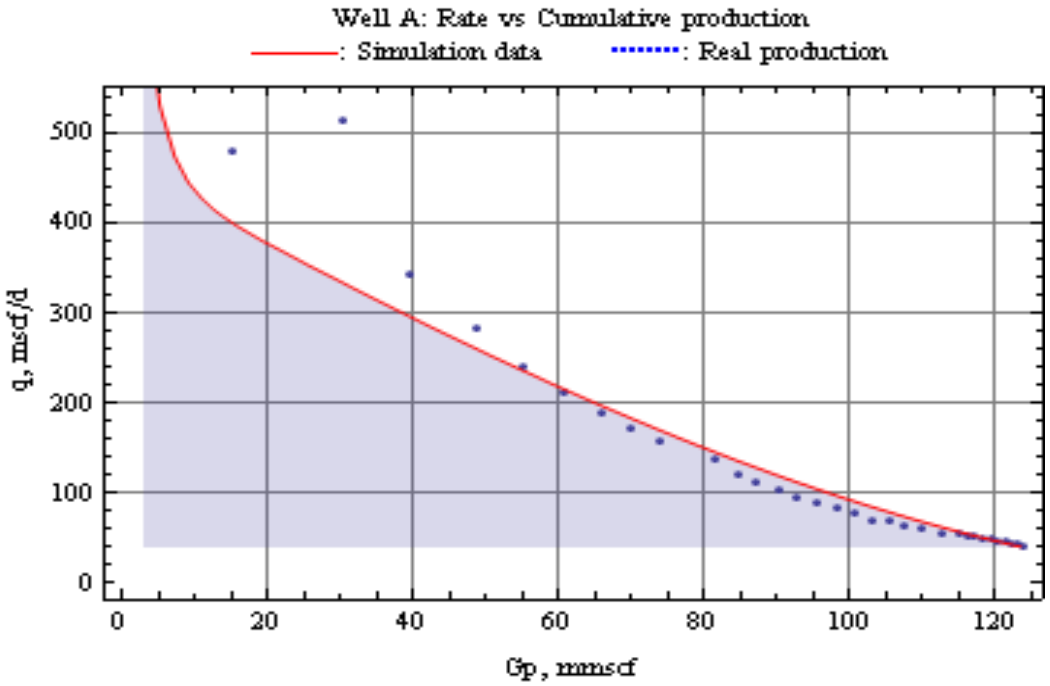

Fig. 4.5—Comparison result of rate versus cumulative production for Well A

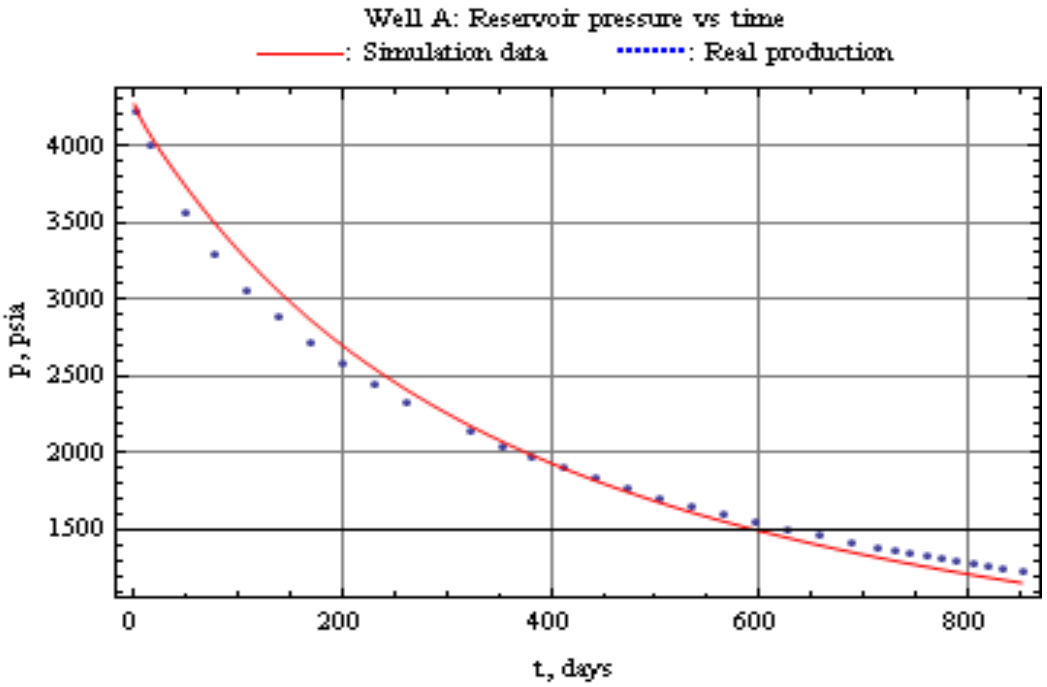

Fig. 4.6—Comparison result of reservoir pressure versus time for Well A

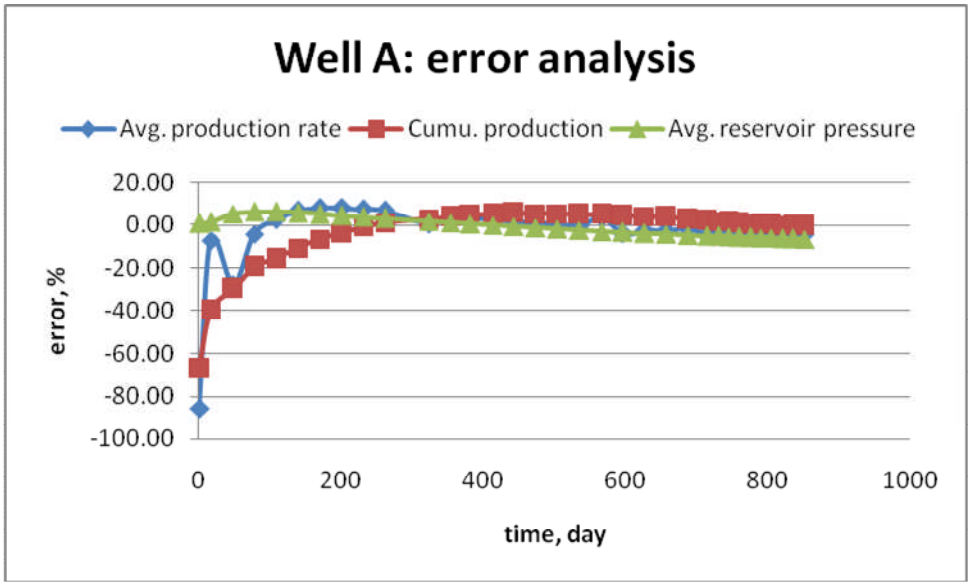

Fig. 4.7—Error analysis for Well A

The discrepancy between simulated data and real data is generally within 10% and is decreasing as production flows as can be seen in the error analysis plots in **Fig. 4.7** for Well A. The same results can be seen for Well B and Well C listed in **APPENDIX C**.

4.4 Conclusions

From the field studies, the discrepancy between simulation and real production is within 10% and is decreasing with elapsed time. Prudent choice of input data for our model can guarantee an accurate production forecasting for a typical hydraulically fractured vertical well in low-permeability reservoir. From another point of view, our model can be used as the design tool to choose the optimum hydraulic fracturing treatment.

4.5 Concluding Remarks

In this chapter, we first introduced the concept of unconventional gas and their common characteristics: ultra-low matrix permeability. Generally, those reservoirs require massive hydraulic fracturing treatment before they can be produced commercially. The crucial question is to how to choose the size of fracture treatment based on formation permeability and well spacing.

Then, we described the methodology for choosing and validating the input data for production forecasting. There are two methods we use for estimating the fracture width and proppant packed permeability. They can be used independently and they complement each other if used prudently.

In the next sections, we demonstrated the application to three hydraulically fractured gas wells as the field examples.

CHAPTER V

SUMMARY AND CONCLUSIONS

5.1 Summary

For conventional reservoirs, well productivity is usually calculated using the pressure response of the reservoir in its pseudosteady-state period. There are numerous studies for different well completion schemes, which developed correlations for pseudosteady-state productivity index for specific cases. Most of the developed models for complex well completion schemes use some approximations for productivity index calculation and they have some limitations in use. Furthermore, as the petroleum industry goes toward producing lower quality reservoirs like TGS, the period of transient flow covers larger part of the well lifetime and these pseudosteady-state productivity calculations become less applicable in prediction of the reservoir's production behavior.

In this research, well performance of a vertical well intersected by a vertical fracture is modeled with incorporation of details of the hydraulic fracture. Inside the vertical fracture, the spatial variance is investigated in details, which will directly affect the well performance. The varying proppant packed permeability is treated with a linear distribution along the fracture from the wellbore to the fracture tips. The varying fracture width is treated with an elliptic distribution along an ellipse. The varying fracture height is treated with an elliptic distribution along an ellipse well contained within the pay zone. Field data are used to validate the accuracy of the model in the field studies. As other simulators require, the carefulness of choosing the input data is crucial. They are formation permeability, well spacing and hydraulic fracture parameters.

5.2 Conclusions

On the basis of the work done during this research project, the following conclusions are offered:

1. The DVS method has been approved to be a fast, robust and reliable method, as compared to conventional methods, to calculate the well productivity, especially for complex completion schemes.
2. The combination of the DVS method with material balance is an effective way to forecast the production of different hydraulically fractured wells.
3. For hydraulically fractured wells, the details of fracture could be incorporated into the model, which directly affect the fractured well performance.
4. Investigation of varying fracture parameters shows that it will affect the well productivity index in both the transient and pseudo-steady state flow regimes but for production forecasting, its effect is often negligible.
5. Field examples show that good match can be achieved between simulated and observed production. At the very beginning of production, we found about 10% difference between the simulated data and real data, which could partially be attributed to the fluctuation of early production. But eventually, the difference will diminish at long-term production.
6. The good match of simulated data and field data shows that our model, combination of DVS method and material balance, is reliable and accurate enough to be used as a tool to optimize hydraulic fracture treatments.

NOMENCLATURE

Variables

A	=	reservoir drainage area, ft^2
c_t	=	total compressibility, psi^{-1}
c_{trad}	=	conversion factor
c_x	=	position of the center of the source in x direction, ft
c_y	=	position of the center of the source in y direction, ft
c_z	=	position of the center of the source in z direction, ft
f	=	1D solution to the flow equation
J_D	=	dimensionless productivity index
$J_{D,\ trand}$	=	traditional definition of dimensionless productivity index
k	=	permeability, reference permeability, md
k_x	=	directional permeability in x direction, md
k_y	=	directional permeability in y direction, md
k_z	=	directional permeability in z direction, md
p	=	pressure, psi
p_i	=	initial pressure, psi
p_{wf}	=	well flowing pressure, psi
$p_{\delta D}$	=	dimensionless pressure due to instantaneous source
PI	=	productivity index, STB/d/psi
p_{uD}	=	dimensionless pressure due to continuous source

t	=	time
t_D	=	dimensionless time
t_{DA}	=	dimensionless time with regard to reference drainage volume
$t_{DA,\ trad}$	=	dimensionless time with regard to fracture half-length
w_x	=	source width in x direction, ft
w_y	=	source width in y direction, ft
w_z	=	source width in z direction, ft
x_D	=	dimensionless length in x direction, x/xe
x_e	=	length of outer box, ft
y_D	=	dimensionless width in y direction, y/ye
y_e	=	width of the outer box, ft
z_D	=	dimensionless height in z direction, z/ze
z_e	=	height of the outer box, ft

Greek Symbols

ϕ	=	porosity, fraction
μ	=	viscosity, cp

REFERENCES

1. Gidley, J.L., Holditch, S.A., Nierode, D.E. and Veatch Jr, R.W.: *Recent Advances in Hydraulic Fracturing*, SPE Monograph Vol. 12, SPE, Richardson, TX 2001
2. Amini, S.(2007): *Development and Application of the Method of Distributed Volumetric Sources to the Problem of Unsteady State Fluid Flow in Reservoirs*, Ph.D. dissertation, Texas A&M U., College Station, TX
3. Valkó, P. P. and Amini, S.: "The Method of Distributed Volumetric Sources for Calculating the Transient and Pseudo-steady State Productivity of Complex Well-Fracture Configurations," Paper SPE 106729 presented at the 2007 SPE Hydraulic Fracturing Technology Conference held in College Station, TX, U.S.A., 29-31 January 2007
4. Economides, M. J. and Martin, T.: *Modern Fracturing-Enhancing Natural Gas Production*, ET Publishing, Houston, TX, 2007
5. Economides, M., Oligney, R. and Valkó, P.: *Unified Fracture Design-Bridging the Gap Between Theory and Practice*, Orsa Press, Alvin, TX 2002
6. Romero, D. J., Valkó, P. P. and Economides, M. J.: "Optimization of the Productivity Index and the Fracture Geometry of a Stimulated Well with Fracture Face and Choke Skins," SPE Paper 73758, SPE, Richardson, TX 2002.
7. Economides, M.J. and Nolte, K.G.: *Reservoir Stimulation*, 3rd Edition, Schlumberger Educational Services, Sugar Land, TX 1998.
8. Lee, J., Rollins, J.B. and Spivey, J.P.: *Pressure Transient Testing*, SPE Textbook

Series Vol. 9, SPE, Richardson, TX 2003.

9. FAST RTA Technical Documentation, Fekete Associate Inc. 2005
10. Kumar, A.(2008): *Effective Fracture Geometry Obtained With Large Water Sand Ratio*, M.S. Thesis, Texas A&M U., College Station, TX
11. McGuire, W.J. and Sikora, V.J.: "The Effect of Vertical Fractures on Well Productivity," *Trans.*, AIME 219, 401-03, 1960.
12. Tannich, J.D. and Nierode, D.E.: "The Effect of Vertical Fractures on Gas Well Productivity," Paper SPE 15902, SPE, Richardson, TX 1985.
13. Balen, R.M., Meng, H-Z. and Economides, M.J.: "Applications of the Net Present Value (NPV) in the Optimization of Hydraulic Fractures," Paper SPE 18541, SPE, Richardson, TX 1988.
14. Cinco-Ley, H. and Samaniego, F.: "Transient Pressure Analysis for Fractured Wells," Paper SPE 7490, SPE, Richardson, TX 1981.
15. Prats, M.: "Effect of Vertical Fracture on Reservoir Behavior-Incompressible Fluid Case," *SPE Journal*, 1, 105-118, 1961.
16. Bennett, C.O., Reynolds, A.C., Raghavan, R. and Elbel, J.L.: "Performance of Finite-Conductivity, Vertically Fractured Wells in Single-Layer Reservoirs", SPE Formation Evaluation, SPE, Richardson, TX 1986.
17. Ehrl, E., Schueler, S.K.: "Simulation of a Tight Gas Reservoir with Horizontal Multifractured Wells," Paper SPE 65108, presented at SPE European Petroleum Conference, 24-25 October 2000, Paris, France.
18. Behr, A., Mtchedllishvili, G., Friedel, G. and Haefner, F.: "Consideration of Damage

Zone in Tight Gas Reservoir Model with Hydraulically Fractured Wells," SPE 82298, presented at SPE European Formation Damage Conference, 2003, The Hague, The Netherlands.

19. Shaoul, J.R., Behr A. and Mtchedllishvili, G.: "Developing a Tool for 3D Reservoir Simulation of Hydraulically Fractured Wells," IPTC 10182 presented at the International Petroleum Technology Conference held in Doha, Qatar, 21-23 November, 2005.
20. Lolon, E.P., Shaoul, J.R. and Mayerhofer, M.J.: "Application of 3D Reservoir Simulator for Hydraulically Fractured Wells," Paper SPE 110093 presented at the 2007 Asia Pacific Oil and Gas Conference and Exhibition held in Jakarta, Indonesia, 30 October-1 November 2007.
21. Meng, H.Z., Proano, E.A., Buhidma, I.M. and Mach, J.M.: "Production Systems Analysis of Vertically Fractured Wells," Paper SPE 10842 presented at the SPE/DOE Unconventional Gas Recovery Symposium held at Pittsburgh, PA, May 16-18, 1982.
22. Lee, J. and Wattenbarger, R. A.: *Gas Reservoir Engineering*, SPE Textbook Series Vol. 5, SPE, Richardson, TX 1996.
23. Houpeurt, A.: "On the Flow of Gases in Porous Media," *Revue de L'Institut Francais du Petrole* (1959) XIV (11), 1468-1684.
24. Rawlins, E.L. and Schellhardt, M.A.: *Backpressure Data on Natural Gas Wells and Their Applications to Production Practices*, Monograph Series, United States Bureau of Mines (USBM) 1937.

25. Gringarten, A.C. and Ramey, H.J. Jr.: "The Use of Source and Green's Functions in Solving Unsteady-Flow Problems in Reservoirs," *SPEJ* (October 1973) **285**, Trans., AIME, 255.
26. Marongiu-Porcu, M., Economides, M.J. and Holditch, S.A.: "Economic and Physical Optimization of Hydraulic Fracturing," Paper SPE 111793, SPE, Richardson, TX 2008.
27. Zhu, D. at al. "Predicting the Productivity of Multiple Fractured Horizontal Gas Wells," Paper SPE 106280, SPE, Richardson, TX 2007.
28. Chen, H. Y. and Asaad, N.: "Horizontal-Well Productivity Equations With Both Uniform-Flux and Uniform-Pressure Wellbore Models," Paper SPE 97190 presented at the 2005 SPE Annual Technical Conference and Exhibition, Dallas, TX, 9-12 October 2005
29. Al-Hussainy, R. and Ramey, H. J.: "Application of Real Gas Flow Theory to Well Testing and Deliverability Forecasting," Paper SPE 1243 presented at SPE Annual Fall Meeting held in Denver, CO., Oct. 3-6, 1965
30. Helmy, M. W. and Wattenbarger, R. A.: "Simplified Productivity Equations for Horizontal Wells Producing at Constant Rate and Constant Pressure," Paper SPE 49090 presented at the 1998 SPE Annual Technical Conference and Exhibition, New Orleans, Louisiana, 27-30 September 1998
31. Valkó, P. P.: *User's Manual for Gas14.nb*, Crisman Institute, Petroleum Engineering Department, Texas A&M U., College Station, TX, April 2008.

32. MATHEMATICA, Version Number 6.0.1.0, Wolfram Research Inc., Champaign, IL (2007).

33. Holditch, S.A.: “Tight Gas Sands,” Paper SPE 103356, SPE, Richardson, TX 2006

34. Guo, B.Y. and Ghalambor, A.: *Natural Gas Engineering Handbook*, Gulf Publishing Company, Houston, TX, 2005.

35. Economides, M. J., Hill, A. D. and Economides, C. E.: *Petroleum Production Systems*, Prentice Hall PTR, Upper Saddle River, NJ, 1993

APPENDIX A

PROCEDURE OF CALCULATING RESERVOIR ROCK AND GAS PROPERTIES

For calculating the gas properties, we refer to the calculations and correlations in Guo and Ghalambor's book[34] and Lee and Wattenbarger's book[22].

1. Apparent Molecular Weight, M_g

$$M_g = 29\gamma_g \quad \text{..... (A.1)}$$

2. Systematic Procedure for Calculating Pseudocritical Gas Properties for a given Specific Gravity: Sutton's Correlation

---

1. Estimate pseudocritical pressure, p_{pc}, and temperature, T_{pc}.

   1. Estimate the hydrocarbon gas gravity, γ_h

      a. If the gas contains no contaminants, then:

         1. If separator gas gravity, γ_g, is used, then $\gamma_h = \gamma_g$ for a dry gas.

         2. If the gravity of the wellstream fluid, γ_w, is used, then $\gamma_h = \gamma_w$ for a wet gas or a gas condensate. If the gas/liquid ratio and separator gas gravity of each separation stage and the stock-tank-liquid gravity are known, calculate γ_w with Equ. 2.23.

$$\gamma_w = \frac{R_1\gamma_1 + 4602\gamma_o + R_2\gamma_2 + R_3\gamma_3}{R_1 + (133316\gamma_o / M_o) + R_2 + R_3} \quad \text{..... (A.2)}$$

      b. If the gas contains more than 12*mol*% of CO2, more than 3*mol*% of N2, or any H2S, then calculate the hydrocarbon gas gravity, γ_h, with Equ. 2.24.

$$\gamma_h = \frac{\gamma_w - 1.1767y_{H2S} - 1.5196y_{CO2} - 0.9672y_{N2} - 0.6220y_{H2O}}{1 - y_{H2S} - y_{CO2} - y_{N2} - y_{H2O}} \quad \text{..... (A.3)}$$

   2. Calculate p_{pch} and T_{pch} with Eqs. 2.25 and Eqs. 2.26, respectively.

$$p_{pch} = 756.8 - 131.0\gamma_h - 3.6\gamma_h^2 \quad \text{..... (A.4)}$$

$$T_{pch} = 169.2 + 349.5\gamma_h - 74.0\gamma_h^2 \quad \text{..... (A.5)}$$

---

3. Calculate p_{pc} and T_{pc} with Eqs. 2.27.

$$p_{pc} = (1 - y_{H2S} - y_{CO2} - y_{N2} - y_{H2O})p_{pch} + 1306y_{H2S} + 1071y_{CO2} + 493.1y_{N2} + 3200y_{H2O}$$

$$T_{pc} = (1 - y_{H2S} - y_{CO2} - y_{N2} - y_{H2O})T_{pch} + 672.35y_{H2S} + 547.58y_{CO2} + 227.16y_{N2} + 1164.9y_{H2O} \quad \text{..... (A.6)}$$

2. Correct the pseudocritical properties for H2S and CO2 contamination.

   A. If the gas does not contain H2S or CO2, then $p'_{pc} = p_{pc}$ and $T'_{pc} = T_{pc}$.

   B. If the gas contains H2S and/or CO2, then calculate the corrected pseudocritical properties, p'_{pc} and T'_{pc}, with the Wichert and Aziz correlation.

3. Correct the pseudocritical properties for nitrogen and water vapor using Casey's method.

   A. If the gas does not contain nitrogen or water vapor, then $p''_{pc} = p'_{pc}$ and $T''_{pc} = T'_{pc}$.

   B. If the gas contains nitrogen and/or water vapor, then calculate p'_{pc} and T'_{pc}.

4. p''_{pc} and T''_{pc} are the appropriate values to use in correlations for z facor, compressibility, and viscosity.

4. Brill and Beggs Correlation for z Factor

1. Calculate pseudocritical properties corrected for H2S, CO2, N2, and H2O, p''_{pc} and T''_{pc}. Use the procedure outlined in section 3.

2. Calculate reduced properties, $p_r = p / p''_{pc}$ and $T_r = T / T''_{pc}$.

3. Estimate z factor.

$$z = A + \frac{1 - A}{e^B} + Cp_r^D \quad \text{..... (A.7)}$$

Where,

$$A = 1.39(T_{pr} - 0.92)^{0.5} - 0.36T_{pr} - 0.10 \quad \text{(A.8)}$$

$$B = (0.62 - 0.23T_{pr})p_{pr} + (\frac{0.066}{T_{pr} - 0.86} - 0.037)p_{pr}^2 + \frac{0.32p_{pr}^6}{10^E} \quad \text{(A.9)}$$

$$C = 0.132 - 0.32\log(T_{pr}) \quad \text{(A.10)}$$

$$D = 10^F \quad \text{(A.11)}$$

$$E = 9(T_{pr} - 1) \quad \text{(A.12)}$$

$$F = 0.3106 - 0.49T_{pr} + 0.1824T_{pr}^2 \quad \text{(A.13)}$$

5. Gas FVF

$$B_g = \frac{p_{sc}}{T_{sc}}\frac{zT}{p}\frac{ft^3}{scf} \quad \text{(A.14)}$$

6. Gas Density

$$\rho_g = \frac{pM_g}{zRT} \quad \text{(A.15)}$$

7. Gas Compressibility

$$c = \frac{1}{\rho}(\frac{\partial\rho}{\partial p})_T \quad \text{(A.16)}$$

8. Carr, Kobayashi and Burrows Correlation for Gas Viscosity

The gas viscosity correlation of Carr, Kobayashi, and Burrows involves a three-step procedure:

1. The gas viscosity at temperature and atmosphere pressure is estimated first from gas-specific gravity and inorganic compound content

   The atmospheric pressure viscosity can be expressed as:

   $$\mu_1 = \mu_{1HC} + \mu_{1N2} + \mu_{1CO2} + \mu_{1H2S} \quad \text{(A.17)}$$

   Where,

$$\mu_{1HC} = 8.188\times10^{-3} - 6.15\times10^{-3}\log(\gamma_g) + (1.709\times10^{-5} - 2.062\times10^{-6}\gamma_g)T \text{ . (A.19)}$$

$$\mu_{1N2} = [9.59\times10^{-3} + 8.48\times10^{-3}\log(\gamma_g)]y_{N2} \text{ ..... (A.20)}$$

$$\mu_{1CO2} = [6.24\times10^{-3} + 9.08\times10^{-3}\log(\gamma_g)]y_{CO2} \text{ ..... (A.21)}$$

$$\mu_{1H2S} = [3.73\times10^{-3} + 8.49\times10^{-3}\log(\gamma_g)]y_{H2S} \text{ ..... (A.22)}$$

2. The atmospheric value is then adjusted to pressure conditions by means of a correction factor on the basis of reduced temperature and pressure state of the gas Dempsey developed the following relation:

$$\begin{aligned}\mu_r = \ln(\frac{\mu_g}{\mu_1}T_{pr}) &= a_0 + a_1 p_{pr} + a_2 p_{pr}^2 + a_3 p_{pr}^3 \\ &+ T_{pr}(a_4 + a_5 p_{pr} + a_6 p_{pr}^2 + a_7 p_{pr}^3) \\ &+ T_{pr}^2(a_8 + a_9 p_{pr} + a_{10} p_{pr}^2 + a_{11} p_{pr}^3) \\ &+ T_{pr}^3(a_{12} + a_{13} p_{pr} + a_{14} p_{pr}^2 + a_{15} p_{pr}^3)\end{aligned} \text{ ..... (A.23)}$$

Where,

$$a_0 = -2.462, a_1 = 2.97, a_3 = -0.2862, a_4 = 2.808, a_5 = -3.498,$$
$$a_6 = 0.3603, a_7 = -0.01044, a_8 = -0.7933, a_9 = 1.396, a_{10} = -0.1491,$$
$$a_{11} = 0.00441, a_{12} = 0.08393, a_{13} = -0.1864, a_{14} = 0.02033, a_{15} = -0.0006095,$$

3. Gas viscosity at elevated pressure can be readily calculated using the following relation:

$$\mu_g = \frac{\mu_1}{T_{pr}}\exp(\mu_r) \text{ ..... (A.24)}$$

9. The total compressibility

$$\begin{aligned}c_t &= c_{rock} + \varphi S_g c_g + \varphi S_w c_w \\ &= c_{rock} + \varphi(1 - S_w)c_g + \varphi S_w c_w\end{aligned} \text{ ..... (A.25)}$$

10. Pore Volume (PV), Water Volume (WV) and Hydrocarbon Volume (HCV)

$$\begin{aligned}PV &= A\phi[1 - c_{rock}(p_i - p)] \\ WV &= A\phi S_w[1 + c_w(p_i - p)] \\ HCV &= PV - WV\end{aligned} \text{ ..... (A.26)}$$

11. Initial Gas-in-place, G_i

$$G_i = \frac{Ah\varphi S_g}{B_{gi}} \quad \text{……...……...…..} \quad \text{(A.27)}$$

APPENDIX B

EXAMPLE CALCULATIONS

To demonstrate the systematic computation procedures in a vivid manner, the following reservoir in **TABLE B.1** will be investigated. Through this example calculation, one might appreciate the advantage of the DVS method.

TABLE B.1—Reservoir and gas properties

Net Pay (ft)	200
Hor. Permeability (md)	0.9
Vertical-to-horizontal permeability ratio	1:10
Hydrocarbon Porosity (%)	8.8
Initial Pressure (psia)	3500
Reservoir Temperature(°F)	220
Gas Gravity	0.63
rock compressibility (psi)	10^{-5}
Well spacing (acre)	80

Assuming a fully penetrating vertical well of radius 0.25 ft (no damage, no stimulation) and constant bottomhole pressure 500 psia, create a 3-year production forecast combining material balance with

1. Use transient and boundary-dominated stabilized production rate from well known correlations[35] (Traditional Method)
2. Use the boxinbox model[2,3] (DVS Method)

1. Calculation of Reservoir Rock and Gas Properties

Laboratory analysis is the most accurate way to determine the physical and chemical properties of a particular fluid sample; however, in the absence of laboratory data, correlations are viable alternatives for estimating many of the properties.

In this section, we calculate the values of gas and reservoir necessary to the calculation of J_D in traditional method and the DVS method. The input data and the output data are tabulated separately as in **TABLE B.2** and **TABLE B.3**. Initial gas in place is also calculated as in **TABLE B.4**. Functions of computing gas properties are coded in *Mathematica 6.0.1*, so that we can visualize the gas properties changes with reservoir pressure at reservoir temperature. These plots are shown as **Fig. B.1** for z-factor, **Fig. B.2** for viscosity, **Fig. B.3** for compressibility and **Fig. B.4** for pseudopressure.

TABLE B.2—Input data for gas properties calculation

Gas Specific Gravity, γ_g	0.63
Initial Reservoir Pressure, p_i, psi	3500
Reservoir Temperature, T, °F	220
Pressure at the standard conditions, p_{sc}, psia	14.65
Temperature at the standard conditions, T_{sc}, °F	60
The universal gas constant, R, psi ft^3/lb-mol-°R	10.732

TABLE B.3—Calculated value for reservoir and gas properties

Gas Molecular Weight, M_g	18.27
Gas Deviation Factor or z-Factor at initial reservoir pressure, z_{gi}	0.9149
Gas Formation Volume Factor at initial reservoir pressure, B_{gi}	0.003547
Gas Compressibility at initial reservoir pressure, c_{gi}	5.592×10^{-6}
Gas Viscosity at initial reservoir pressure, μ_{gi}	0.01919
Total Compressibility at initial reservoir pressure, c_{ti}	1.04921×10^{-5}

TABLE B.4—Calculated initial gas-in-place

Initial gas-in-place, G_i, MMscf	1.72919×10^{4}

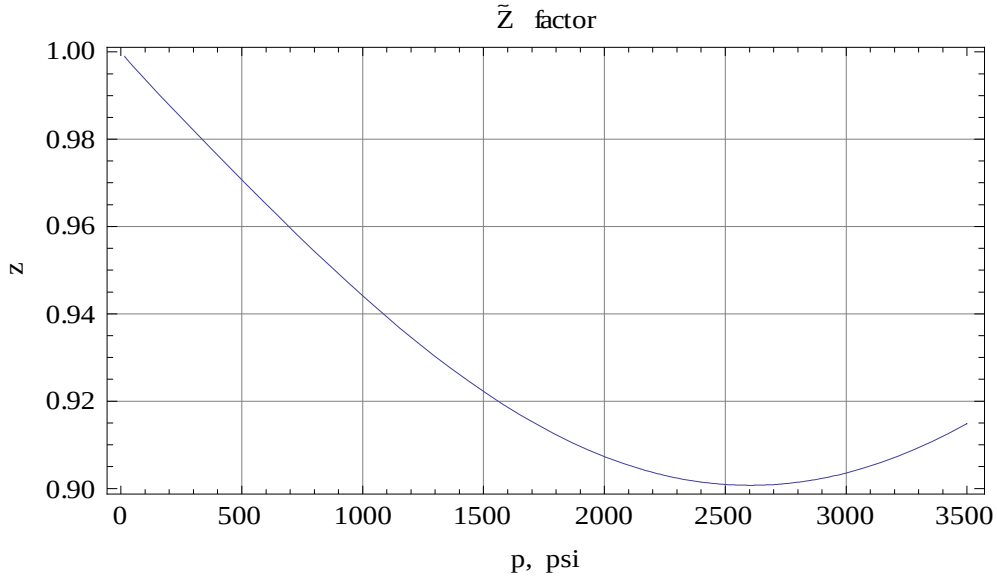

Fig. B.1—Gas z-factor as a function of pressure at reservoir temperature, 220 °F

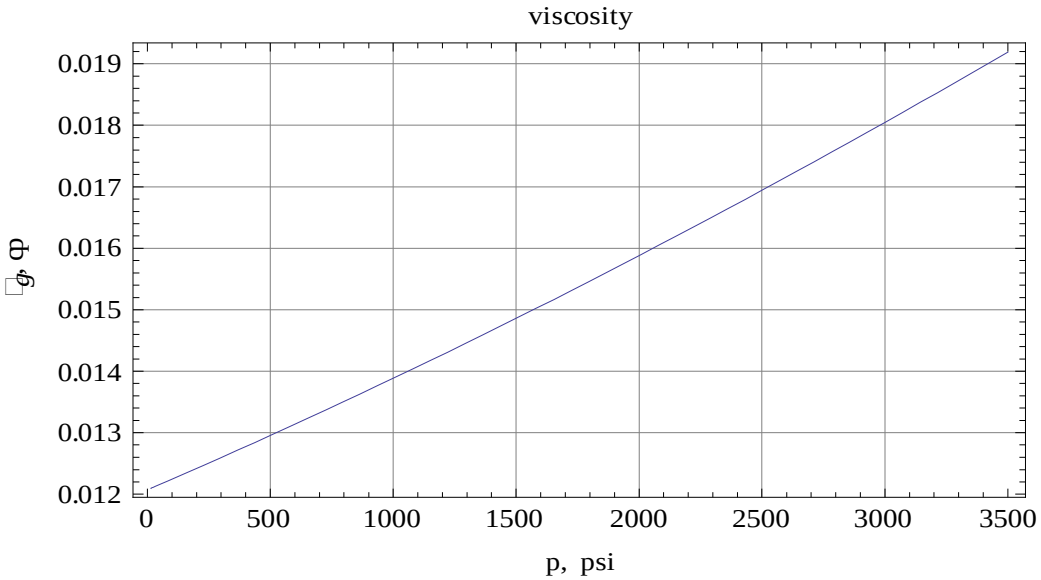

Fig. B.2—Gas viscosity as a function of pressure at reservoir temperature, 220 °F

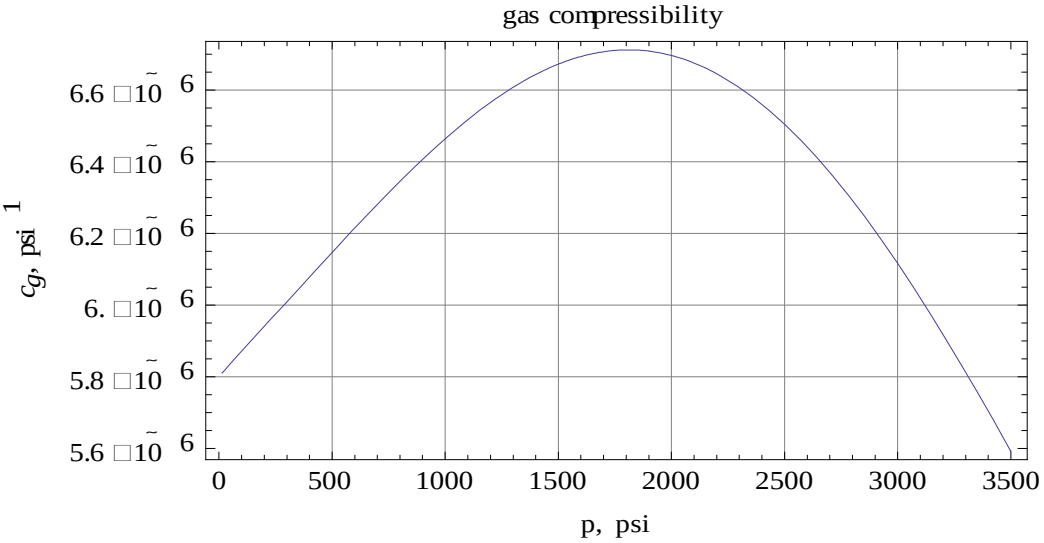

Fig. B.3—Gas compressibility as a function of pressure at reservoir temperature, 220 °F

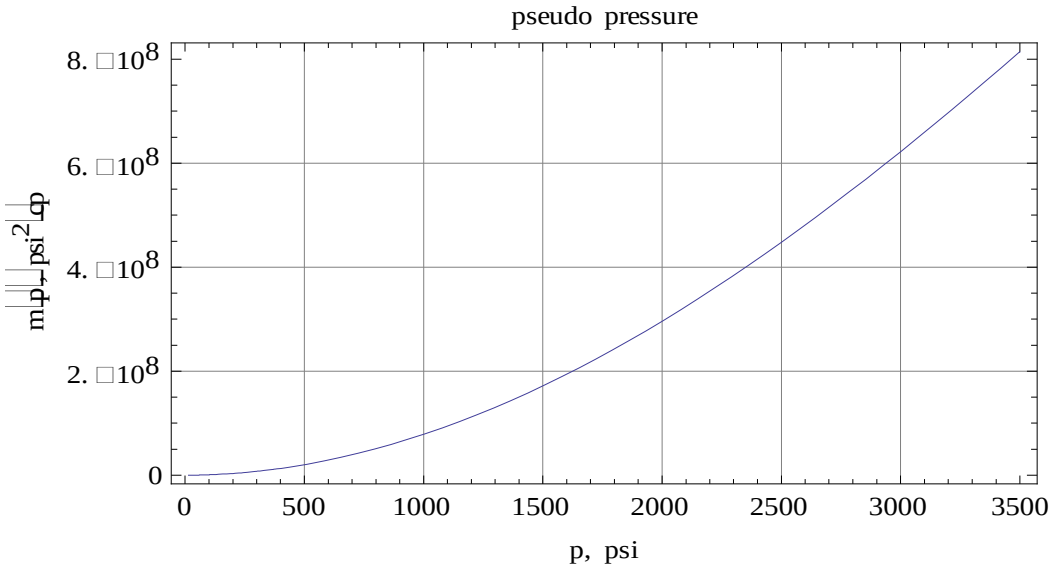

Fig. B.4—Gas pseudopressure function at reservoir temperature, 220 °F

2. Calculation Summary for Traditional Method

TABLE B.5—Input data for traditional method

Reservoir initial pressure, p_i, psia	3500
Horizontal permeability, k_H, md	0.9
Vertical permeability, k_V, md	0.09
Hydrocarbon porosity, phi, fraction	0.088
Rock compressibility, c_{rock}, 1/psi	$1. \times 10^{-5}$
Total compressibility at initial reservoir pressure, c_t, 1/psi	1.04921×10^{-5}
Wellbore radius, r_w, ft	0.25
Well spacing, A, acre	80
t_{DA} for circle/square drainage shape, dimensionless	0.1
Forecasting time span, t_p, yr	3

The input data and calculated data are tabulated in **TABLE B.5** and **TABLE B.6**, respectively. The J_D curve is shown in **Fig. B.5**. The transient flow lasts about 83 hours when the flow stabilizes, which means the onset of pseudosteady state flow. The production forecast results are shown graphically from **Fig. B.6** to **Fig. B.9**.

TABLE B.6—Calculated data for traditional method

Well drainage radius, r_e, ft	1053
Transition time, t_{pss}, hr	83
Productivity of stabilized flow, J_{Dpss}	0.13165

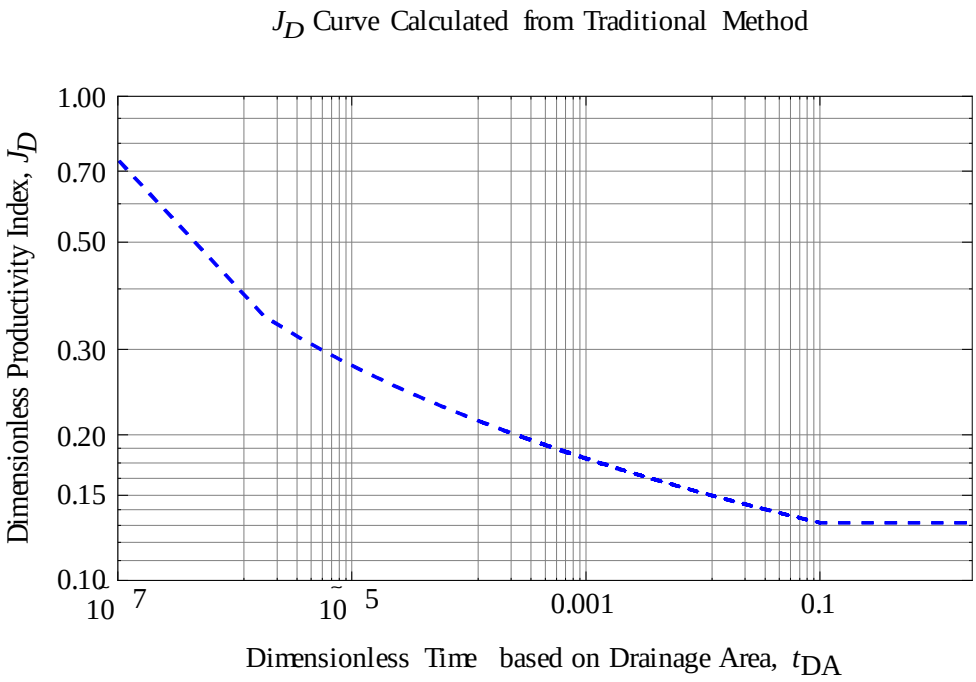

Fig. B.5—Computed J_D curve from Traditional Method: dimensionless productivity index as a function of dimensionless time based on drainage area

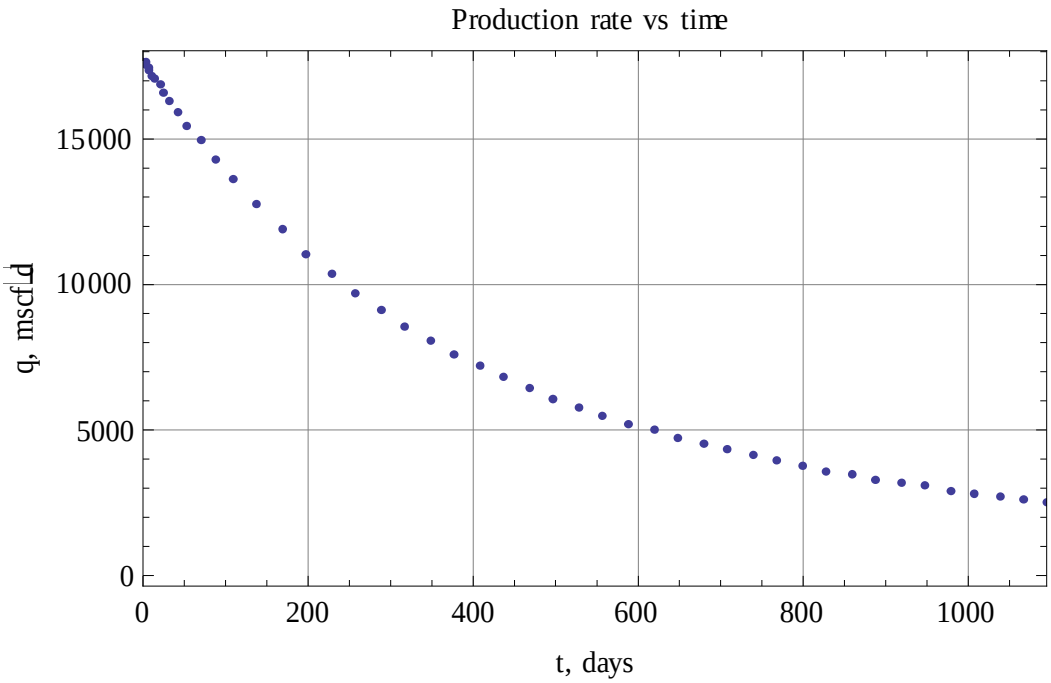

Fig. B.6—Forecasting using Traditional Method: production rate vs time

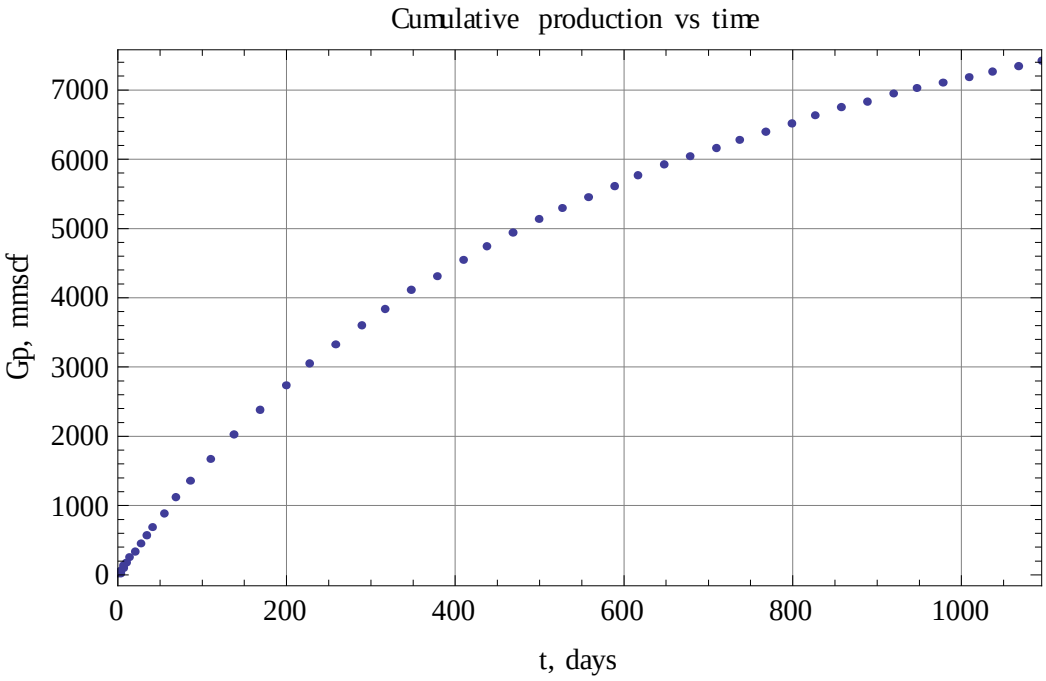

Fig. B.7—Forecasting using Traditional Method: cumulative production vs time

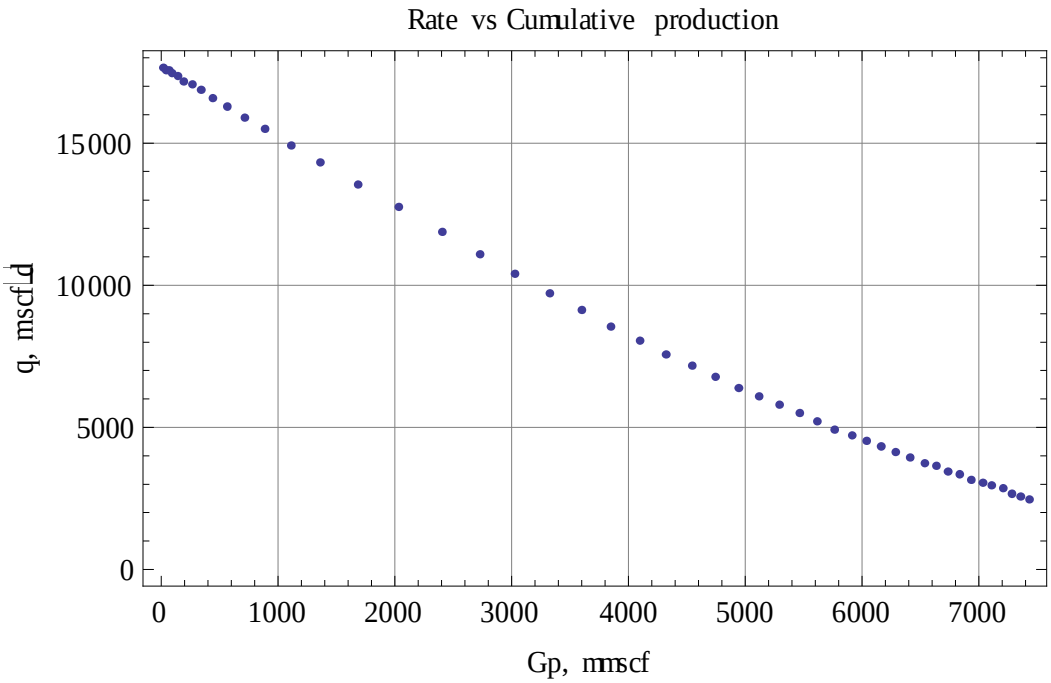

Fig. B.8—Forecasting using Traditional Method: rate vs cumulative production

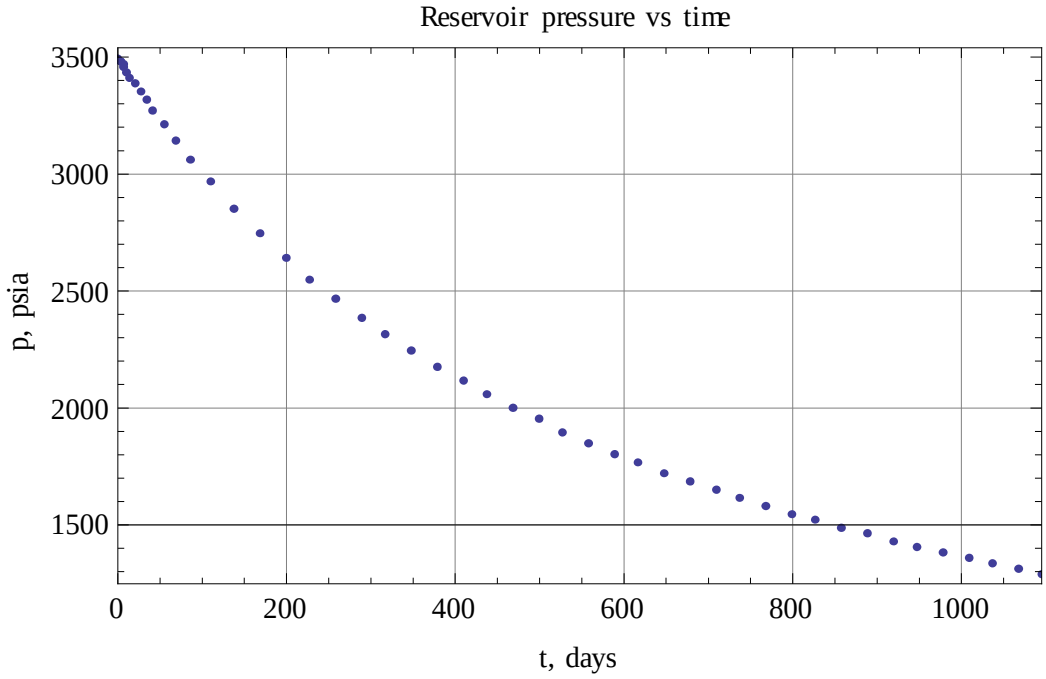

Fig. B.9—Forecasting using Traditional Method: reservoir pressure vs time

3. Calculation Summary for the DVS Method

The input data and calculated data are tabulated in **TABLE B.7** and **TABLE B.8**. The J_D curve is shown in **Fig. B.10**. As we can see, the curve is smooth all the time. The production forecast results are shown graphically from **Fig. B.11** to **Fig. B.14**.

TABLE B.7—Input data for the DVS method

Wellbore radius, r_w, ft	0.25
Well spacing, A, acre	80
Net pay, z_e, ft	200
Horizontal permeability, k_H, md	0.9
Vertical permeability, k_V, md	0.09

TABLE B.8—Calculated data for the DVS method

Reference length, L, ft	886.62
Reference permeability, K, md	0.418
Conversion factor between t_D and t_{DA}, c_{trad}	0.486
Onset of stabilized flow, t_{DA}	0.115246
Productivity of stabilized flow, J_{Dpss}	0.131396

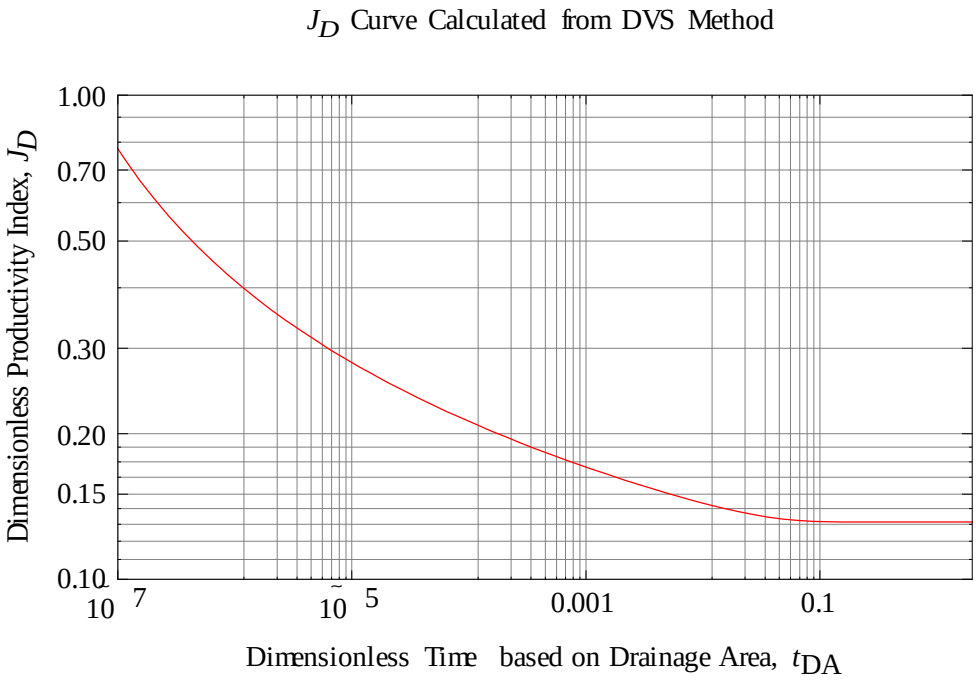

Fig. B.10—Computed J_D curve from the DVS Method: dimensionless productivity index as a function of dimensionless time based on drainage area

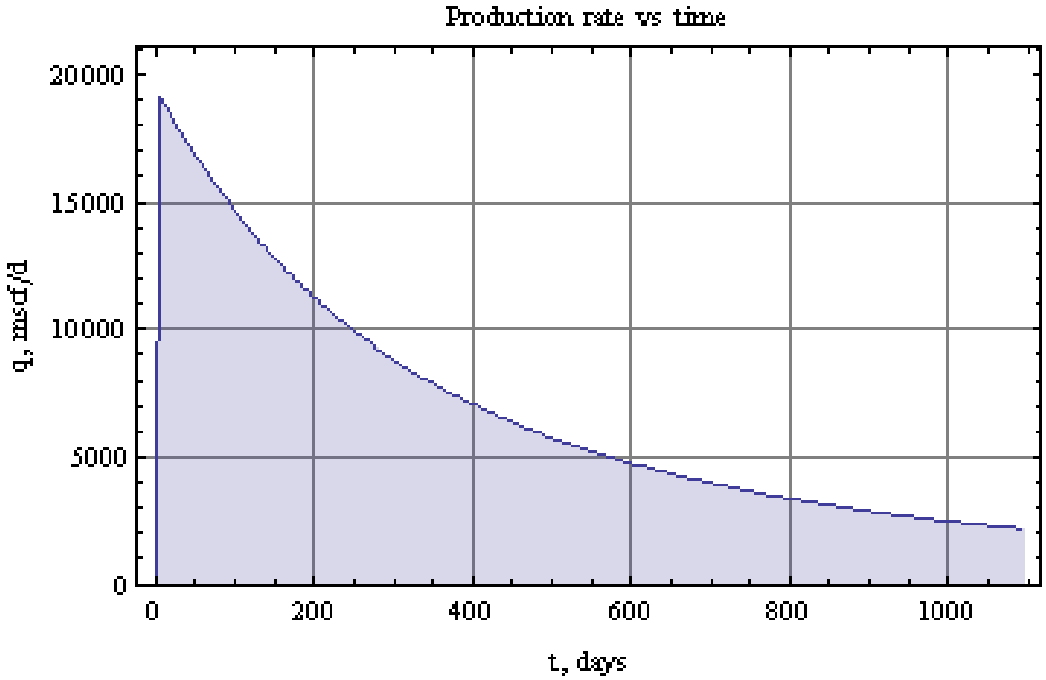

Fig. B.11—Forecasting using the DVS Method: production rate vs time

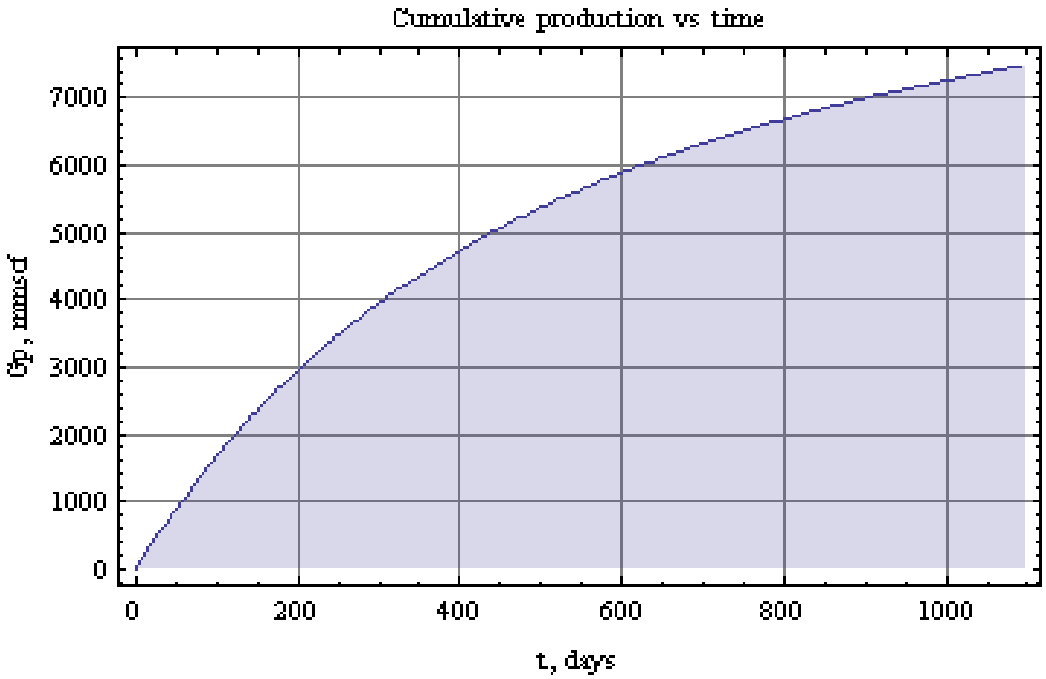

Fig. B.12—Forecasting using the DVS Method: cumulative production vs time

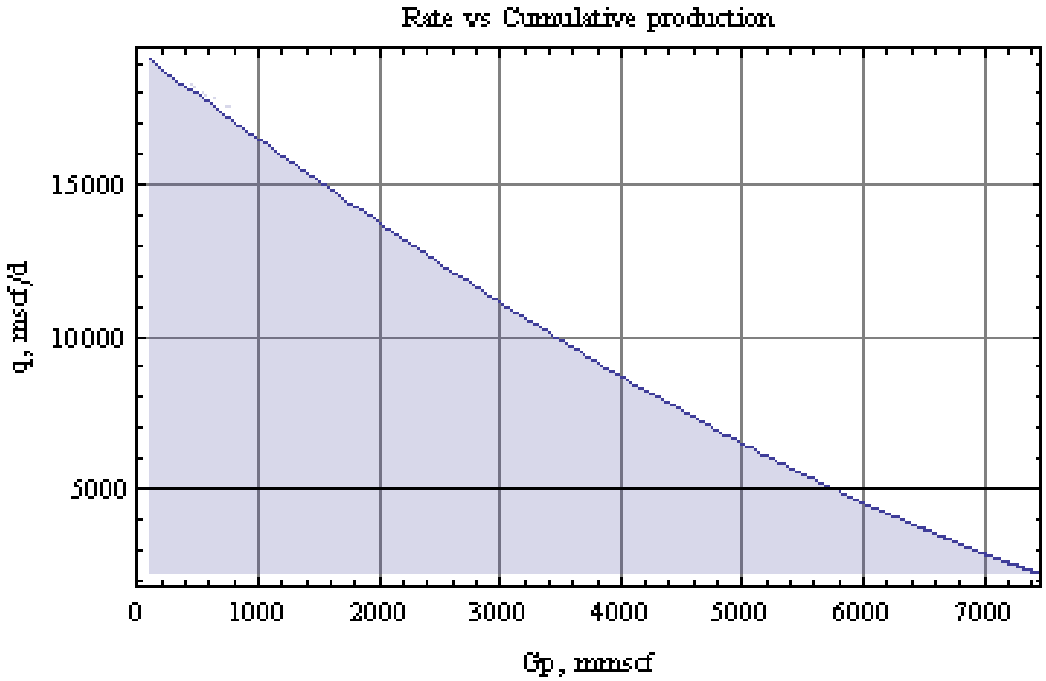

Fig. B.13—Forecasting using the DVS Method: rate vs cumulative production

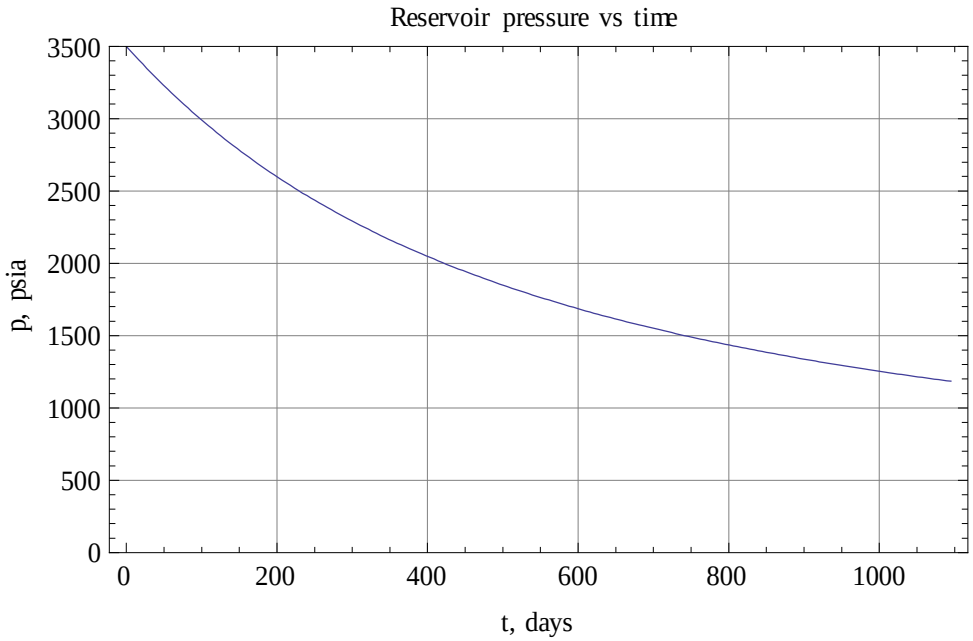

Fig. B.14—Forecasting using the DVS Method: reservoir pressure vs time

4. Comparison of Results

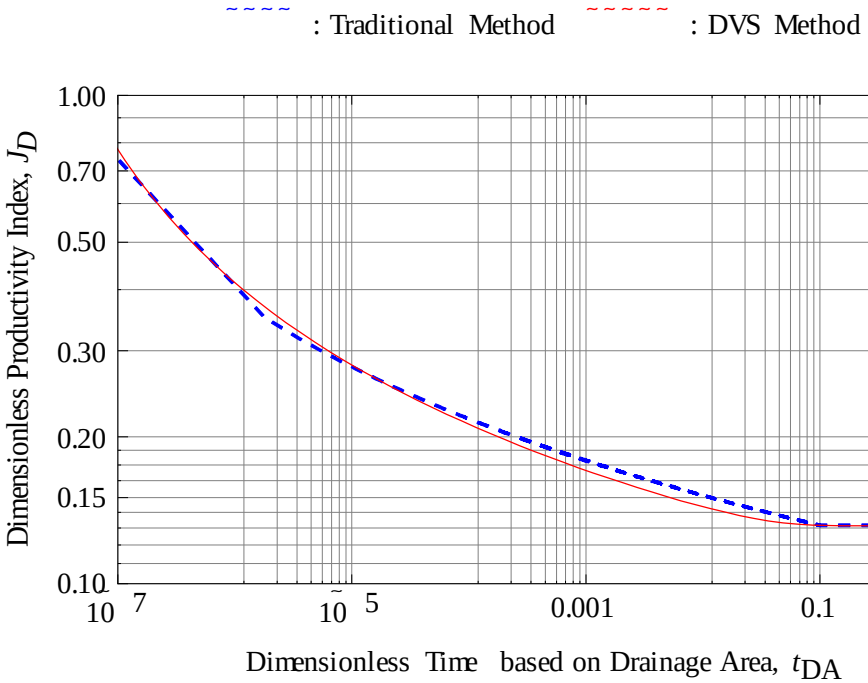

Fig. B.15—Comparison of Dimensionless Productivity Index (J_D) values calculated from Traditional Method and DVS Method

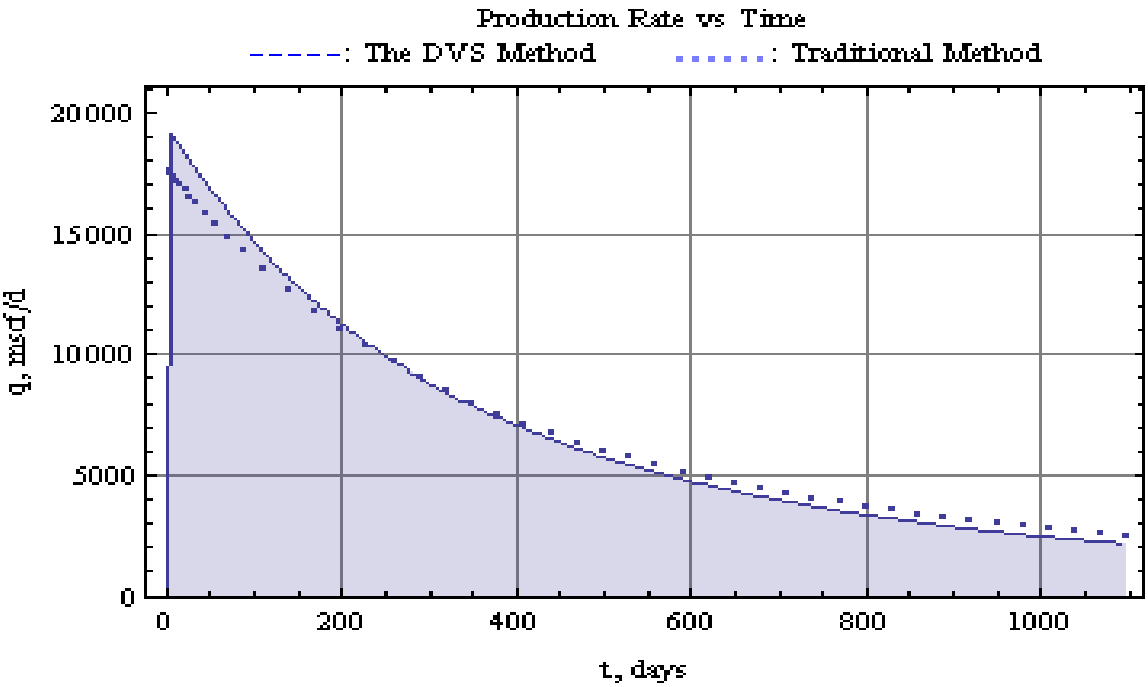

Fig. B.16—Comparison of forecasting results: production rate vs time

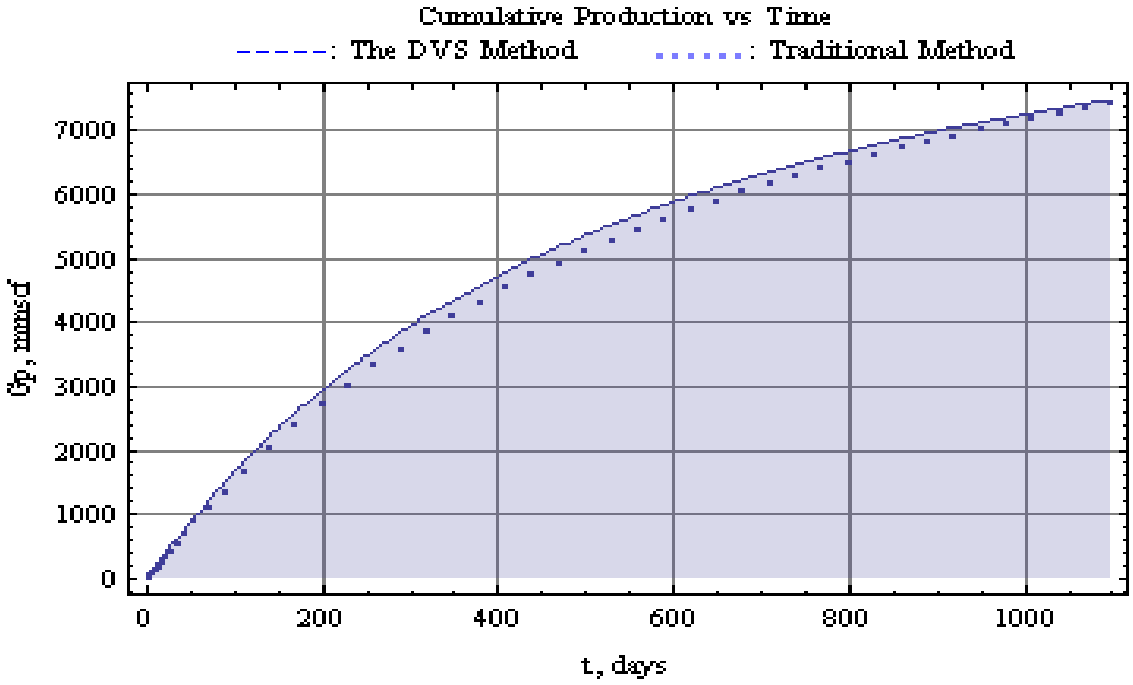

Fig. B.17—Comparison of forecasting results: cumulative production vs time

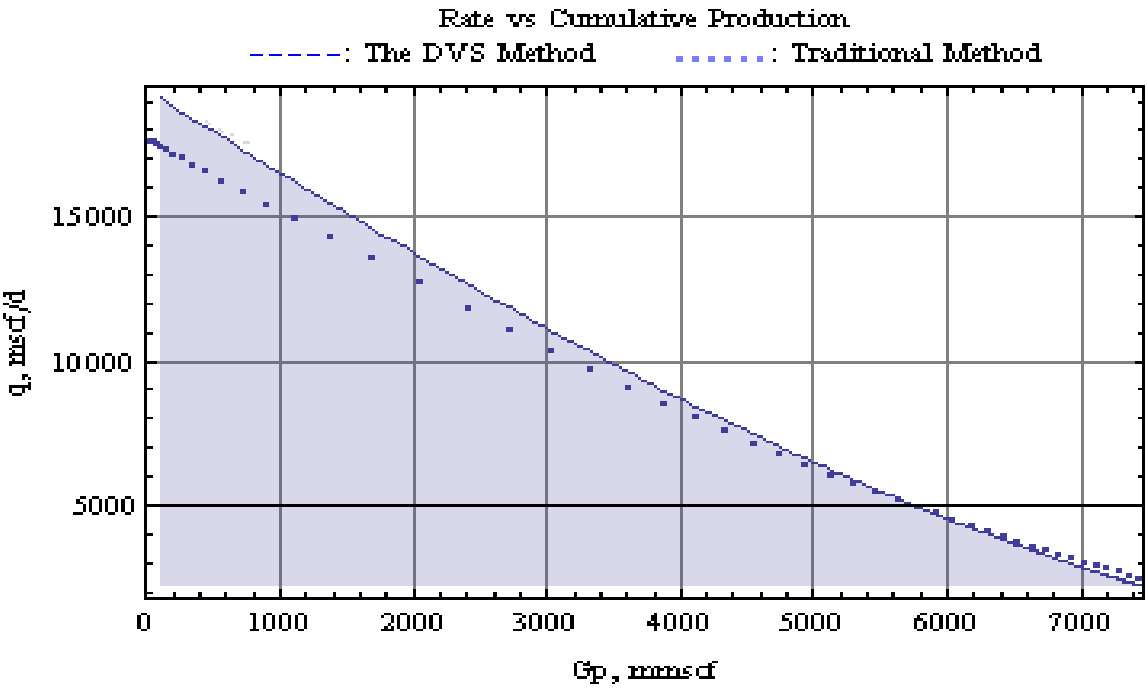

Fig. B.18—Comparison of forecasting results: rate vs cumulative production

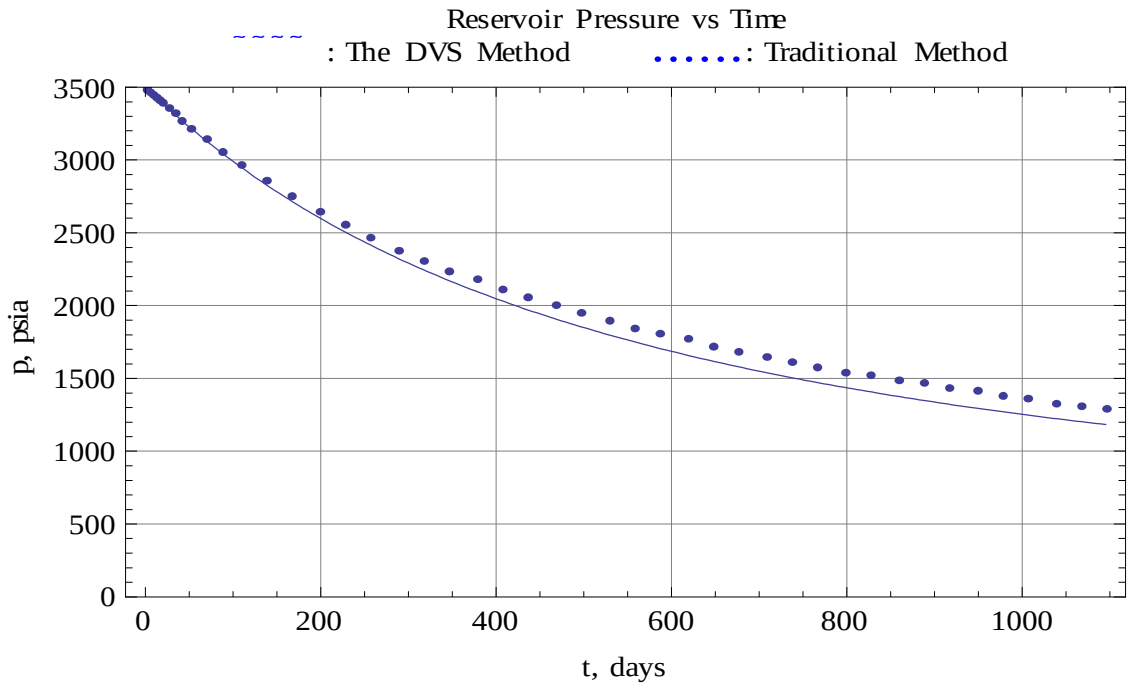

Fig. B.19—Comparison of forecasting results: reservoir pressure vs time

APPENDIX C

FIELD EXAMPLES STUDIES RESULTS

FOR WELL B AND WELL C

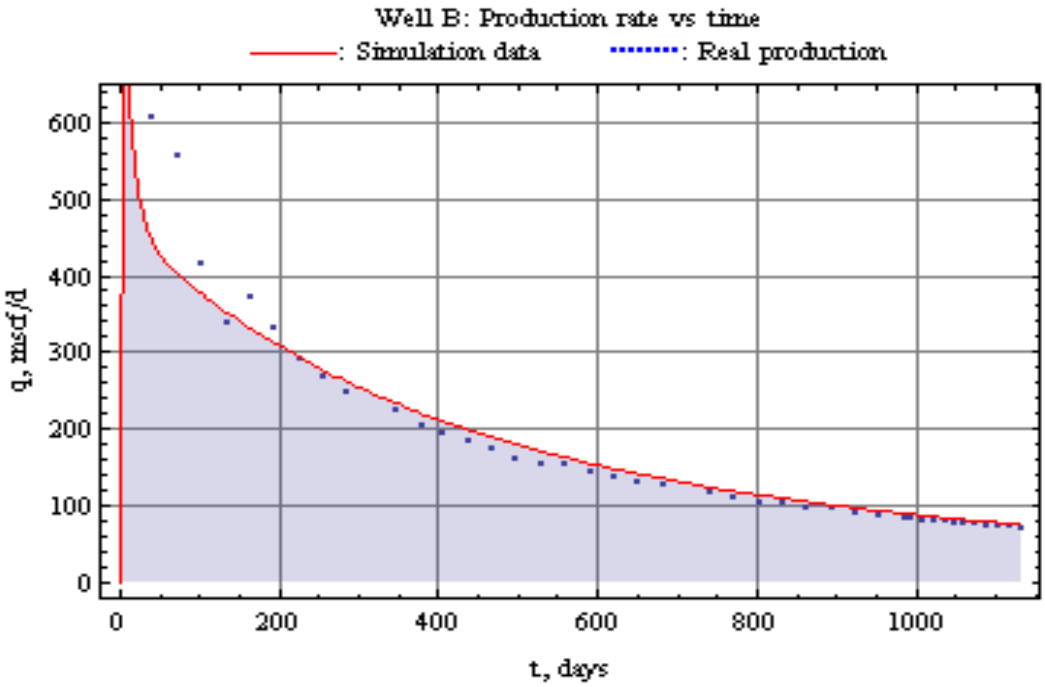

Fig.C.1—Comparison result of production rate versus time for Well B

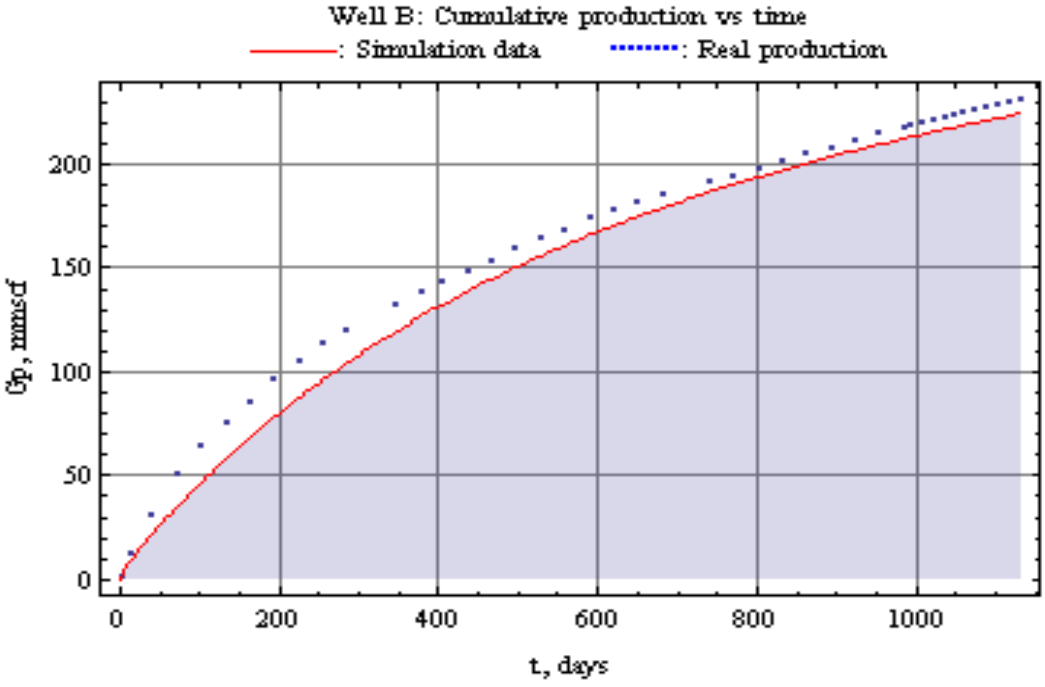

Fig. C.2—Comparison result of cumulative production versus time for Well B

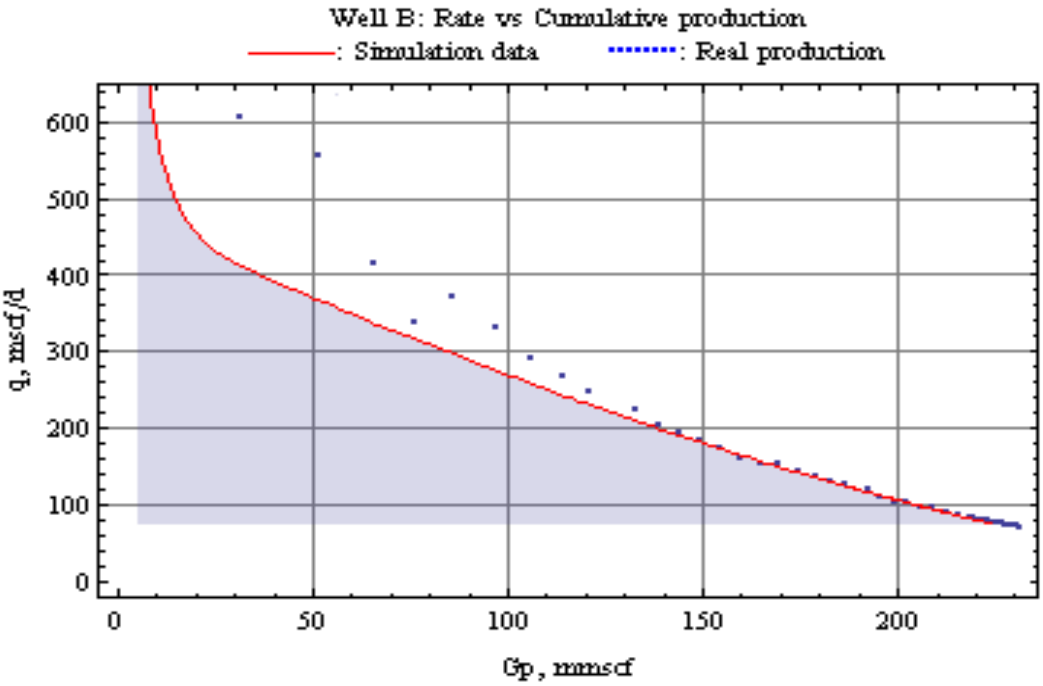

Fig. C.3—Comparison result of rate versus cumulative production for Well B

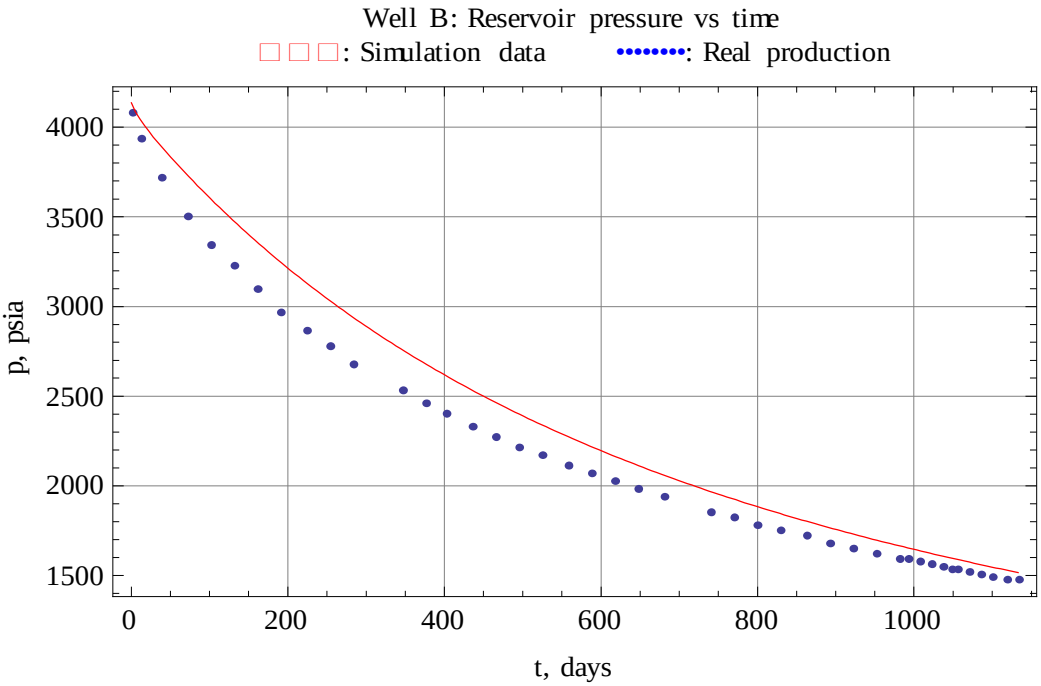

Fig. C.4—Comparison result of reservoir pressure versus time for Well B

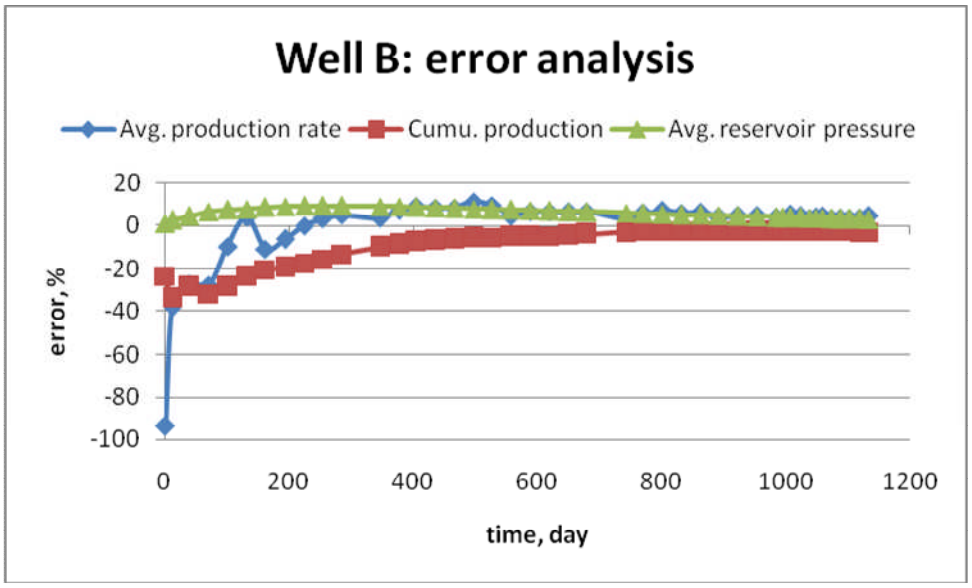

Fig. C.5—Error analysis for Well B

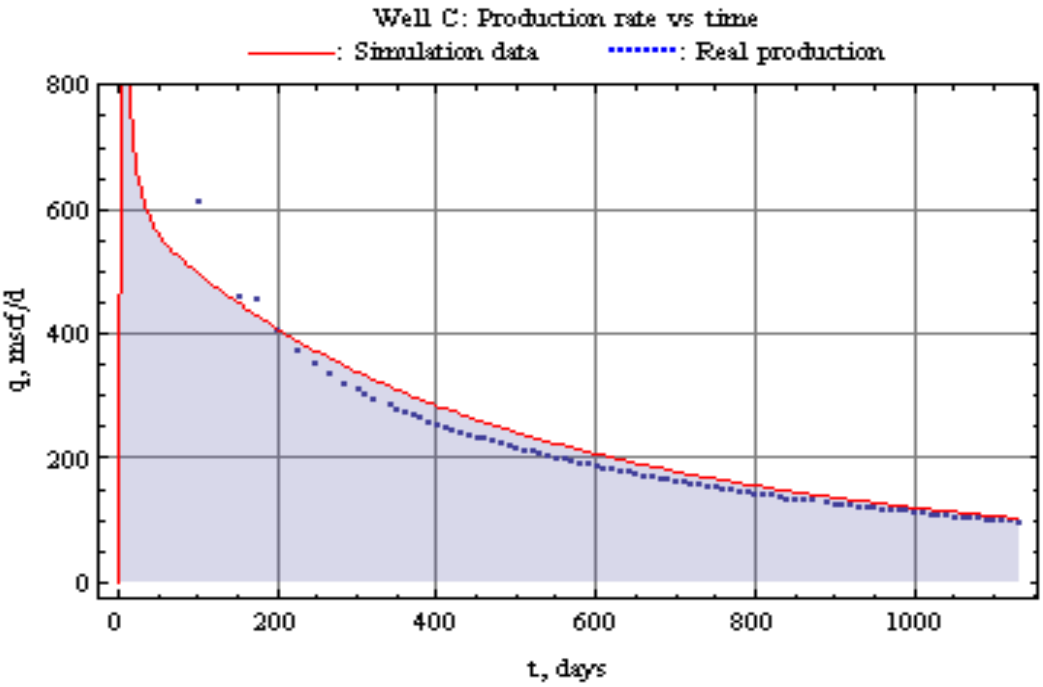

Fig.C.6—Comparison result of production rate versus time for Well C

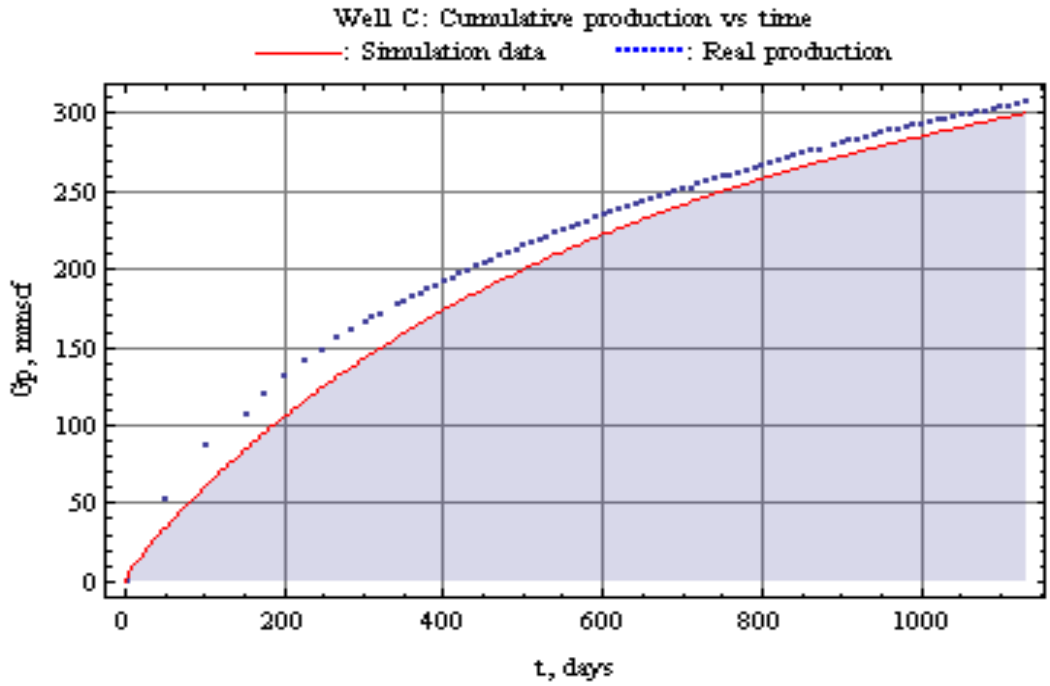

Fig. C.7—Comparison result of cumulative production versus time for Well C

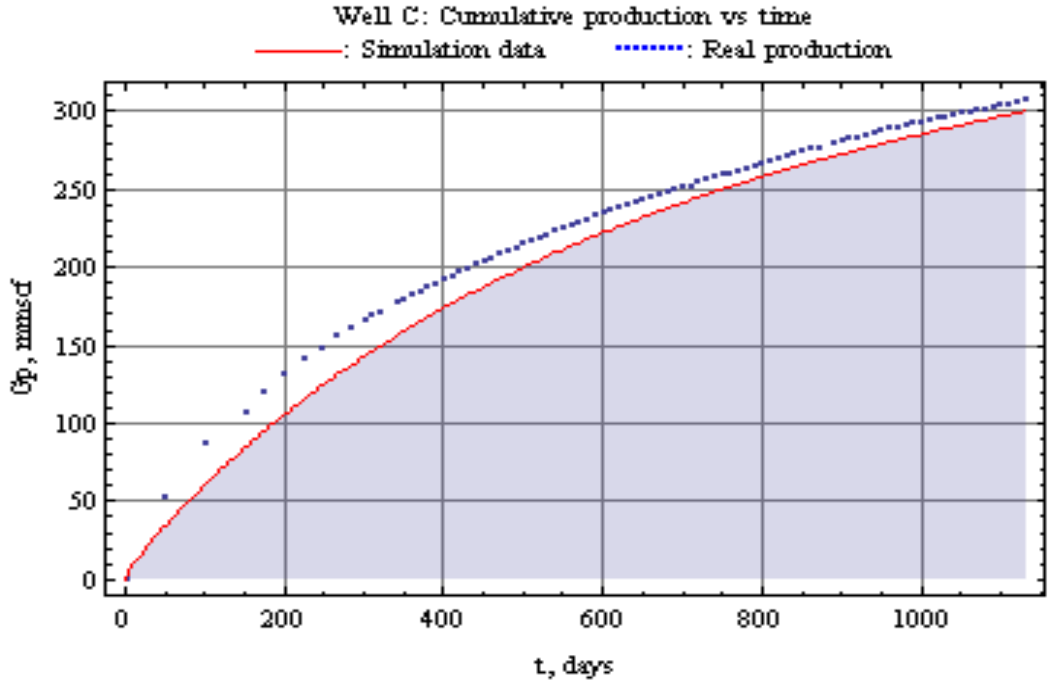

Fig. C.8—Comparison result of rate versus cumulative production for Well C

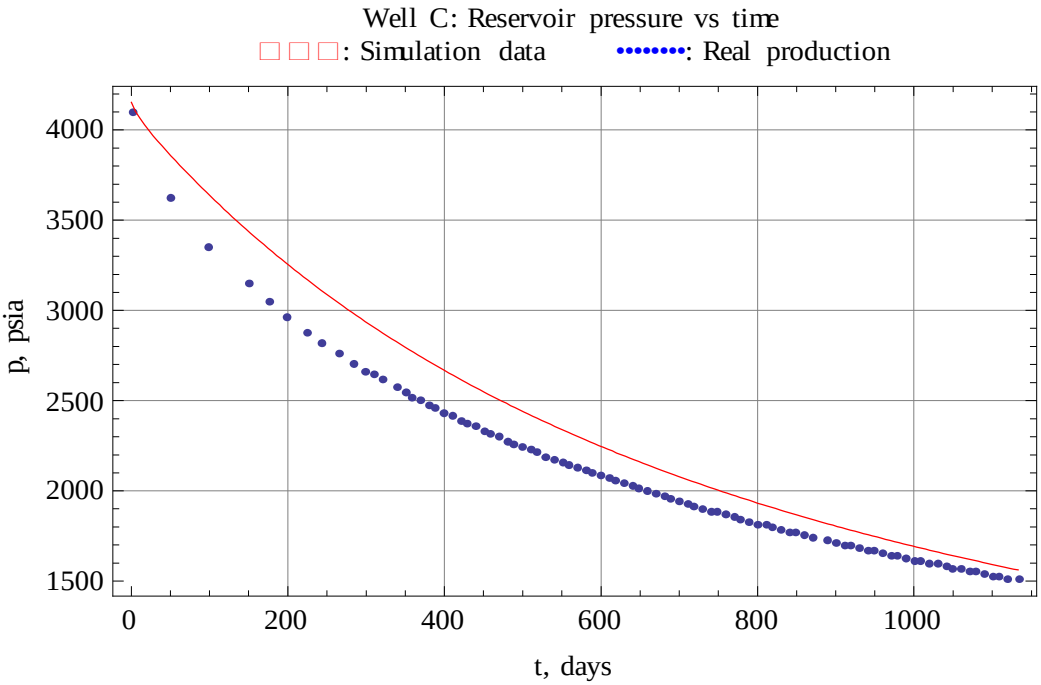

Fig. C.9—Comparison result of reservoir pressure versus time for Well C

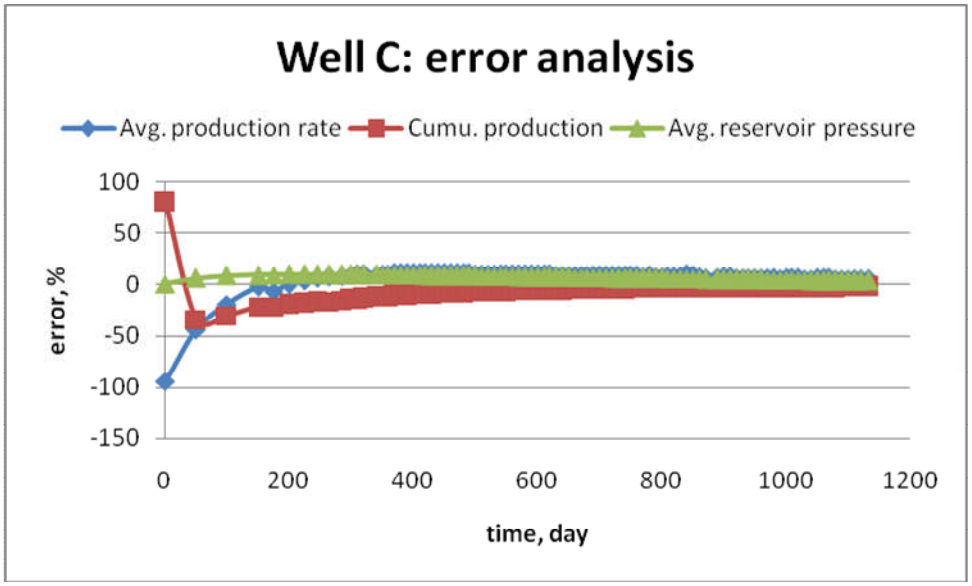

Fig. C.10—Error analysis for Well C

VITA

Name:	Xiaoze Jin
Born:	Shanxi, China
Permanent Address:	Harold Vance Department of Petroleum Engineering, 3116 TAMU, College Station, TX 77841
Email Address:	jinxz168@hotmail.com
Education:	M.S., Petroleum Engineering, Texas A&M University, December 2008 B.S., Polymer Science and Engineering, University of Science and Technology of China, July 2005
Affiliation:	Society of Petroleum Engineers